UNDERSTANDING THE ROLE OF RAB10 IN NEURONAL RESILIENCE

PREPARED BY:

WYATT BUNNER

December, 2023

Director of Dissertation: Erzsebet Szatmari

Major Department: Physical Therapy

Neuroresilience refers to the remarkable capacity of the brain to maintain its normal functioning and safeguard against cognitive decline even in the face of stress or trauma. The exploration of genes and pathways that play a role in mediating neuroresilience has garnered significant attention in recent years with the small GTPase known as Rab10 emerging as one of significant note. Functioning as a "resilience factor," a rare variant of Rab10 that has reduced activity has been found to confer resilience against Alzheimer's disease (AD). The primary objectives of this dissertation were to shed new light on the intricate functions of Rab10 and to contribute to the identification of novel biomarkers for neuroresilience, as well as therapeutic targets for the treatment of neurodegenerative disorders.

Nanostring nCounter platform was utilized for the analysis of 880 genes involved in neurodegeneration. This showed that $Rab10^{+/-}$ mice have increased activation of pathways associated with neuronal metabolism, structural integrity, neurotransmission, and neuroplasticity compared with their $Rab10^{+/+}$ littermates. Lower activation was observed for pathways involved in neuroinflammation and aging. We identified and validated several differentially expressed genes (DEGs), including Stx2, Stx1b, Vegfa, and Lrrc25 (downregulated) and Prkaa2, Syt4, and Grin2d (upregulated). Behavioral testing showed that $Rab10^{+/-}$ mice perform better in a hippocampal-dependent spatial task (object in place test), while their performance in a classical conditioning task (trace eyeblink classical conditioning, TECC) was significantly impaired.

We also identified different central and peripheral immune targets that Rab10 may help grant to combat neurodegeneration. Of note, basal microglia activation is significantly less in $Rab10^{+/-}$. Peripheral immune profiling of $Rab10^{+/-}$ mice showed reduced Natural Killer cells and a different phenotype distribution of CD8+ and CD4+ positive T-cells. Finally, Rab10 may provide a neuroprotective role via its ability to lower the production of inflammatory cytokines such as interleukin-1β, tumor necrosis factor-alpha, and interferon gamma. Further work is needed to evaluate whether any of these changes mediates the behavioral phenotypes and the resilience that Rab10 confers. We conclude that $Rab10^{+/-}$ mice described here can be a valuable tool to study the mechanisms of resilience in AD model mice and to identify novel therapeutical targets to prevent cognitive decline associated with normal and pathologic aging.

Understanding the Role of Rab10 in Neuronal Resilience

A Dissertation

Presented to the Faculty of the Department of Physical Therapy

East Carolina University

In Partial Fulfillment of the Requirements for the Degree

DOCTOR OF PHILOSOPHY

in

REHABILITATION SCIENCES

By

Wyatt Bunner

December, 2023

Director of Dissertation: Erzsebet M. Szatmari, Ph.D.
Thesis Committee Members:
Alessandro Didonna, Ph.D.
Robert M. Hughes, Ph.D.

UNDERSTANDING THE ROLE OF RAB10 IN NEURONAL RESILIENCE

By,

Wyatt Paul Bunner

APPROVED BY:

DIRECTOR OF DISSERTATION:

_____

Erzsebet M. Szatmari, PhD

COMMITTEE MEMBER:

_____

Robert Hughes, PhD

COMMITTEE MEMBER:

_____

Alessandro Didonna, PhD

CHAIR OF THE DEPARTMENT OF PHYSICAL THERAPY

_____

Amy Gross McMillan, PhD

DEAN OF THE GRADUATE SCHOOL

_____

Kathleen Cox, PhD

Acknowledgements

I would like to begin with a special thank you to my mentor, Dr. Erzsebet Szatmari, who took a chance on me and provided me the tools, opportunities, and guidance to thrive during my doctoral studies. Second, Drs. Robert Hughes and Alessandro Didonna who comprised my dissertation committee, providing priceless insight facilitating experimental development, data collection, analysis, and conclusions of my project. Finally, I would like to thank the many members of the East Carolina School of Dental Medicine and the College of Allied Health Sciences who provided technical and emotional support daily.

Table of Contents

Contents

List of Tables

Chapter 2-

List of Figures

Chapter 1-

Chapter 2-

List of Abbreviations

ACh- Acetylcholine
AChE- Acetylcholinesterase
AD- Alzheimer's disease
AP2- adipocyte Protein 2
APP- Amyloid Precursor Protein
Atm- Ataxia- telangiectasia mutation
Atp6v1d- ATPase H+ Transporting V1 Subunit D
Axin1- Axis inhibition protein 1
Aβ- Amyloid beta
Aβ40- 40-amino acid β amyloid
Aβ42- 42-amino acid β amyloid
BAC- Bacterial artificial chromosome
CCV- Clathrin coated vesicles
CD- Chron's disease
CD33- Sialic acid binding Ig-like lectin 3
cDNA- Complementary DNA
CHAT- Choline acetyltransferase
cKO- Conditional knockout
Cnot10- CCR4-NOT Transcription Complex Subunit 10
CNS- Central Nervous System
COPI- Coat complex subunit alpha
CR- Conditioned Response
CS- Conditioned Stimulus
DAPI- 4′,6-diamidino-2-phenylindole
DEG- Differentially expressed genes
DENND4- DENN domain-containing protein 4
DIV- Days in vitro
DOC- Deoxycholic acid
ECC- Eyeblink Classical Conditioning
ECL- Enhanced chemiluminescence
EMCN- Endomucin
EMG- Electromyography
EPM- Elevated plus maze
ERK- Extracellular signal-regulated kinase
ES- Embryonic stem cells
FACS- fluorescence-activated cell sorting
FBS- Fetal bovine serum
FC- Fear conditioning
FDA- Food and Drug Administration
GAPDH- glyceraldehyde-3-phosphate dehydrogenase

GAPs- GTPase activating proteins
GDI- GDP dissociation inhibitor
GDP- Guanosine diphosphate
GEFs- Guanine nucleotide exchange factors
GFAP- Glial fibrillary acidic protein
GLUT4- Glucose transporter type 4
GRIN2D- Glutamate Ionotropic Receptor NMDA Type Subunit 2D
GS- Griscelli syndrome
GTP- Guanosine triphosphate
HET- Heterozygous
HRP- Horseradish peroxidase
HSV- High speed video
Iba1- Ionized calcium binding adaptor molecule 1
INF-Gamma –Interferon gamma
IL1-beta- Interleukin-1 beta
ITI- Intertrial interval
KO- Knockout
LAMP2- Lysosome-associated membrane protein 2
Lrrc25- Leucine rich repeat containing 25
LRRK2- Leucine rich repeat kinase 2
Lsr- lipolysis stimulated lipoprotein receptor
LTD- Long term depression
LTP- Long-term potentiation
M1- Primary motor cortex
M6PR- Mannose-6-phosphate receptor
MABs- Monoclonal Antibodies
Mtorc1- Mammalian target of rapamycin complex 1
MWM- Morris Water Maze
NE- Northeast
NeuN- Neuronal nuclear protein
NFTs- neurofibrillary tangles
NK- Natural Killer
NMDA- N-methyl-D-aspartate
NMDAR- N-methyl-D-aspartate receptors
NW- Northwest
OIP- Object in place
PBS- Phosphate-buffered saline
PD- Parkinson’s disease
Phf21a- PHD finger protein 21A
PI3K- Phosphoinositide 3-kinase
PLD3- phospholipase D
PET- Positron emission topography
Ppp2r5e- Protein Phosphatase 2 Regulatory Subunit B'Epsilon
Prkaa- Protein Kinase AMP-Activated Catalytic Subunit Alpha 2
PSEN1- presenilin 1
PSEN2- presenilin 2

PVDF- Polyvinylidene fluoride
qPCR- Quantitative polymerase chain reaction
RanGap1- Ran GTPase activating protein 1
Rela- REL-associated protein
REP1- Rab escort protein 1
RNAi- Ribonucleic acid interference
RR- Rota-rod
RT-PCR- reverse transcriptase polymerase chain reaction
SA- Spontaneous alteration
SDS-PAGE- Sodium dodecyl-sulfate polyacrylamide gel electrophoresis
SNARE- Soluble N-ethylmaleimide sensitive factor attachment protein
SR- Startle response
Stx1b- Syntaxin 1b
SynGap1- Synaptic Ras-GTPase-activating protein
SYT4- Synaptotagmin 4
TBS-T- Tris-buffered saline with triton
TECC- Trace Eyeblink Classical Conditioning
TGN- Trans-Golgi network
TIP47- Perilipin 3
TLR4- Toll-like receptor 4
TNF-α- tumor necrosis factor-alpha
TRAPPCB- Trafficking protein particle complex subunit 9
TRAPPc9- Trafficking protein particle complex subunit 9
TREM2- Triggering Receptor Expressed On Myeloid Cells 2
TrkB- Tropomyosin receptor kinase B
TrkC- Tropomyosin receptor kinase C
UR- Unconditioned response
US- Unconditioned Stimulus
UTR- untranslated region
Vegfa- Vascular Endothelia Growth Factor A
WGS- Whole genome sequencing
WT- Wild-type

Chapter 1

Introduction

1.1 Alzheimer's Disease Prevalence and Current Hypothesis

Alzheimer's disease (AD) is the most prevalent neurodegenerative disorder, characterized by cognitive decline, cumulative memory loss and maladaptive behavior (Wimo et al., 2023). Currently, there are around 50 million AD patients worldwide, and this number is projected to double every 5 years (Saw et al., 2023). Despite being characterized by Alois Alzheimer in 1906, a cure or even therapeutic interventions to attenuate the progression for this devastating disease have yet to be discovered with the drugs approved by the FDA working only to alleviate some of the symptoms (Saw et al., 2023).

AD is commonly characterized by the presence of Amyloid-beta (Aβ) peptide, a small peptide consisting of 40-42 amino acids that forms amyloid plaques (Portelius et al., 2010). Another hallmark of AD are the intracellular deposits of hyperphosphorylated tau protein, termed neurofibrillary tangles (Portelius et al., 2010). Aβ may initiate the misplacement of tau in dendrites, thereby affecting the accumulation of Aβ (Tu et al., 2014). Interestingly, experiments conducted in a human neural cell culture system demonstrated that elevated levels of Aβ alone were sufficient to increase neurofibrillary tangles in neurons (Kwak et al., 2020). Furthermore, studies involving mouse models exhibiting both Aβ and tau pathologies revealed that Aβ accelerates neurofibrillary tangle pathology, whereas the same doesn't occur conversely when tau is present (Hurtado et al., 2010). Independent of tau pathology, Aβ has also been shown to contribute to cognitive impairment. For instance, secreted oligomers derived from Aβ in human brains diagnosed with AD have been found to reduce dendritic spine density in hippocampal pyramidal neurons (Shankar et al., 2008). These oligomers have also been observed to induce

increased synaptic long-term depression (LTD) in rodent hippocampal slice cultures, suggesting that Aβ can influence synaptic plasticity (Li et al., 2009).

While the underlying cause of AD is still unknown, it is considered a multifactorial disease with two current hypotheses proposed as the main source: the cholinergic and amyloid hypotheses. Early studies in AD reported presynaptic cholinergic deficits related to the enzyme choline acetyltransferase (ChAT) (Sims et al., 1983). One role of ChAT is the synthesis of acetylcholine (ACh), which plays a vital role in cognitive function (Winkler et al., 1995). Degeneration of cholinergic neurons occurs in patients afflicted with AD leading to cognitive function decline and memory loss (Winkler et al., 1995). Increasing cholinergic levels due to the reductions in acetylcholine biosynthesis is considered one possible therapeutic strategy for AD. One way this is accomplished is by inhibiting acetylcholinesterase (AChE). This is achieved via AChE inhibitors which inhibit ACh degradation in synapses resulting in the accumulation of ACh and the activation of cholinergic receptors (Singh et al., 2013). The first FDA-approved cholinesterase inhibitor approved for the treatment of AD was Tacrine (Davis & Powchik, 1995). Newer generations of AChE inhibitors also show some promise, but this class of drugs has only been shown to attenuate the onset of the major symptoms of AD, and many of the drugs that have been developed largely fail during clinical trials with the side effects outweighing the therapeutic effects (Zhou et al., 2021). Though as we continue to try to cure or attenuate this disease, cholinergic interventions are likely to maintain their critical role in slowing the onset of symptoms.

Another hypothesis used when developing therapeutic targets in AD is the amyloid hypothesis (also known as the Aβ hypothesis). A major component of the accumulated Aβ in the brain is Aβ 42 and Aβ 40 residues. An increase in these residues, especially Aβ 42, is a major

inducer of Aβ fibril formation (Savage et al., 1995). These accumulated fibrils develop into senile plaques, which can cause the induction of another hallmark of AD tau pathology and neurotoxicity, leading to neuron cell death and neurodegeneration (Maccioni et al., 2010). With this hypothesis, targets for clearing Aβ plaques have led the therapeutic charge of developing treatment for AD for over a decade. One major therapeutic strategy that has been developed to target amyloid are anti-amyloid monoclonal antibodies (mABs). The goal of mABs is to clear toxic Aβ species, thus preventing the amyloid cascade and halting the neurodegeneration and cognitive decline associated with AD (Van Dyck, 2018). While the results of testing these therapeutics was originally fraught with failure, this therapy has shown some promise in recent years. Aducanumab was the first antibody targeting Aβ to show a possible dose-dependent reduction in humans determined by positron emission tomography (PET) (Rodriquez et al., 2023). In 2021 it was granted accelerated approval by the Food and Drug Administration, but it was terminated in both of its phase 3 trials due to conflicting evidence of its efficiency (Rodriquez et al., 2023). January 2023 brought even more promise in this class of drugs with the introduction of Lecanemab. Since its accelerated approval patients with mild AD progression showed a 27% slower cognitive decline compared to individuals treated with a placebo (Söderberg et al., 2023). This data combined with the reduction of Aβ in PET scans cleared the way for the full approval of the drug in July 2023 (Mahase et al., 2023).

1.2 Inflammation and AD

While the exact cause of Alzheimer's remains unknown, emerging evidence suggests that chronic inflammation in the brain plays a crucial role in its pathogenesis (Heneka et al., 2015; Onyango et al., 2021). This chronic inflammation can be triggered by various factors, including

the aggregation of abnormal proteins, oxidative stress, and aberrant function of the immune system (Bettcher et al., 2021; Butterfield et al., 2019). Neuroinflammation refers to the activation of immune cells and inflammatory mediators in the brain. In Alzheimer's disease, microglia, the brain's resident immune cells, become chronically activated, releasing pro-inflammatory cytokines, such as interleukin-1β (IL-1β) and tumor necrosis factor-alpha (TNF-α) (Torres-Acosta et al., 2020; Scarabino et al., 2020). Additionally, astrocytes, another type of glial cell, contribute to the inflammatory response by releasing inflammatory molecules. This neuroinflammation disrupts normal brain function and exacerbates neuronal damage (Preman et al., 2021). The traditional hallmark features of AD are accumulation of two abnormal proteins: Aβ plaques and tau tangles. Aβ is derived from the APP, and in a healthy brain, it is cleared efficiently (Withington et al., 2022). However, in AD, the clearance mechanisms are impaired, leading to the formation of Aβ plaques. These plaques trigger an immune response, attracting microglia to the site of deposition (Hansen et al., 2018). While microglia attempt to clear the Aβ, their inflammatory response can inadvertently cause neuronal damage (Hansen et al., 2018).

Similarly, tau protein is essential for stabilizing microtubules in neurons, but in Alzheimer's, tau becomes hyperphosphorylated, leading to its aggregation into neurofibrillary tangles (Stoothoff et al., 2005). These tangles are associated with neuroinflammation, as they promote the activation of microglia and the release of pro-inflammatory molecules (Pascoal et al., 2021). Compounding on this, when neurons are destroyed from this tau-induced microglia activation, the newly destroyed neurons will release inflammatory peptides that serve to re-activate microglia creating a dangerous neurodegeneration cascade (Maccioni et al., 2010). Modulation of this inflammatory cascade is likely to lead to future pharmaceutical intervention strategies for combating or preventing the cognitive decline that this debilitating disease induces.

1.3 Small Rab GTPases

Human cells exhibit nearly 70 distinct Rab GTPase family members, many which actively regulate the formation and transport of vesicles (Wandinger-Ness & Zerial, 2014). Like other small GTPases, Rab proteins undergo a dynamic cycle, transitioning between an active state (bound to GTP) and an inactive state (bound to GDP). The switch between these states is finely regulated by effector proteins that interact with the switch I and II regions of Rab GTPases, inducing conformational changes (Seabra & Wasmeier, 2004). The primary regulation of GTPase activity is facilitated by GAPs, such as SynGAP1, Axin1, and RanGap1, which promote the hydrolysis of GTP to GDP, resulting in the inactivation of the GTPases (Stenmark, 2009). To stabilize Rab proteins in their inactive form, GDIs like Rab GDI and REP-1 bind to them, preventing reactivation by GEFs such as TRAPPc9, TRAPPC6B, and Alsin (Stenmark, 2009). The temporal control of Rab GTPases and the regulation of their duration of activity are profoundly influenced by GEFs and GAPs (D'Adamo et al., 2014). GEFs catalyze the activation of Rab GTPases by facilitating the exchange of GDP for GTP. Rab-GAPs can augment the intrinsic activity of GTPases, enabling swift hydrolysis of GTP to GDP. For example, when Rab5 is active, it concurrently recruits TBC-4, a Rab10 GAP, which significantly reduces Rab10 activity. Contrariwise, DENND4 functions as a GEF for Rab10, triggering the conversion of Rab10 from its GDP-bound to GTP-bound form, thus enabling its participation in various cellular functions like GLUT4 translocation (Saraste, 2016).

Each Rab protein has a diverse number of functions through interactions with different effectors, including motor proteins, coat proteins, tethering complexes, and SNAREs (Hunter et al., 2013). These downstream effectors guide Rab signaling toward different stages of membrane transport such as vesicle budding, tethering, and mobility. Notably, coat proteins such as COPI

and COPII play a crucial role in the formation of cytosolic coat complexes around cargo (Bonifacino & Glick, 2004). Additionally, Rab GTPases contributes to ensuring precise coat recruitment to intracellular membranes. An example is found in Rab9 signaling, which facilitates the recycling of mannose-6-phosphate receptors (M6PRs) from late endosomes to the trans-Golgi network. TIP47, a sorting adaptor and an effector of Rab9, recognizes the tail of M6PRs (Carroll et al., 2001). Interaction between Rab9 and M6PRs recruits TIP47 to late endosome membranes, enhancing its affinity for cargo and facilitating the sorting of M6PRs into late endosomal recycling buds (Carroll et al., 2001).

Following cargo sorting and vesicle budding from the donor membrane, it is necessary to remove coat proteins to allow vesicles to fuse with the acceptor membrane. A well-studied model in this context is the AP2 adaptor complex and clathrin coat involved in endocytosis vesicles. AP2 is capable of recruiting clathrin to the newly formed vesicles and regulating the endocytosis process of clathrin-coated vesicles (CCVs) (Carroll et al., 2001). The μ2 subunit of AP2, when phosphorylated, enhances its interaction with cargo and vesicles (Jackson et al., 2003). Moreover, during clathrin-mediated endocytosis, PIP2 plays a crucial role in recruiting AP2 to the vesicles (Zoncu et al., 2007).

Rab5 has been identified as a key regulator of clathrin uncoating by influencing AP2 function. Rab5 is localized on CCVs and exerts its influence on CCV uncoating through two mechanisms. Firstly, Rab5 inhibits the phosphorylation of the μ2 subunit of AP2, which reduces its interaction with vesicles and promotes uncoating. Secondly, Rab5 facilitates the turnover of PIP2 by recruiting PI3K or PI phosphatases, consequently reducing the AP2 levels and facilitating uncoating (Semerdjieva et al., 2008; Shin et al., 2005).

Rab proteins play a crucial role in regulating vesicle trafficking along both actin filaments and microtubules. Specifically, Rab proteins can interact with actin motors of the myosin V family through specific Rab effectors, facilitating vesicle trafficking along actin filaments (Stenmark, 2009). For instance, Rab11 interacts with Myosin Vb via its effector Rab11-FIP2, effectively controlling the transport of various receptors from recycling endosomes to the plasma membrane in both neuronal and non-neuronal cells (Wang et al., 2008). Another example is Rab27, which interacts with myosin V through its effector melanophilin, facilitating the trafficking of melanosomes to the plasma membrane (Wu, 2002).

Intriguingly, Rab proteins can also interact with microtubule motors such as kinesin or dynein to regulate vesicle trafficking along microtubules. For example, GTP-bound Rab6 directly interacts with a kinesin called Rabkinesin-6 (also known as kinesin family member 20A), thereby regulating directional membrane transport and Golgi dynamics (Fontijn et al., 2001). Additionally, Rab6 indirectly interacts with microtubule motors through its effector Bicaudal D1, controlling COPI-independent Golgi-ER transport (Matanis et al., 2002). Another notable example is Rab7, which regulates trafficking between late endosomes and lysosomes. Rab7 recruits the dynein-dynactin motor complex by interacting with its effector RILP, facilitating the trafficking of late endosomes to lysosomes (Matanis et al., 2002).

1.4 Rab Proteins in Neuronal Function

The intricate structure and function of neuronal cells heavily rely on the precise regulation of membrane trafficking. In neurons, the transport of molecules and membranes is essential over long distances along dendrites and axons, with some axons being a meter or more in length (Campenot & Eng, 2000). As a result, neurons have developed specific mechanisms to

tightly control the transport of proteins, organelles, and receptors across these extensive pathways.

Several Rab proteins are intricately involved in the tight regulation of these neuronal processes. At the synapse, Rab5, Rab4, Rab11, and Rab35 govern clathrin-mediated endocytosis, ensuring efficient membrane retrieval, synaptic vesicle homeostasis, and recycling (Cousin, 2015). Additionally, Rab3 and Rab27 play crucial roles in synaptic vesicle exocytosis and neurotransmitter release (Pavlos & Jahn, 2011). Several Rab GTPases contribute to the trafficking and turnover of neurotransmitter receptors at the postsynaptic site, controlling receptor delivery (Rab8), receptor maturation (Rab39b), insertion and removal at the plasma membrane (Rab4, Rab11), thereby regulating the number of surface neurotransmitter receptors(Rab17) (Pavlos & Jahn, 2011; Stenmark, 2009).

Notably, Rab proteins also play vital roles in anterograde and retrograde axonal transport. For instance, Rab3, Rab27, and Rab10 mediate transport to the axon terminals through their interaction with kinesin motor proteins (Raiborg et al., 2015; Szodorai et al., 2009). Rab7a also participates in sorting plasma membrane proteins for degradation at the axon terminal (Zhang et al., 2009). Given their pivotal roles in multiple transport pathways within neurons, including dendrite branching, morphogenesis, neurite outgrowth, and neuronal migration during development, dysregulation of these Rab-mediated processes has been associated with neurodegenerative disorders, including Alzheimer's disease, Parkinson's disease, amyotrophic lateral sclerosis, and Charcot–Marie–Tooth disease (Bellucci et al., 2022; Seabra et al., 2002).

1.4 Rab GTPases in AD

AD is the most prevalent form of neurodegeneration and dementia. Most AD cases are sporadic and not linked to genetic alterations or mutations, while around 5-10% of cases are

associated with mutations in Presenilin 1 (PSEN1), Presenilin 2 (PSEN2), and amyloid precursor protein (Wimo et al.) (Giau et al., 2019). These mutations disrupt the normal production of amyloid-β peptide (Aβ), leading to the accumulation of Aβ as extracellular deposits in the brain. Aβ plaques, along with neurofibrillary tangles, are key components of AD pathogenesis. PSEN1 and PSEN2 are proteases present in the endoplasmic reticulum (ER), trans-Golgi network (TGN), and vesicles, where they act as the catalytic component of the γ-secretase enzyme (Vetrivel et al., 2006). This enzyme cleaves APP, generating Aβ of different lengths. Mutations in PSEN1, PSEN2, or APP increase the relative ratio of long and short Aβ amyloid peptides, which can form neurotoxic oligomers (Hampel et al., 2021). Additionally, PSEN1 plays a role in regulating membrane transport by binding to Rab GDP dissociation inhibitor (GDI). In PSEN1-deficient neurons, the association of Rab GDI with membranes decreases, resulting in reduced levels of membrane-associated Rab GTPases (Scheper et al., 2000). Notably, the levels of membrane associated active Rab6 are decreased in PSEN1 knockout-cells. As Rab6 is involved in Golgi-to-ER transport, this reduction in Rab6 association with membranes could lead to defective vesicle recycling from the Golgi to the ER in AD patients (Scheper et al., 2004). Rab6 has also been implicated in the regulation of ER stress response in AD, but the specific mechanism for its contribution is still under investigation (Scheper et al., 2007).

Dysfunction in other Rab proteins is also implicated in Aβ alterations, neurodegeneration, and AD pathology. For example, Rab11 and Rab3 play important roles in membrane trafficking events that regulate Aβ production (Udayar et al., 2013). Genetic association studies have revealed a significant link between Rab11 and late-onset AD, suggesting a causal relationship (Udayar et al., 2013). Moreover, PC12 cells expressing the A260V mutant of PSEN1 exhibit reduced expression levels of Rab8 and decreased Aβ production (Kim et al., 2016). This

reduction is attributed to impaired transport of the Aβ precursor, leading to its accumulation in vesicles involved in TGN-to-plasma membrane transport (Kim et al., 2016). These findings emphasize the impact of PSEN mutations or deficiency on Rab-mediated protein trafficking, with Rab GTPase dysfunctions affecting the production of Aβ.

Conversely, sporadic AD cases often display upregulation of Rab GTPase transcripts. For instance, early endosomal Rab GTPases such as Rab4 and Rab5 are upregulated in cholinergic basal forebrain neurons, and their expression levels correlate with cognitive decline in individuals with mild cognitive impairment and AD (de Wit et al., 2001). Hippocampal CA1 neurons from AD patients also exhibit overexpression of Rab5 and Rab7a (Chen et al., 2012; Deinhardt et al., 2006). Rab5 overexpression in these neurons is associated with downregulation of genes encoding neurotrophic receptors TrkB and TrkC, which leads to long-term deficits in hippocampal neurotrophic signaling, another feature of AD pathology (Deinhardt et al., 2006). Additionally, the Rab5 effector APPL1 is involved in the overactivation of Rab5 in AD, resulting in accelerated endocytosis, enlargement and impaired axonal transport of early endosomes (Deinhardt et al., 2006). Therefore, targeting Rab GTPases and their associated effectors holds promise as a therapeutic strategy to disrupt the trafficking pathways that drive the progression of AD.

1.5 Rab GTPases in Cancer

Emerging evidence demonstrates a strong connection between aberrant expression of Rab GTPases and tumorigenesis. Several Rab proteins, including Rab1, Rab8, Rab11, Rab21, Rab23, Rab25 Rab35 among others, have been implicated in tumor cell migration and invasion, influencing tumorigenesis and metastasis through their ability to regulate intracellular signal transduction (Hooper et al., 2010; Mendoza et al., 2013). One example of note is the oncogenic

Rab1 which is frequently overexpressed in various cancer types and correlates with poor cancer survival. In colorectal cancer, overexpression of Rab1A enhances tumor progression and invasion by promoting mTORC1 signaling and oncogenic growth in response to amino acid stimulation (Xu et al., 2015). Similarly, gene amplification and overexpression of Rab23 are associated with enhanced cancer cell invasion and advanced-stage gastric cancer (Wang et al., 2016). Another example of note can be found in Rab2A, which has been identified as a driver of breast cancer stem cell expansion through the activation of Erk signaling (Wang et al., 2016). High expression of Rab25 is often linked to poor prognosis in breast and ovarian cancer (Cheng et al., 2004). In another resent study, two gain-of-function mutations in tumor cells have revealed the oncogenic potential of Rab35 (Wheeler et al., 2015). Constitutively active Rab35 mediates the internalization of platelet-derived growth factor receptor α to LAMP2-positive endosomal membranes, leading to the activation of oncogenic PI3K/Akt signaling (Wheeler et al., 2015). These findings highlight the collaborative role of Rabs-mediated vesicle dynamics and oncogenic signaling in driving tumor progression.

While most of the studies in cancer that highlight Rab GTPases implicate Rab proteins as promoters of tumor progression, recent studies have also found instances where Rab GTPases serve as tumor suppressors. For example, in esophageal squamous cell carcinoma, Rab25 acts as a tumor suppressor by inhibiting invasive and angiogenic activities (Denning et al., 2007). Conversely, in the intestines of $Rab25^{-/-}$;$Apc^{Min/-}$ mice, Rab25 deficiency leads to an increase in malignant tumor formation (Tzeng & Wang, 2016). These contrasting roles of Rab25 in tumorigenesis highlight its cell-type-dependent functions.

1.6 Rab Proteins in Infectious Diseases and Immune Disorders

Rab GTPases also are involved in host-pathogen interactions during infectious diseases. Intracellular pathogens have evolved strategies to hijack the host's Rab GTPase machinery to facilitate their entry, replication, and spread inside their host T-cells. These pathogens can manipulate Rab GTPases to modulate vesicular trafficking, evade host immune responses, and establish their replicative niche. For example, some bacteria and viruses exploit Rab5 and Rab7 to direct their internalization into host T-cells or to escape from the phagolysosome (Mottola, 2014).

Rab GTPases have also been implicated in immune disorders, one example being Rab27a. This Rab protein is involved in Griscelli syndrome (GS) and choroideremia (Barral et al., 2002). GS is a rare autosomal recessive disorder characterized by hypopigmentation of the skin and hair, along with abnormal accumulation of melanosomes in melanocytes. Patients with GS who have mutations in the rab27a gene also experience uncontrolled activation of T-lymphocytes and macrophages (Barral et al., 2002). Notably, T-cells deficient in Rab27a display reduced cytotoxicity and impaired exocytosis of cytolytic granules, which are vital for maintaining immune homeostasis (Barral et al., 2002). Defects in the transport pathways regulated by Rab27a are associated with choroideremia, an X-linked retinal degeneration. Mutations in Rab escort protein 1 (REP1), crucial for the prenylation of Rab GTPases, result in the accumulation of unprenylated Rab27a, contributing to the disease (Seabra et al., 1995). Additionally, disruptions in the transport pathways governed by Rab13 have been implicated in Crohn's disease (CD). CD is characterized by cell-cell junction aberrations, leading to the loss of mucosal barrier integrity, and increased intestinal permeability. The dysregulation of Rab13 at

the basolateral junctions observed in CD patients is thought to contribute to the defects of tight junctions (Teshima et al., 2012).

1.7 Rab10 in Neurodegenerative Disorders

One Rab GTPase that has garnered significant attention in recent years in the context of neurodegenerative disorders, is Rab10. This member of the Rab GTPase family has been implicated in various cellular processes and disease contexts. Of note are recent studies implicating a possible neuroprotective role that Rab10 may confer to individuals at high risk to develop AD. In a study utilizing whole genome sequencing (WGS), a rare functional variant in the Rab10 gene was found to provide resilience to AD in elderly individuals who were not just at risk because of their advanced age, but also due to carrying genetic risk factors for AD as well (Ridge et al., 2017). Further evidence for Rab10's ability to provide AD resilience was found in a cellular model of AD, where the suppression of Rab10 led to a decrease in the production of Aβ42 and a reduction in the Aβ42/40 ratio, while overexpression of Rab10 had the opposite effect (Ridge et al., 2017; Udayar et al., 2013). Additionally, there is evidence linking Rab10 to the tau pathology associated with AD. In postmortem human hippocampal samples, Rab10 was found to be hyperphosphorylated at the T73 residue and co-localized with neurofibrillary tangles (NFTs) (Yan et al., 2018). This hyperphosphorylation of Rab10 at T73 leads to abnormal membrane and vesicle trafficking contributing to neurodegeneration. Moreover, this process is mediated by the protein kinase leucine-rich repeat kinase 2 (LRRK2). LRRK2 variants are common genetic risk factors for Parkinson's disease (PD), preceding only AD in incidence worldwide (Ross et al., 2008). Some variants of this protein kinase also promote LRKK2 activity toward Rab10. Many recent therapeutic interventions for PD inhibit this LRRK2-Rab signaling

pathway to help restore normal membrane trafficking and lysosomal activity (Jennings et al., 2022).

1.9 Thesis Purpose

Due to the abundant roles that Rab10 has throughout the body combined with the different hypothesis presented in this introduction, a multifaceted approach will be used to help elucidate the role this signaling protein has in granting resilience to AD. The first part of this thesis will focus on the behavioral and transcriptional characterization of mice transgenically designed to have reduced levels of Rab10. Whereas the second part will examine different markers of inflammation both centrally and peripherally in $Rab10^{+/-}$ mice and their $Rab10^{+/+}$ counterparts.

Chapter 1 Figures

Figure Legend:

Figure 1.1 Schematic diagram of the Rab-GTPase activation and inactivation

A, In their inactive forms, Rab-GTPases are GDP-bound. The switch from GDP to GTP is mediated by Rab-GEF proteins and leads to Rab activation. Rab-GAP proteins hydrolyze the Rab-bound GTP to GDP and thus the Rab-GTPase returns to its inactive form. Cytosolic GDI proteins prevent the exchange of GDP for GTP and therefore keep the Rab protein in its inactive form. Representative Rab-GEF and Rab-GAP proteins linked to neurodegenerative disorders are given as examples.

A.

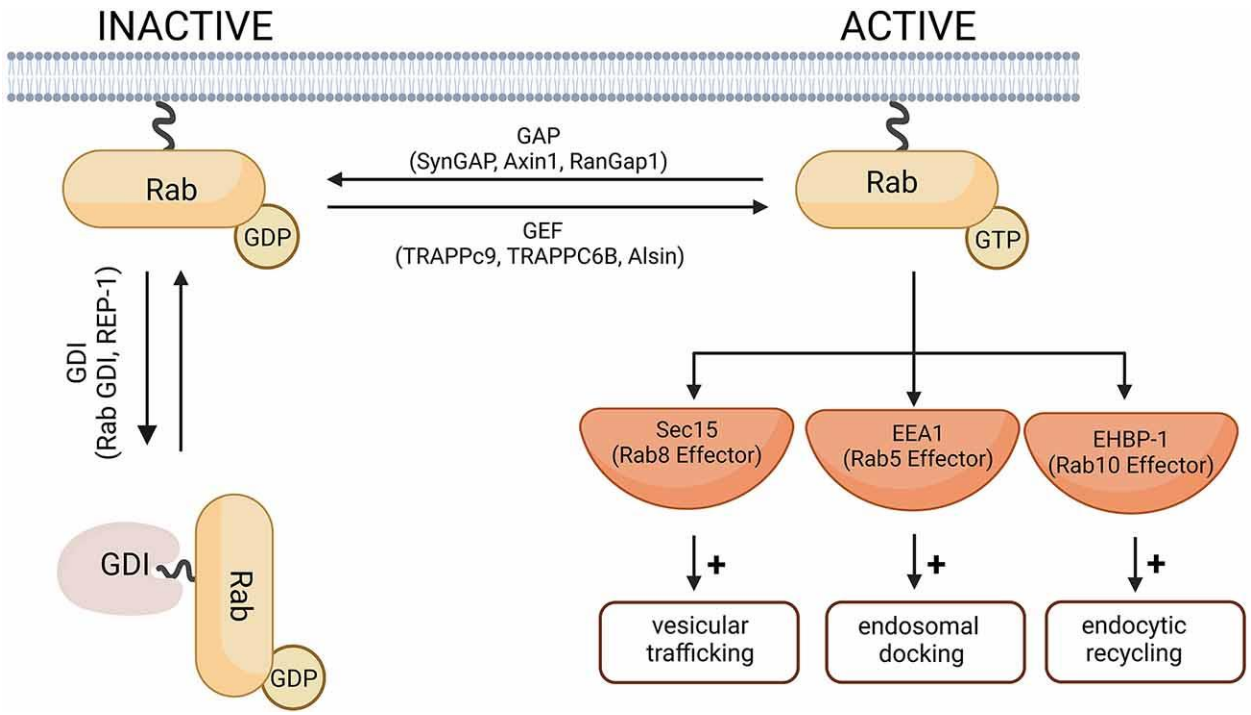
INACTIVE
ACTIVE
Rab
GDP
GAP
(SynGAP, Axin1, RanGap1)
GEF
(TRAPPc9, TRAPPC6B, Alsin)
Rab
GTP
GDI
(Rab GDI, REP-1)
GDI
Rab
GDP
Sec15
(Rab8 Effector)
EEA1
(Rab5 Effector)
EHBP-1
(Rab10 Effector)
+
+
+
vesicular
trafficking
endosomal
docking
endocytic
recycling

Statement of Problem

Alzheimer's disease, the leading cause of dementia worldwide, results in a sustained deterioration in cognition. The consequences of this devasting disorder include increased mortality, decreased quality of life, and a tremendous economic burden that is continuing to skyrocket as the average lifespan of individuals continues to increase. This neurodegenerative disorder is particularly devastating due to the almost non-existent number of diseases modifying therapies available. As a result, investigation into therapeutic interventions that mediate the onset of progression of disease is critical.

Current hypotheses show AD progression to be primarily characterized by the abnormal build-up of β-amyloid within plaques and phosphorylated tau within neurofibrillary tangles. This accumulation leads to neurodegeneration via neuronal and synaptic loss. Interestingly, there are elderly individuals who harbor these plaques and tangles that can maintain their cognitive abilities, and do not show typical AD symptoms in their lifetime. Recent studies have suggested that the small GTPase Rab10 as a possible mediator of "cognitive resilience" against AD. Thus, providing an exciting target for possible therapeutic intervention.

Main Objective

Ras-related protein Rab10 is a GTP-binding protein that is crucial for the regulation of intracellular trafficking. In the CNS, this small GTPase is highly involved in axonal development, dendritic arborization, and glutamate receptor trafficking during synaptic plasticity. Recent research developments have also suggested that mutations in this signaling protein can possibly dull the devastating cognitive effects that are brought on an individual by AD.

This dissertation aimed to identify and characterize the molecular mechanisms of neuroresilience conferred by reduced level of Rab10.

Hypothesis

Considering Rab10's high expression throughout the brain, particularly in the areas that are among the first affected by AD neurodegeneration such as the hippocampus, I hypothesized that exploring the cellular and molecular mechanisms affected by reducing Rab10 levels will offer novel insight into the mechanisms of neuroresilience and help pave the way for novel therapeutic interventions against neurodegeneration.

Chapter 2

Behavioral and Transcriptome Profiling of Heterozygous Rab10 Knock-Out Mice

Abstract

Ras-related Rab proteins are signaling molecules with well documented abilities to facilitate membrane trafficking; however, their roles in facilitating neuroresilience is much less explored. The current studies' focus was to characterize $Rab10^{+/-}$ mice behaviorally and molecularly, and to identify downstream targets of Rab10-dependent resilience against neurodegeneration. Comprehensive multiplex gene expression analysis of 880 different genes associated with neurodegeneration in the brain in $Rab10^{+/-}$ mice were compared to their $Rab10^{+/+}$ littermates by harnessing the advantages of the nCounter Analysis System. Lower activation was observed for genetic pathways involved in neuroinflammation and aging. Furthermore, deferentially expressed genes (DEGs) identified between the two genotypes included Stx2, Stx1b, Vegfa, and Lrrc25 (downregulated) and Prkaa2, Syt4, and Grin2d (upregulated). Next, we performed a battery of behavioral tests, particularly those involved in learning and memory. $Rab10^{+/-}$ mice had significantly better performance in the hippocampus-dependent object in place test, while the opposite was observed in the trace eyeblink classical conditioning task. Thus, these results provided evidence for the first time that Rab10 differentially controls the brain circuitry of spatial memory task compared to higher-order behavior that requires communication between multiple areas of the brain. These results indicate that the $Rab10^{+/-}$ mice described in this study can be valuable for decoding the mechanisms of resilience against neurodegenerative disorders and providing potential targets for developing novel therapeutics strategies.

Bunner, Wyatt, Jie Wang, Sarah Cohen, Denys Bashtovyy, et al. "Behavioral and Transcriptome Profiling of Heterozygous Rab10 Knock-Out Mice." *Eneuro* 10, no. 5 (2023). DOI: https://doi.org/10.1523/ENEURO.0459-22.2023

2.1 Introduction

2.1.1 Background- Rab10 is a small monomeric Ras-related GTP-binding protein widely expressed in the intracellular membranes. It is highly conserved from *Caenorhabditis elegans* to humans, with a predicted molecular weight of ~23 kDa (Lv et al., 2015). Similar to other Rab proteins, Rab10 regulates intracellular trafficking by recruiting effectors and binding proteins (Homma et al., 2021). Among the 60 human Rab GTPases, only 24 Rab proteins are specific to or enriched in neurons (Brighouse et al., 2010; D'Adamo et al., 2014; Diekmann et al., 2011; Homma et al., 2021; Stenmark & Olkkonen, 2001). In the central nervous system (CNS), Rab protein-dependent membrane trafficking (including vesicle biogenesis, sorting, fission, transport, tethering, docking, and fusion) is essential for the development of neuronal asymmetry and the formation of neuronal circuits (Mignogna & D'Adamo, 2018). Rab10 is a crucial regulator of axonal development, dendritic arborization, and glutamate receptor trafficking during synaptic plasticity (Deng et al., 2014; Homma et al., 2021; Mignogna & D'Adamo, 2018; Taylor et al., 2015; Zou et al., 2015).

As small GTPases, Rab proteins are switched between the guanosine diphosphate (GDP)-bound "inactive" state and the GTP-bound "active" state. Specific guanine nucleotide exchange factors (GEFs) regulate the conversion from "active" to "inactive" state, while GTPase activating proteins (GAPs) control the opposite way (Stenmark et al., 2009). Activated Rab GTPases interact with diverse downstream effectors to coordinate the intracellular transport of proteins and lipids (Hutagalung & Novick, 2011). In neurons, membrane trafficking is essential to the maintenance of asymmetric morphology and synaptic activity. Several Rab proteins have been implicated in neurodegenerative disorders, including Alzheimer's disease (AD), Parkinson's

disease (PD), Huntington's disease, and motor neuron degeneration (Bezprozvanny & Hiesinger, 2013; Kiral et al., 2018)

Although aging is the main risk factor associated with sporadic Alzheimer's disease, several genetic risk factors have been identified, including rare variants in APP, PLD3, and TREM2 (Cruchaga et al., 2014; Guerreiro et al., 2013; Jonsson et al., 2013) along with a few protective rare variants in APP and CD33 (Griciuc et al., 2013; Jonsson et al., 2012; Medway et al., 2014). A recent whole genome sequencing (WGS) study identified a rare functional variant in Rab10 which confers "resilience" against AD even for high-risk individuals (Ridge et al., 2017; Tavana et al., 2019). Moreover, in a cellular model of AD, silencing of Rab10 reduced Aβ42 production and Aβ42/40 ratio, while Rab10 overexpression had the opposite effect (Ridge et al., 2017). Another line of evidence implicates Rab10 in AD-associated tau pathology. Rab10 was found to be hyperphosphorylated at the T73 residue and co-localized with neurofibrillary tangles (NFTs) in the postmortem human hippocampus. Rab10 hyperphosphorylation at T73 in human AD hippocampus was shown to be mediated by the serine/threonine protein kinase, leucine-rich repeat kinase 2 (LRRK2), leading to the aberrant membrane and vesicle trafficking and progression of neurodegeneration (Yan et al., 2018). This discovery has allowed researchers to develop a new approach towards the disease modification of Parkinson's disease via inhibition of the LRRK2-Rab signaling pathway (Jennings et al., 2022).

Despite the emerging roles of Rab10 in brain function and neurodegeneration (particularly in AD and PD pathophysiology), our mechanistic understanding of Rab10's functions are still limited. Here, using heterozygous knock-out mice for Rab10 ($Rab10^{+/-}$), we performed cellular, molecular, and behavioral assessments of the effects of a reduced Rab10 level in the mouse brain. We provide evidence that Rab10 differentially regulates spatial memory

and higher-order learning. Transcriptome profiling suggests that Rab10 downregulation leads to elevated activation of signaling pathways associated with neuronal metabolism, structural integrity, neurotransmission, and neuroplasticity, as well as reduced activation of neuroinflammatory and aging pathways in $Rab10^{+/-}$ mice. Differentially expressed genes (DEGs) in $Rab10^{+/-}$ mice (downregulated: Stx2, Stx1b, Vegfa, and Lrrc25; upregulated: Prkaa2, Syt4, and Grin2d) are associated with neuronal metabolism, structural integrity, and synaptic transmission.

2.1.2. Main objective/hypothesis- The current study investigates the novel roles for Rab10 in the brain and identifies potential mediators of neuroresilience provided by a reduced level of Rab10.

2.2. Methods

2.2.1 Experimental animals- All mice were housed in the Animal Resource Facilities compliant with the National Institutes of Health *Guide for Care and Use of Laboratory Animals*. Rab10 conditional knock-out (Ali et al., 2022) mice were generated from C57BL/6 mice. A targeting vector for BAC recombineering was generated with two 50 bp homology regions located 265–365 bp upstream of Rab10 exon 2. The two homology regions were upstream and downstream of a frt site-flanked neomycin cassette with a single lox site at the 3′ end. This vector was inserted into a Rab10 locus-containing BAC (RP24-278M14; CHORI) through homologous recombination in *Escherichia coli* (Murphy, 1998; Muyrers et al., 1999; Yu et al., 2000; Zhang et al., 1998), thereby placing a neo cassette and one lox site 265 bp upstream of exon 2. The second 3′ lox site was placed 169 bp downstream of exon 2 by co-integration during the above homologous recombination process of a PCR fragment containing the lox site flanked by 300 bp

homology regions. Subsequently, an embryonic stem (ES) cell targeting vector containing the modified Rab10 locus was retrieved through recombineering the BAC into a plasmid vector [PL253; P. (Liu et al., 2003)]. In 129 Sv ES cells [R1;(Nagy et al., 1993)], homologous targeting of the Rab10 locus was achieved by electroporation of the linearized targeting vector, selection of neo-resistant colonies, and PCR screening for homologous integration of the targeting vector. Correctly modified ES cells were then injected into C57BL/6 blastocysts following standard procedures. Chimeric males were mated with black wild-type (WT) females (C57BL/6) to generate heterozygous transgenic mice and further crossed with Flp mice to remove the neo cassette. The heterozygous Rab10 cKO mice were further crossed with CMV-Cre mice to generate the heterozygous constitutive Rab10 KO mice in all tissues.

In all experiments, the genotype of each mouse was verified by PCR of genomic DNA extracted from the tail before experiments and by Western blotting of brain samples after experiments. The experimental groups are heterozygous Rab10 cKO X CMV-Cre mice, and controls are the wild-type littermates, ensuring that the mice are from the same parents, living in the same cage and are uniformly affected by any environmental effect.

2.2.2 Behavioral Testing- Behavioral testing included open field (OF), object-in-place (OIP), elevated plus maze (EPM), spontaneous alternation (SA), Rota-Rod (RR), Morris water maze (MWM), trace fear conditioning (FC), and trace eyeblink classical conditioning (TECC).

2.2.2.1 Open field test- Locomotor behavior was measured in 43.2 × 43.2 cm square acrylic open field chambers. Before testing, uniformity of light across the arena was confirmed using a light intensity meter, and the chambers were cleaned with 1% Micro-90 before and between trials.

Background white noise (~72 dB) was used during trials. Mice were placed into the center of the chamber to begin testing, and activity was recorded for 30 min. Data were analyzed in 10 min blocks.

2.2.2.2. Elevated plus maze test- Mice were placed in the center of the plus maze (Med Associates) and allowed to explore the maze for 5 min. Time spent in open and closed arms, number of arm entries, latency to initially enter an open arm, and total distance moved were recorded using EthoVision XT (Noldus Information Technology Inc.). Uniformity in lighting was confirmed across the maze, and the maze was cleaned with 1% Micro-90 before each trial. Background white noise used during trials was ~72 dB.

2.2.2.3. Trace fear condition- In trace fear conditioning, there is a temporal gap during which an association can develop between the termination of the tone (CS, conditioned stimulus) and the onset of the aversive stimulus (US, unconditioned stimulus). During the conditioning, mice gradually acquire an appropriately timed anticipatory conditioned freezing response. The strength and accuracy of this temporally guided fear memory then can be assessed during a subsequent test session. As previously described (Zhang & Stackman Jr, 2015), briefly each mouse was allowed to freely explore a conditioning chamber during a 10 min Context A preexposure session. Context A consisted of rectangular chambers (30.5 × 24.1 × 21 cm) constructed of brushed aluminum side walls and clear Plexiglas front, back, and top walls. The chamber floor was constructed of parallel stainless-steel rods (36 rods, 3.2 mm in diameter, placed 7.9 mm apart). Before each trial, the chamber floors were cleaned thoroughly with a 10% ethanol solution then with 1% LiquiNox to remove olfactory cues. Twenty-four hours later, each

mouse was returned to Context A. After a 60 s exploration interval (used to establish baseline freezing), a tone (90 dB, 5000 Hz, CS) was presented for 15 s followed by a 30 s stimulus-free interval, and then a 0.5 s, 0.75 mA foot shock (US) was presented. The CS-US pairing was repeated eight times with a 210 s intertrial interval (Udayar et al.). Sixty seconds after the final CS-US pairing, each mouse was removed from their chamber and returned to their home cages. Twenty-four hours later, each mouse was tested for freezing to the CS tone in a modified chamber (Context B). Context B chamber consisted of a white Plexiglas floor, a black Plexiglas triangular insert, and several drops of 10% acetic acid on the tray under the floor. Thus, Context B provided an altered floor texture, light intensity, chamber geometry, and odor. Sixty seconds after the introduction of a mouse into Context B, eight unpaired 15 s CSs were presented with an ITI of 210 s. Freezing, a rodent's conditioned response to a threatening stimulus, was recorded and automatically scored by the Video Freezing software (MED Associates).

2.2.2.4. Morris water maze test- The water maze consisted of a 1.4 m diameter white tank with a 10 cm diameter platform submerged ~1 cm below the surface of the water. The water was made opaque by the addition of nontoxic white washable paint that made the platform invisible during trials. The temperature of the water was kept at 22–24°C. Visual cues were placed in the testing room around the tank for spatial reference. Before water maze training, mice received a visual platform test where the spatial cues were removed, and the platform was elevated above the surface of the water and marked with a cue, so it could clearly be discerned. Mice were given four trials, and the platform location was changed each trial. Visible platform training served to verify the visual ability of the mice and to ensure that the mice had no deficit that would affect their ability to swim to the platform. For the hidden platform training, mice were given four

acquisition trials per day for eight consecutive days. The start location was varied for each trial, and the mice were allowed 60 s to find the platform. Mice were left on the platform for 15 s before removing them from the water maze. If a mouse did not find the platform within 60 s, it was placed on or guided to the platform and kept there for 15 s. Mice were dried after each trial and placed into cages located atop heating pads to reduce the opportunity for hypothermia. Measures from the daily four-trial block of acquisition trials (escape latency, cumulative distance, and swim speed) were averaged for analysis. On day 9, mice were given a 60 s probe test during which the platform was not present. Activity and performance were tracked using EthoVision XT (Noldus Information Technology Inc.). Total time spent in each quadrant, total number of entries into the target quadrant, total number of platform crossings, latency to first platform crossing, and average distance to the platform center were recorded from each probe test.

2.2.2.5. Spontaneous alteration test- Mice received two tests, each separated by 3 d. Two mazes were used, each turned in a different configuration to increase novelty to the maze on the second test. Each maze contained three arms with walls made opaque including a start box (17.8 × 7.3 cm) at the base of the start arm (38.1 × 7.3 cm) and adjoined to a central choice area (10.2 × 10.2 cm) with two choice arms (30.5 × 7.3 cm) radiating 180 degrees from the central choice area (forming a “T”). Automatic guillotine doors were installed at the entry of each arm that were controlled by EthoVision. Each test was conducted as follows: a mouse was placed in a start box and the door to the maze subsequently opened, allowing the mouse to enter the maze and explore to the T intersection. Upon reaching the intersection, the mouse chose an arm (free choice trial) and, after three body points had entered that arm, the door closed automatically,

detaining the mouse in that arm for a period of 10 s. During the 10 s, a cloth lightly sprayed with 70% ethanol was used to wipe the maze outside the chosen arm to remove possible odor cues. After 10 s, the mouse was placed back in the start box for a second free choice trial, after which the door to that arm again closed, detaining the mouse in that arm until prompt removal. Of the two tests the mouse was given, one allowed the mouse to immediately enter the maze for the second trial (no delay trial) and one kept the mouse in the start box for 60 s before the door opened to allow the mouse to enter the maze for a second trial (delay trial). Groups were balanced for maze, test day, and delay. Alternation success was calculated for each test. If a mouse did not leave the start box to enter the maze after 60 s, it was gently nudged with a cotton swab. The maze was cleaned with 70% ethanol between mice. Background white noise (~72 dB) was present during trials.

2.2.2.6. Object-in-place memory test- The OIP test was performed as previously described (Szatmari et al., 2021). Briefly, the apparatus consisted of two open-top, high-walled square arenas made of white ABS plastic (each: 37.5 × 37.5 × 50.0 cm). A salient landmark cue (blue plastic tarp, 20.3 × 25.4 cm) was affixed with clear tape to the center of the north wall. Each mouse was habituated to one of the arenas for 10 min/day for two consecutive days. On days 3 and 4, each mouse was returned to the familiar arena that contained 2 novel toy objects (stainless steel cabinet leveling foot attached to a Plexiglas base, 4.2 cm in diameter and 6.0 cm tall; metal spring attached to a Plexiglas base, 2.0 cm in diameter and 4.8 cm tall) for 10 min training sessions. The two objects were positioned on the arena floor 2 cm from the corners on either side of the landmark cue (NW and NE). During the test session 24 h later (day 5), each mouse was given a 5 min test session in the familiar arena, yet one of the toy objects was transferred to the

opposing southern corner. The objects, the arena floor, and walls were cleaned with 70% ethanol after each session. All behavioral testing data were digitally acquired by the EthoVision XT software package. Object exploration was scored off-line from the digital video files by experimenters that were blind to the genotype of the mice. Object-in-place memory was inferred from the preference ratio, calculated for each subject by dividing the time spent exploring the familiar object in the novel location by the total time spent exploring both objects. Preference ratios range from 0 to 1, with 0.5 indicating chance performance, a lack of preference for one object location over another, and positive ratios indicating preference for exploring the object in the novel location. During training, mice that did not explore the objects for a minimum of 50 s were excluded from analyses. The data for mice that did not explore the objects for a minimum of 20 s during the test session were also excluded from all analyses.

2.2.2.7. Trace eyeblink conditioning test- All surgical, testing, and analysis procedures were conducted as previously described in rats (Rufer et al., 2012; Thomas & Tran, 2012; Tran et al., 2017) and scaled for application in mice.

2.2.2.7 Surgery- Mice were implanted with two size 3T stainless steel recording electrodes (Pyrofuze Corp/Medwire) in the left orbicularis oculi muscle and a bipolar stimulating electrode (P1 Technologies) adjacent to the left eye. The recording electrodes were for measurement of electromyographic (EMG) activity during blink responses and the bipolar electrode was for shock stimulation. Mice were allowed to recover for 72 h post-surgery.

2.2.3. TECC procedure- Mice were placed in a modified operant box (Med Associates) containing a house light and a fan (55 dB), which was housed inside a sound-attenuating box

(Med Associates) fitted with acoustic foam. The EMG wires from the animals were plugged into a commutator (P1 Technologies), which enabled uninterrupted electrical signaling while they moved freely. The operant boxes consisted of cabling that connected to a Windows PC equipped with proprietary eyeblink conditioning software (JSA Designs) that recorded EMG activity and delivered the training stimuli [conditioned (CS) and unconditioned (US)]. During each trial, a tone of 80 dB, 2.8 kHz (CS) was presented first and remained on by itself for 380 ms. The tone then terminated and after a 500 ms delay, the shock (US) was delivered and remained on for 100 ms. This 500 ms time window represented the trace interval in which the animal is required to bridge the association between the offset of the tone (CS) and the onset of the shock (US). A total of 90 CS-US trials were presented each session. On every 10th trial, the tone (CS) was presented by itself to test for learning of the conditioned response (CR). In total, there were 100 trials per session with an average intertrial interval of 30 s (18–42 s). Acquisition occurred over six consecutive days (one session per day). Each training session lasted ~54 min.

2.2.4. TECC data collection- Data were prescreened for "acceptable" and "unacceptable" trials within each session using established criteria in rodent ECC (Skelton, 1988; Stanton & Goodlett, 1998). All relevant measures (below) associated with "acceptable" trials were averaged within session. This was conducted with assistance from proprietary data analysis software (JSA Designs), which divided each trial epoch into four discrete EMG sampling periods: (1) a 280 ms pre-CS baseline before CS onset, (2) a startle response (Zhang et al.) period during the first 80 ms after CS onset (EMG activity related exclusively to a non-associative reaction), (3) a 200 ms adaptive CR period that allowed for measuring well-timed CRs before US onset, and (4) a UR (unconditioned response) period which measured EMG activity that occurred from the onset

of the US to the end of the trial (140 ms). Any EMG activity that exceeded the pre-CS baseline mean by at least 0.4V (2 standard deviations) was registered by the software as an SR, CR, and/or UR during their respective sampling periods. The reason for analyzing the adaptive CR is that it represents a well-timed eyeblink response just before US onset. Percentage and amplitude of SRs, adaptive CRs, and URs were measured and analyzed as previously described (Brown et al., 2007; Rufer et al., 2012; Tran et al., 2005; Tran et al., 2007).

2.2.5. Immunofluorescence staining- Adult mice (four to seven months old of both sexes) were deeply anesthetized with Isoflurane until lack of response to toe pinch was recorded, then intracardially perfused with a PBS followed by 10% neutral buffered formalin (fixative). Brains were collected, stored in fixative for 24 h, then incubated in 30% sucrose at 4°C for at least 24 h before sectioning. Coronal sections were cut at 20-μm thickness using a freezing microtome (Leica VT1000 S). Brain sections were washed in PBS, then blocked in 3% normal donkey serum in PBS with 0.03% Triton X-100 (PBST) for 1 h at room temperature. Brain sections were then incubated overnight at room temperature in blocking solution containing anti-NeuN primary antiserum (ABN78, rabbit polyclonal, Millipore; diluted 1:1000). Sections were then washed in PBS and incubated in blocking solution containing anti-rabbit Alexa 488-conjugated secondary antibodies (Life Technologies; diluted 1:500) at room temperature for 1 h. Sections were rinsed in PBS and mounted on Superfrost Plus slides (ThermoFisher) using ProLong Gold with DAPI mounting medium (Invitrogen). Images were taken on a BZ-X800 digital microscope (Keyence). A 10× objective was used to image a whole glass slide containing coronal sections from both genotypes. The stitching function on the BZ-X800 Viewer software (Keyence) was then used to generate images of the whole coronal section.

2.2.6. SDS-Page and immunoblotting- Brain tissue was extracted with NP-40 buffer (Invitrogen) supplemented with inhibitors for proteases and phosphatases (Roche) and 1% deoxycholic acid (DOC). Lysates were then centrifuged at 15,000 × *g* for 15 min at 4°C and the supernatants were used for further analysis. Samples were prepared for standard SDS-PAGE and separated on AnyKD acrylamide gels (Mini-PROTEAN TGX precast gels; Bio-Rad), then transferred onto 0.2-μm pore size PVDF membranes (Millipore) using semi-dry immunoblotting (transfer buffer containing 25 mm Tris, 200 mm glycine and 20% methanol). Membranes were blocked with 5% nonfat milk in TBS-T (tris-buffered saline with 0.1% Tween 20) for 1 h at room temperature, then incubated overnight at 4°C with primary antibodies diluted in 5% BSA in TBS-T. We used the following commercially available primary antibodies: rabbit anti-Rab10 (1:500; Cell Signaling Technology), rabbit anti-GAPDH (1:2000; Sigma), and rabbit anti-GRIN2D (1:500; LSBio). Membranes were washed three times for 15 min in TBS-T, followed by incubation for 2 h at room temperature with HRP-conjugated goat anti-rabbit or goat anti-mouse secondary antibodies (Bio-Rad), diluted 1:5000 in 5% nonfat milk in TBS-T. Membranes were washed three times for 15 min in TBS-T, then incubated with Pierce ECL Plus Western blotting substrate or Pierce ECL Western blotting substrate (for GAPDH) to detect Western blotted proteins using a Bio-Rad Chemidoc touch imaging system. Fiji software was used for Western blot quantification (Schindelin et al., 2012).

2.2.7. RNA extraction and analysis- RNA was isolated from frozen mouse forebrain tissue. Isolated RNA was purified using the QIAGEN RNeasy kit following the manufacturer's instructions. The concentration of RNA was determined using Nanodrop (Thermo Fisher

Scientific) and the quality of RNA was confirmed using the ECU Genomic Core's Bioanalyzer system with RNA pico chips.

2.2.8. Gene expression analysis- Gene expression analysis was performed using NanoString Mouse Neuropathology and Neuroinflammation gene expression panel (NanoString Technologies Inc.). Briefly, RNA isolated from fresh-frozen forebrain tissue was used for experiments; 100 ng of total RNA was hybridized with reporter and capture probes for nCounter Gene Expression code sets (Neuropathology and Neuroinflammation) according to the instructions from manufacturer (NanoString Technologies Inc.). Using the NanoString nSolver Analysis system, data were normalized to spiked positive controls and housekeeping genes. Transcript counts less than the mean of the negative control transcripts plus 2STDEV for each sample were considered background. RNA isolated from five mice per genotype was used for Nanostring mRNA analysis.

2.2.9. quantitative RT-PCR analysis- Complementary DNA (cDNA) was synthesized with the High-Capacity cDNA Reverse Transcription kit (Applied Biosystems) following manufacturer's instructions. Quantitative RT-PCR was performed (Power SYBR Green PCR Master Mix; Applied Biosystems) in triplicate using the Applied Biosystems ViiA 7 system. mRNA gene expression was normalized to mouse 18s ribosomal RNA, with expression fold change calculated using the $2^{-\Delta\Delta Ct}$ method.

The following primer sequences were used for qPCR analysis: Vegfa: forward, CTGAAGGTCAAAGGGAATGTG and reverse, GGACAGAGTCTTGATGATCTC; Prkaa 2: forward, CGGCGCCTTTCCTTGAATAT and reverse, GGCCTGTTCCTCACGGTATTA;

Grin2d: forward, CAGCTGCAGGTCATTTTTGA and reverse, GGATCTGCGCACTGACACTA; Syt4: forward, ATGGCTCCTATCACCACCAG and reverse, AGCAGATCCAGGCAAAGAGA; EmCN: forward, AATACCAGGCATCGTGTCAGT and reverse, CTGATTCTCAGTCTTGTTCTGGG; Mouse 18s rRNA: forward, GTAACCCGTTGAACCCCATT and reverse, CCATCCAATCGGTAGTAGCG.

2.2.10. Experimental design and statistical analysis- For all experiments mice of both genotypes were processed in parallel. Both sexes were used for adult behavior studies, immunofluorescence staining, biochemistry, and gene expression studies. GraphPad Prism (version 9.4.1 for Windows, GraphPad Software) was used for the majority of statistical analysis. Student's *t* test was used to compare two independent datasets. For multiple comparisons, we used ANOVA followed by Dunnett's test. Differences between genotypes or samples were considered significant at $p < 0.05$. This software was also used to calculate a 95% confidence interval (CI) for a difference between means where applicable (Calin-Jageman and Cumming, 2019). In figures and tables, data are reported as mean ± SEM, unless otherwise stated.

2.3 Results

2.3.1. Normal gross brain morphology and physical attributes of Rab10$^{+/-}$ mice

Rab10 conditional knock-out mice were generated from C57BL/6 mice at Duke University Transgenic Core Facility using a strategy described in Materials and Methods. To generate Rab10 constitutive knock-out mice, we further crossed Rab10 cKO mice with CMV-Cre mice, which express Cre in all tissues during early embryogenesis. Because of the previously reported embryonic lethality caused by rab10 deletion (Lv et al., 2015), we were able to generate heterozygous knock-out mice for Rab10 (Rab10$^{+/-}$) instead of homozygous. Immunoblotting analysis showed an ~50% reduction in the expression of Rab10 in the hippocampus of Rab10$^{+/-}$ (heterozygous; HET) mice compared with their non-transgenic littermates (Rab10$^{+/+}$; wild-type; WT; Fig. 2.1[B]). To assess whether Rab10 reduction affects gross brain structure, we compared the overall brain morphology between Rab10$^{+/+}$ and Rab10$^{+/-}$ mice. NeuN immunostaining of coronal sections was indistinguishable between the two genotypes (Fig. 2.2[A]). Considering Rab10 is involved in metabolic regulation (Brumfield et al., 2021), we compared the body weight between Rab10$^{+/-}$ mice and their non-transgenic littermates (Rab10$^{+/+}$). The body weight (in grams) of Rab10$^{+/-}$ and Rab10$^{+/+}$ mice (Fig. 2.2[B,C]) was indistinguishable for both males (Rab10$^{+/+}$: 38.45 ± 12.15, $n = 10$; Rab10$^{+/-}$: 38.71 ± 11.09, $n = 12$; $t_{(9)} = 0.251$, $p = 0.9$, 95% CI [−6.457, 5.169]; SEM; two-tailed unpaired *t* test) and females (Rab10$^{+/+}$: 33.15 ± 9.19, $n = 13$; Rab10$^{+/-}$: 30.71 ± 8.2; $n = 14$; $t_{(12)} = 0.728$, $p = 0.39$, 95% CI [−6.898, 3.502]; SEM; two-tailed unpaired *t* test).

2.3.2. Differentially expressed genes between Rab10$^{+/-}$ and Rab10$^{+/+}$ mice

To gain insights into the signaling pathways driving Rab10-dependent neuroresilience, we employed the NanoString nCounter platform to interrogate gene expression profiles in our cohorts. We isolated RNA from the frontal cortical tissue of Rab10$^{+/-}$ and Rab10$^{+/+}$ mice, and identified 16 differentially expressed genes (DEGs), of which 11 were significantly downregulated (Table 2.1) and five of which were significantly upregulated (Table 2. 2). We used a heatmap analysis to depict hierarchical clustering of upregulated (blue) and downregulated (yellow) genes (Fig. 2.3). Gene expression profiling also revealed distinct pathways and cell-type changes in the Rab10$^{+/-}$ mice compared with their control Rab10$^{+/+}$ littermates (Table 2.3). The identified DEGs are associated with signaling pathways mediating neuroinflammation (Vegfa, Galc, Lrrc25); neuroplasticity, development, and aging (Vegfa, Phf21a, Rela, Prkaa2, Emcn, Atm); metabolism (Stx2, Lsr, Atp6v0d1, Galc, Rela, Prkaa2, Ppp2r5e); compartmentalization and structural integrity (Stx2, Atp6v0d1, Syt4, Grin2d, Stx1b); neuron-glia interaction (Rela) and neurotransmission (Stx2, Atp6v0d1, Syt4, Rela. Grin2d, Ppp2r5e, Stx1b). We validated several significantly altered genes by quantitative RT-PCR (qRT-PCR) analysis (Fig.2. 4[A–E]), which was performed on RNA isolated from the corresponding frozen tissue specimens used for NanoString nCounter analysis (Crist et al., 2021; Prokop et al., 2019). Similar changes were observed in the subset of genes tested (Vegfa, Fig. 2.4[A]; Rab10$^{+/+}$: 1.0 ± 0.28, $n = 12$; Rab10$^{+/-}$: 0.56 ± 0.14, $n = 16$; $t_{(26)} = 2.304$, $p = 0.029$, 95% CI [−1.34, −0.077]; SEM; Emcn, Fig. 2.4[B]; Rab10$^{+/+}$: 1.0 ± 0.30, $n = 12$; Rab10$^{+/-}$: 0.67 ± 0.16, $n = 16$; $t_{(27)} = 0.827$, $p = 0.33$, 95% CI [−0.762, 0.922]; SEM; Prkaa, Fig. 2.4[C]; Rab10$^{+/+}$: 1.0 ± 0.27, $n = 14$; Rab10$^{+/-}$: 1.84 ± 039, $n = 22$; $t_{(34)} = 1.654$, $p = 0.107$, 95% CI [−0.206, 2.008]; SEM; Syt4, Fig. 2.[4]D; Rab10$^{+/+}$: 1.0 ± 0.27, $n = 14$; Rab10$^{+/-}$: 2.03 ± 0.43, $n = 22$; $t_{(34)} = 1.580$,

p = 0.13, 95% CI [−0.339 2.710]; SEM; Grin2d, Fig. 2.4[E]; $Rab10^{+/+}$: 1.0 ± 0.29, n = 12; $Rab10^{+/-}$: 3.3 ± 0.82, n = 17; $t_{(28)}$ = 2.875, p = 0.01, 95% CI [0.746, 4.440]; SEM), with two individual genes (Vegfa and Grin2d) showing statistical significance in the qRT-PCR analysis. Next, we validated the NanoString and qRT-PCR results using biochemical analysis of the corresponding frozen tissue specimens. Western blot analysis of GRIN2D protein level in hippocampal samples (Fig. 2.4[F]) showed increased expression of GRIN2D in $Rab10^{+/-}$ mice ($Rab10^{+/+}$: 1.0 ± 0.31, $n = 10$; $Rab10^{+/-}$: 2.6 ± 1.16, $n = 5$; $t_{(13)}$ = 2.249, $p = 0.028$, 95% CI [0.063, 3.132]; SEM; Fig. 2.4[G]).

2.3.3. Behavioral characterizations of $Rab10^{+/-}$ mice

We examined the behavior of $Rab10^{+/-}$ mice and their control littermates on several standard tasks. Baseline behaviors showed no statistically significant difference between genotypes as indicated by similar levels of anxiety-like behavior in the open field and elevated plus maze test. However, during the OF test, there was a statistically significant difference between genotypes in total distance moved ($Rab10^{+/+}$: 5289.2 ± 300.1, $n = 16$; $Rab10^{+/-}$: 6102.1 ± 260.6, $n = 14$; $t_{(28)}$ = 2.056, $p = 0.05$, 95% CI = [3.01, 1623]; SEM). This is likely a result of the $Rab10^{+/-}$ mice having increased interest in contextual novelty. The fact that both groups performed well indicates that it is not likely that this difference is because of a decrease in learning ability. In addition, working memory measured by spontaneous alteration test was intact in $Rab10^{+/-}$ mice. Therefore, reducing Rab10 expression had no statistically significant effect on motor activity, anxiety-like behavior, and working memory in mice. It should be noted, that if tested in other behavioral tasks, these mice may demonstrate performance deficits. Next, we performed the Morris water maze (MWM) task, a commonly used test for hippocampal-

dependent spatial learning and memory. We evaluated swim speed and latency to a platform in the visible platform version of the MWM, and found no statistically significant difference between genotypes, indicating no impairment of escape motivation, vision, and motor skills. Subsequently, the mice were trained in the hidden platform version of MWM using four trials per day for 8 d, with an intertrial interval of 20–30 min. On day 9, we administered a probe test without the platform present. There was no statistically significant difference between genotypes in the MWM test. Next, we conducted hippocampal-dependent trace fear conditioning in which the conditioned stimulus (CS) and unconditioned stimulus (US) become associated across a stimulus-free time interval (the "trace"). Both genotypes exhibited greater freezing during the "anticipatory" trace period as compared with the tone, suggesting successful hippocampal-dependent learning. We did not find significant differences between genotypes. We also evaluated spatial and contextual memory performance in an object-in-place memory task (OIP). Memory in the OIP task depends on the interaction between the hippocampus, perirhinal cortex and medial prefrontal cortex (Barker & Warburton, 2015). Briefly, we trained mice to learn the location of two objects, in a familiar arena. During a subsequent test session, one object was moved to a new location in the arena. If the mouse recognized the location change, it would exhibit a preference for exploring the moved object. The experimental design of OIP test is presented in (Figure 2.5[A]). Mice were habituated to the arena for 10 min/d for two consecutive days. The habituation sessions were followed by 2 d of training that consisted of 10 min/d in the arena that now contained two toy objects. For male mice (Fig. 2.5[B,C]), during the OIP training sessions there was no difference in total object exploration time (s) between genotypes (mean total object exploration for the first training session: $Rab10^{+/+} = 102.36 \pm 8.23$; $Rab10^{+/-} = 97.088 \pm 5.74$; $t_{(13)} = 0.5235$, $p = 0.56$, 95% CI [−36.69, 22.37]; mean total object exploration for

second training session: $Rab10^{+/+}$ = 91.39 ± 8.27; $Rab10^{+/-}$ = 92.86 ± 5.99; $t_{(12)}$ = 1.145, p = 0.25, 95% CI [−44.30, 13.78]; n = 13 for $Rab10^{+/+}$ and n = 20 for $Rab10^{+/-}$; Fig. 2.5[B]). One day after the completion of the training session, we performed a 5 min OIP test session in the familiar arena, with one toy object transferred to the opposing southern corner. We found that male $Rab10^{+/-}$ mice preferred the object in the novel location significantly more than their control littermates (preference ratio: $Rab10^{+/+}$ = 0.57 ± 0.03; $Rab10^{+/-}$ = 0.65 ± 0.02; $t_{(31)}$ = 2.530, p = 0.0167, 95% CI [0.015, 0.139]; Fig. 2.5[C]). Next, we performed the OIP experiments using age-matched female $Rab10^{+/-}$ mice and their control littermates (Fig. 2.5[D,E]). Similar to male mice, during the OIP training session there was no difference in total object exploration time(s) between genotypes (mean total object exploration for the first training session: $Rab10^{+/+}$ = 117.87 ± 15.5; $Rab10^{+/-}$ = 110.71 ± 4.63; $t_{(13)}$ = 0.5235, p = 0.56, p = 0.61, 95% CI [−36.69, 22.37]; mean total object exploration for second training session: $Rab10^{+/+}$ = 120.22 ± 11.4; $Rab10^{+/-}$ = 103.75 ± 6.98; $t_{(13)}$ = 1.145, p = 0.21, [−44.30, 13.78]; Fig. 2.5[D]). However, during the object location preference testing session, the females did not reveal significant difference between genotypes (preference ratio: $Rab10^{+/+}$ = 0.59 ± 0.03; $Rab10^{+/-}$ = 0.55 ± 0.04; $t_{(13)}$ = 0.708, p = 0.492, 95% CI [−0.039, 0.079]; n = 6 for $Rab10^{+/+}$ and n = 9 for $Rab10^{+/-}$; Fig. 2.5[E]). These results suggest that there may be a sex-dependent effect of Rab10 signaling on spatial recognition memory performance.

It has been hypothesized that cue-response association (such as eyeblink conditioning) occurs in the primary motor cortex (M1) and requires the activity of NMDA receptors (Hasan et al., 2013). Eyeblink classical conditioning (ECC) is widely used to understand the mechanisms of learning and memory consolidation. In ECC, a CS (tone) is paired with the US (a mild shock to the eyelid). In untrained animals, the US applied alone will elicit an unconditioned response

(UR, eyeblink). Following repetitive CS-UR pairing, the CS alone will elicit an eyeblink as a conditioned response (CR). In trace eyeblink classical conditioning (TECC), there is a stimulus-free period (trace interval) between CS and US. The TECC requires the participation of the cerebellum, cortex, and hippocampus (Tran et al., 2017; Tran et al., 2007). To evaluate the involvement of Rab10 in cue-response association, we performed TECC in both male and female mice. The experimental design of TECC test is presented in Figure 2.6[A]. Acquisition of trace conditioned responses indicated that male $Rab10^{+/-}$ mice exhibit a statistically significant deficit in acquisition of CR during the terminal sessions (4–6) of the acquisition curve (Fig. 2.6[B–E]). The difference between genotypes was significant both in adaptive CR percentage ($Rab10^{+/+}$= 44.261 ± 13.996; $Rab10^{+/-}$ = 31.793 ± 10.597; $t_{(41)} = 3.335$, $p = 0.0323$, 95% CI [6.268, 25.510]; Fig. 2.6[B,C]) and adaptive CR amplitude ($Rab10^{+/+}$= 0.505 ± 0.159; $Rab10^{+/-}$ = 0.341 ± 0.113; $t_{(41)} = 2.883$, $p = 0.0443$, 95% CI [0.056, 0.317]; Fig. 2.6[D,E]). To verify whether learning was affected by sensorimotor performance, we evaluated unconditioned responses. The two genotypes showed no significant difference for both UR percentage ($Rab10^{+/+}$ = 83.963 ± 26.551; $Rab10^{+/-}$ = 88.518 ± 29.506; $t_{(41)} = 0.489$, $p = 0.2807$, 95% CI [−4.902, 8.032]; Fig. 2.7[A,B]) and UR amplitude ($Rab10^{+/+}$ = 2.817 ± 0.89; $Rab10^{+/-}$ = 3.130 ± 1.043; $t_{(41)} = 0.200$, $p = 0.728$, 95% CI [−1.216, 0.997]; Fig. 2.7[C,D]).

Next, we analyzed the acquisition of trace CR in female mice (Fig. 2.8). Our data show that female $Rab10^{+/-}$ mice have a statistically significant deficit both in adaptive CR percentage ($Rab10^{+/+}$= 53.038 ± 15.310; $Rab10^{+/-}$ = 30.283 ± 8.742; $F_{(5,127)} = 2.502$, $p = 0.0257$; Fig. 2.8[A]) and adaptive CR amplitude ($Rab10^{+/+}$= 0.613 ± 0.177; $Rab10^{+/-}$ = 0.330 ± 0.095; $F_{(5,132)} = 2.419$, $p = 0.0335$; Fig. 2.8[C]) in the last session (S6) of the TECC acquisition curve. Similar to male mice, the averaged S4-S6 terminal sessions were also significantly different for both CR

percentage ($Rab10^{+/+}$= 49.391 ± 14.258; $Rab10^{+/-}$ = 32.804 ± 9.469; $t_{(22)}$ = 2.964, p = 0.0072, 95% CI [5.64, 31.93]; Fig. 2.8[B]) and CR amplitude ($Rab10^{+/+}$=0.572 ± 0.165; $Rab10^{+/-}$ = 0.362 ± 0.104; $t_{(22)}$ = 2.086, p = 0.0488, 95% CI [−0.417, −0.001]; Fig. 2.8[D]).

Unconditioned responses were recorded to evaluate whether learning was affected by sensorimotor performance. Similar to male mice, female mice of both genotypes had similar UR percentage ($Rab10^{+/+}$ = 83.270 ± 24.038; $Rab10^{+/-}$ = 82.624 ± 23.851; $t_{(22)}$ = 0.136, p = 0.893, 95% CI [−10.515, 9.222]; Fig. 2.9[A,B]) and UR amplitude ($Rab10^{+/+}$ = 3.393 ± 0.979; $Rab10^{+/-}$ = 2.919 ± 0.842; $t_{(22)}$ = 0.634, p = 0.533, 95% CI [−2.031, 1.082]; Fig. 2.9[C,D]).

2.4 Discussion

These findings collectively suggest that reducing Rab10 leads to changes in the expression of genes associated with neuroinflammation, aging, and neurotransmission. Behavioral phenotypes of $Rab10^{+/-}$ mice include a sex-dependent improvement in hippocampus-dependent associative learning (OIP test) and a significant impairment in trace eyeblink classical conditioning. These data indicate an opposing role of Rab10 in brain areas involved in contextual versus associative learning.

Identification of genes and pathways that mediate molecular neuroresilience against Alzheimer's disease may represent promising avenues of therapeutic development. Given that membrane trafficking has been implicated in nearly every aspect of brain function, including neuronal plasticity, maintenance and degeneration, AD risk genes involved in organelle composition, endocytosis, lipid biology and neuroimmune function may represent potential targets for prevention and treatment. Indeed, many AD-associated proteins are involved in intracellular trafficking, and some of them are directly regulated by Rab proteins. As one central hub for membrane trafficking, Rab GTPases have been directly and indirectly implicated in the progression of neurodegeneration (Kiral et al., 2018). This is not surprising, given that neuron-specific Rab-GTPases are highly enriched in synapses and localized on endosomes, suggesting a crucial role of Rab-dependent membrane trafficking in synaptic functions (Chan et al., 2011; Jin et al., 2012). Moreover, in postmortem cholinergic basal forebrain neurons and CA1 pyramidal neurons of sporadic AD patients, several Rab proteins are upregulated, including Rab4, Rab5, Rab6, Rab7, and Rab27, indicating an overactivation of the endocytic machinery (Ginsberg et al., 2010; Ginsberg et al., 2011; Scheper et al., 2007). However, it is unclear whether Rab protein upregulation drives pathology or is a protective compensatory mechanism. Several recent studies

focused on Rab10 GTPase as a potential protective factor in AD. A whole genome sequencing identified a rare variant (rs142787485) in the 3′ untranslated region (UTR) of Rab10 gene that reduces Rab10 activity and confers resilience against AD even in elderly individuals with genetic risk for AD (Ridge et al., 2017). Additionally, RNAi screening of Rab proteins in APP processing revealed that silencing several Rab proteins including Rab10 leads to a reduction in amyloid level (Udayar et al., 2013). Moreover, a recent study also implicated Rab10 in AD-associated tau pathology, showing that LRRK2-mediated phosphorylation of Rab10 at Threonine 73 (pRab10-T73) leads to colocalization of pRab10-T73 with pTau (Yan et al., 2018). Additionally, LRRK2-pRab10 signaling controls immunologic response by driving micropinocytosis in phagocytic cells via the PI3K-Akt pathway (Liu et al., 2020). Considering that the genetic variation in LRRK2 enhances susceptibility to the second most common neurodegenerative disorder, Parkinson's disease (Tolosa et al., 2020), these findings render Rab10 signaling pathways as the common mechanisms of neurodegeneration (Wareham et al., 2022).

In the current study, we have used Rab10-deficient mice to evaluate *in vivo* the contribution of Rab10 to neuronal function, and to identify Rab10 targets that might be the molecular mediators of resilience against neurodegeneration. Differentially expressed genes in the Rab10-deficient mouse brain are associated with neuroinflammation (Vegfa, Galc) and neuron-glia interaction (Rela); neuroplasticity, neurodevelopment, and aging (Vegfa, Phf21a, Rela, Prkaa2, Emcn, Atm); metabolism (Stx2, Lsr, Atp6v0d1, Galc, Rela, Prkaa2, Ppp2r5e); compartmentalization and structural integrity (Stx2, Atp6v0d1, Syt4, Grin2d, Stx1b); and neurotransmission (Stx2, Atp6v0d1, Syt4, Rela. Grin2d, Ppp2r5e, Stx1b). Among the downregulated genes, a potential therapeutical target is the vascular endothelial growth factor

(VEGF) signaling protein expressed by endothelial cells and neurons for cell growth and maintenance. Although an increasing number of studies associate VEGF proteins with clinical manifestation of AD, the role of these proteins in neurodegeneration is complex because of the diverse signaling pathways that are VEGF dependent. Several recent studies indicate that upregulation of VEGF is associated with blood brain barrier dysfunction, more severe tau pathology and accelerated cognitive decline (Ali et al., 2022; Mahoney et al., 2021; Thomas et al., 2015). In addition, Endomucin (Emcn), an endothelial marker and modulator of VEGF signaling (Park-Windhol et al., 2017), was also downregulated in the cortex of Rab10-deficient mice.

Interestingly, the genes upregulated in Rab10-deficient mice are primarily associated with neuroplasticity, neurotransmission, as well as compartmentalization and structural integrity. It was reported that the overall level of Syt4 is downregulated in the brain of AD model mice (Parra-Damas et al., 2014). However, in dystrophic axons surrounding amyloid plaques, Syt4 is upregulated as an attempt at regenerative sprouting by damaged axons (Parra-Damas et al., 2014; Tratnjek et al., 2013).

Another gene differentially expressed in the Rab10$^{+/-}$ brain is PRKAA2, which encodes the AMPKα2 isoform. As a master kinase of energy metabolism homeostasis, AMPK has been associated with cellular dysfunctions observed in AD (Wang et al., 2019). Surprisingly, AMPKα2 is reduced in the hippocampus in sporadic AD, but not in familial AD, while the AMPKα1 isoform is upregulated in both forms of AD and in murine models of the disease (Zimmermann et al., 2020).

Another surprising DEG upregulated in the Rab-deficient mice is Grin2d, which encodes glutamate ionotropic receptor NMDA type subunit 2D (GluN2D/GRIN2D). Recent studies have shown that Grin2d genetic variants are linked to developmental and early infantile epileptic encephalopathy (XiangWei et al., 2019; Zimmermann et al., 2020). Recently identified variants were shown to reduce the surface-to-total protein level ratio, indicating a deficit in the trafficking of GluN2D subunit (XiangWei et al., 2019). Interestingly, treatment with memantine was shown to ameliorate seizure in these patients (XiangWei et al., 2019). Memantine is an Alzheimer's disease drug that strongly impacts cognitive function by preferentially inhibiting GluN2C-containing and/or GluN2D-containing NMDARs (Kotermanski & Johnson, 2009; Kotermanski et al., 2009). Whether abnormal trafficking of GluN2D occurs in AD and if this is regulated by Rab10 has not been addressed yet.

Next, we examined whether Rab10-deficiency impacts behavior. We showed that reducing Rab10 level enhances spatial recognition memory performance, in the OIP task where the subject associates an object with the place in which it was previously presented. OIP measures hippocampus-dependent spatial memory and depends on the interaction between the hippocampus, perirhinal cortex and the medial prefrontal cortex (Denninger et al., 2018). OIP memory requires activation of the hippocampal glutamatergic receptor transmission (Barker and Warburton, 2015). It has been shown that OIP performance is sex dependent (Cost et al., 2012), which is consistent with our result showing improved OIP performance in male Rab10-deficient mice, but not in females. The signaling pathways mediating sex dependent OIP performance are yet to be identified. It is important to note that OIP memory deficit occurs in AD patients (Fowler et al., 2002). Thus, our finding that reducing Rab10 enhances OIP performance provides the behavioral evidence for Rab10-mediated neuroresilience. Although the precise molecular

mechanism of Rab10-dependent inhibition of spatial learning is unknown, we propose that the molecular mechanism involves downregulation of signaling pathways that control neurotransmission, neuronal metabolism, and neuroplasticity.

Contrary to OIP, behavioral performance in trace eyeblink classical conditioning was negatively affected by Rab10 deficiency. TECC is a higher-order procedure that has common features with declarative memory formation in humans. Similar to simple eyeblink conditioning, TECC relies on intact cerebellar-brainstem circuitry, but also requires network interdependency across multiple higher-level brain structures, including the dorsal hippocampus and the cortex (Cheng et al., 2008) It has been established that the memory of the acquired trace eyeblink-conditioned responses is localized in the primary motor cortex (M1) and involves NMDA-specific glutamate receptor function (Hasan et al., 2013). Notably, deletion of the *grin1* gene (encoding GluN1 subunit), specifically in the M1 cortex, impairs performance in TECC (Hasan et al., 2013). In contrast, *grin1* deletion in the hippocampal CA3 only does not interfere with TECC memory formation (Kishimoto et al., 2006). Given that the NMDA receptors of the dorsal hippocampus are critical for adaptive CR timing memory, and lesions of the hippocampus impair TECC (Kishimoto et al., 2006), it has been proposed that the dorsal hippocampus and the cortex play different roles in TECC memory. In this model, the dorsal hippocampus organizes spatial computations, while the M1 cortex performs spatial memory and temporal associations, as well as acquisition and storage (Hasan et al., 2013). Thus, Rab10-dependent TECC performance indicates that Rab10 is involved in cortical cell assemblies to mediate declarative memory, while it acts as a negative regulator of spatial memory, highly dependent on the dorsal hippocampus. Future studies such as spatial gene expression and spatial proteomics are needed to elucidate the

downstream targets of Rab10 signaling that mediate differential roles of this protein in behavioral paradigms.

Based on the data presented here, we conclude that Rab10-deficient mice can be used to better understand the role of Rab10 in brain function, and that crossing these mice with mouse models of AD can provide insights into the molecular and cellular mechanisms underlying Rab10-dependent molecular neuroresilience.

Chapter 2 Figures

Figure Legends:

Figure 2.1. Generation of Rab10 conditional and constitutive knock-out (KO) mice. ***A***, Schematic drawing of the targeting strategy used to generate Rab10 conditional and constitutive knock-out (KO) mouse lines. In Rab10 conditional KO line, exon 2 of *Rab10* gene was flanked by two lox sites. A frt-flanked neo cassette was placed upstream of the start of exon 2 and further removed by Flp recombination. Rab10 constitutive KO mouse line was generated by crossing Rab10 conditional heterozygous mouse line with CMV-Cre mouse line. Expression and translation of this modified Rab10 locus resulted in a frame shift product of Rab10 protein. ***B***. Immunoblots show that in the hippocampus of $Rab10^{+/-}$ (heterozygous, HET) mice, the level of Rab10 is reduced to 50% compared with the level in the brain of $Rab10^{+/+}$ (wild-type; WT) littermate mice. Numbers under blots represent GAPDH-normalized Rab10 level in four independent experiments.

Figure 2.2 Normal brain gross anatomy and physical attributes of $Rab10^{+/-}$ mice. ***A*,** NeuN immunohistochemistry of coronal sections from six-month-old $Rab10^{+/-}$ and non-transgenic littermate $Rab10^{+/+}$ mice show normal brain morphology in Rab10-deficient mice. Similar results were obtained in three independent experiments. ***B***, ***C***. The body weight (in grams) of $Rab10^{+/-}$ and $Rab10^{+/+}$ mice is not significantly different in males, nor in females. ***B***. The number of male mice was 10 for $Rab10^{+/+}$ and 12 for $Rab10^{+/-}$ genotype. Error bars indicate SEM. Two-tailed unpaired *t* test, $p = 0.9$. ***C***. The number of female mice was 13 for $Rab10^{+/+}$ and 14 for $Rab10^{+/-}$ genotype. Error bars indicate SEM. Two-tailed unpaired *t* test, $p = 0.39$.

Figure 2.3. NanoString nCounter profiling identified several differentially expressed genes in the brain of Rab10$^{+/-}$ mice. Heatmap depicts the hierarchical clustering of 16 differentially expressed genes (DEGs) between genotypes, of which 11 were significantly downregulated (Stx2, Lsr, Lrrc25, Vegfa, Galc, Phf21a, Rela, Emcn, Atm, Ppp2r5e, Stx1b, yellow; Table 1) and five were significantly upregulated (Cnot10, Atp6v1d, Syt4, Prkaa2, Grin2d, blue; Table 2) in the forebrain of Rab10$^{+/-}$ mice compared with their Rab10$^{+/+}$ littermates.

Figure 2.4. Quantitative RT-PCR and Western blotting to validate a subset of DEGs in the brain of Rab10$^{+/-}$ mice. ***A***, Vegfa gene expression evaluated by qRT-PCR. The number of mice was 12 for Rab10$^{+/+}$ and 16 for Rab10$^{+/-}$ genotype. Error bars indicate SEM. Two-tailed unpaired *t* test, $p = 0.029$. ***B***, Emcn gene expression evaluated by qRT-PCR. The number of mice was 12 for Rab10$^{+/+}$ and 16 for Rab10$^{+/-}$ genotype. Error bars indicate SEM. Two-tailed unpaired *t* test, $p = 0.33$. ***C***, Prkaa gene expression evaluated by qRT-PCR. The number of mice was 14 for Rab10$^{+/+}$ and 22 for Rab10$^{+/-}$ genotype. Error bars indicate SEM. Two-tailed unpaired *t* test, $p = 0.107$. ***D***, Syt4 gene expression evaluated by qRT-PCR. The number of mice was 14 for Rab10$^{+/+}$ and 22 for Rab10$^{+/-}$ genotype. Error bars indicate SEM. Two-tailed unpaired *t* test, $p = 0.13$. ***E***, Grin2d gene expression evaluated by qRT-PCR. The number of mice was 12 for Rab10$^{+/+}$ and 17 for Rab10$^{+/-}$ genotype. Error bars indicate SEM. Two-tailed unpaired *t* test, $p = 0.013$. ***F***, Representative images of GRIN2D protein expression in the hippocampus as evaluated by Western blotting. Numbers under the blots represent relative GRIN2D levels, normalized to the house keeping protein, GAPDH. ***G***, Graph showing relative GRIN2D protein expression in the hippocampus evaluated by Western blotting from 10 Rab10$^{+/+}$ and 5 Rab10$^{+/-}$ mice. Error bars indicate SEM. Two-tailed unpaired *t* test, $p = 0.028$.

Figure 2.5. Improved performance of Rab10$^{+/-}$ mice in object in place spatial memory task is sex dependent. ***A***, Diagram of object-in-place (OIP) memory test. Created with BioRender. ***B***, Graph shows no significant difference between genotypes in averaged duration of object exploration during training. The number of male mice was 13 for Rab10$^{+/+}$ and 20 for Rab10$^{+/-}$ genotype. Error bars indicate SEM. Two-tailed unpaired *t* test, $p = 0.25$. ***C***, Male Rab10$^{+/-}$ mice exhibit significant discrimination of the familiar and novel object locations and exhibit strong preference for the object in the novel location as compared with their Rab10$^{+/+}$ littermates during OIP testing session. Error bars indicate SEM. Two-tailed unpaired *t* test, $p = 0.0167$. ***D***, Graph shows no significant difference between genotypes in averaged duration of object exploration during training. The number of female mice was six for Rab10$^{+/+}$ and nine for Rab10$^{+/-}$ genotype. Error bars indicate SEM. Two-tailed unpaired *t* test, $p = 0.21$. ***E***, Female Rab10$^{+/-}$ mice do not exhibit a stronger preference for the object in the novel location as compared with their Rab10$^{+/+}$ littermates during OIP testing session. Error bars indicate SEM. Two-tailed unpaired *t* test, $p = 0.492$.

Figure 2.6. Impaired performance of male Rab10$^{+/-}$ mice in trace eyeblink classical conditioning (TECC). ***A***, Experimental design of TECC: HSV, high speed video recording; CS, conditioned stimulus (tone; 80 dB for 380 ms); US, unconditioned stimulus (a mild shock to the eyelid; 1.6 mA); O.O muscle (orbicularis oculi muscle); created with BioRender. ***B***, Acquisition curve of adaptive conditioned response (CR) percentage. The number of mice was 10 for Rab10$^{+/+}$ and 9 for Rab10$^{+/-}$ genotype. ***C***, Graph indicates that Rab10$^{+/-}$ male mice exhibit a statistically significant deficit in the adaptive conditioned response percentage during the

terminal sessions (4–6) of the TECC acquisition curve. Error bars indicate SEM. Two-tailed unpaired *t* test, $p = 0.0323$. ***D***, Acquisition curve of adaptive conditioned response (CR) amplitude. The number of mice was 10 for $Rab10^{+/+}$ and 9 for $Rab10^{+/-}$ genotype. ***E***, Graph shows that $Rab10^{+/-}$ mice exhibit a statistically significant deficit in the adaptive CR amplitude during the terminal sessions (4–6) of the TECC acquisition curve. Error bars indicate SEM. Two-tailed unpaired *t* test, $p = 0.0443$.

Figure 2.7. Male $Rab10^{+/-}$ mice exhibit normal sensorimotor performance in TECC paradigm. ***A***, Acquisition curve of unconditioned response (UR) percentage. The number of mice was 10 for $Rab10^{+/+}$ and 9 for $Rab10^{+/-}$ genotype. ***B***, Graph shows that there is no significant difference between genotypes in UR percentage during the terminal sessions (4–6) of the TECC acquisition curve. Error bars indicate SEM. Two-tailed unpaired *t* test, $p = 0.2807$. ***C***, Acquisition curve of UR amplitude. The number of mice was 10 for $Rab10^{+/+}$ and 9 for $Rab10^{+/-}$ genotype. ***D***, Graph indicates that $Rab10^{+/-}$ mice do not exhibit deficit in UR amplitude during the terminal sessions (4–6) of the TECC acquisition curve. Error bars indicate SEM. Two-tailed unpaired *t* test, $p = 0.728$.

2.8. Impaired performance of female $Rab10^{+/-}$ mice in TECC. *A*, Acquisition curve of adaptive conditioned response (CR) percentage. The number of mice was 11 for $Rab10^{+/+}$ and 12 for $Rab10^{+/-}$ genotype. Female $Rab10^{+/-}$ mice exhibit a statistically significant deficit in the CR percentage during the terminal S6 session of the TECC acquisition curve. Two-tailed unpaired *t* test, $p = 0.0257$. ***B***, Graph indicates that female $Rab10^{+/-}$ mice exhibit a significant

deficit in the adaptive conditioned response percentage during the terminal sessions (4–6) of the TECC acquisition curve. Error bars indicate SEM. Two-tailed unpaired *t* test, $p = 0.0072$. ***C***, Acquisition curve of adaptive CR amplitude. The number of mice was 11 for $Rab10^{+/+}$ and 12 for $Rab10^{+/-}$ genotype. Female $Rab10^{+/-}$ mice exhibit a statistically significant deficit in the CR amplitude during the terminal S6 session of the TECC acquisition curve. Two-tailed unpaired *t* test, $p = 0.0335$. ***D***, Graph shows that female $Rab10^{+/-}$ mice exhibit a significant deficit in the CR amplitude during the terminal sessions (4–6) of the TECC acquisition curve. Error bars indicate SEM. Two-tailed unpaired *t* test, $p = 0.0488$.

Figure 2.9. Female $Rab10^{+/-}$ mice exhibit normal sensorimotor performance in TECC paradigm. ***A***, Acquisition curve of unconditioned response (UR) percentage. The number of mice was 11 for $Rab10^{+/+}$ and 12 for $Rab10^{+/-}$ genotype. ***B***, Graph shows that there is no significant difference between genotypes in UR percentage during the terminal sessions (4–6) of the TECC acquisition curve. Error bars indicate SEM. Two-tailed unpaired *t* test, $p = 0.8931$. ***C***, Acquisition curve of unconditioned response (UR) amplitude. The number of mice was 11 for $Rab10^{+/+}$ and 12 for $Rab10^{+/-}$ genotype. ***D***, Graph indicates that female $Rab10^{+/-}$ mice do not exhibit deficit in UR amplitude during the terminal sessions (4–6) of the TECC acquisition curve. Error bars indicate SEM. Two-tailed unpaired *t* test, $p = 0.5329$.

Table 2.1. Genes significantly downregulated in the brain of $Rab10^{+/-}$ mice. Table shows differentially expressed genes (DEGs) that are significantly downregulated in the forebrain of $Rab10^{+/-}$ mice. The number of mice was 6 for $Rab10^{+/+}$ and 4 for $Rab10^{+/-}$ genotype. Data are

means± SEM; two-tailed unpaired *t* test was performed and $p < 0.05$ was used for initial filtering and DEG selection.

Table 2.2. Genes significantly upregulated in the Rab10$^{+/-}$ brain. Table shows differentially expressed genes that are significantly upregulated in the forebrain of Rab10$^{+/-}$ mice. The number of mice was 6 for Rab10$^{+/+}$ and 4 for Rab10$^{+/-}$ genotype. Data are mean ± SEM; two-tailed unpaired *t* test was performed and $p < 0.05$ was used for initial filtering and DEG selection.

Table 2.3. Pathway and cell-type changes in the brain of Rab10$^{+/-}$ mice. Table shows enriched pathways and cell-type interactions in the Rab10$^{+/-}$ brain. The number of mice was 6 for Rab10$^{+/+}$ and 4 for Rab10$^{+/-}$ genotype. Up and down arrows indicate upregulated and downregulated genes, respectively. +: DEG is associated with a pathway/cell-type interaction; −: DEG is not associated with a pathway/cell-type interaction.

Figure 2.1

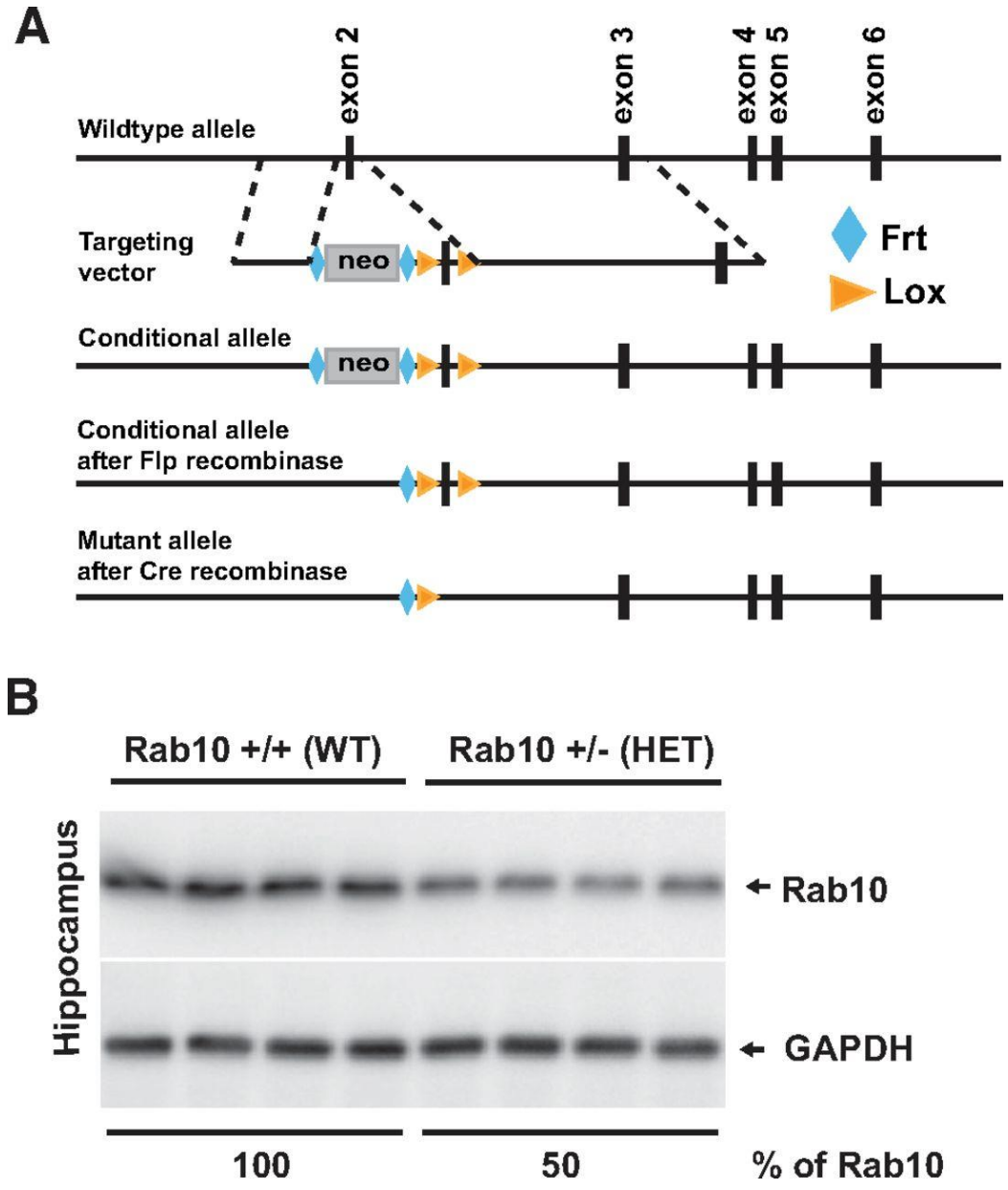
A
exon 2
exon 3
exon 4
exon 5
exon 6
Wildtype allele
Targeting vector
neo
Frt
Lox
Conditional allele
neo
Conditional allele after Flp recombinase
Mutant allele after Cre recombinase
B
Rab10 +/+ (WT)
Rab10 +/- (HET)
Hippocampus
Rab10
GAPDH
100
50
% of Rab10

Figure 2.2.

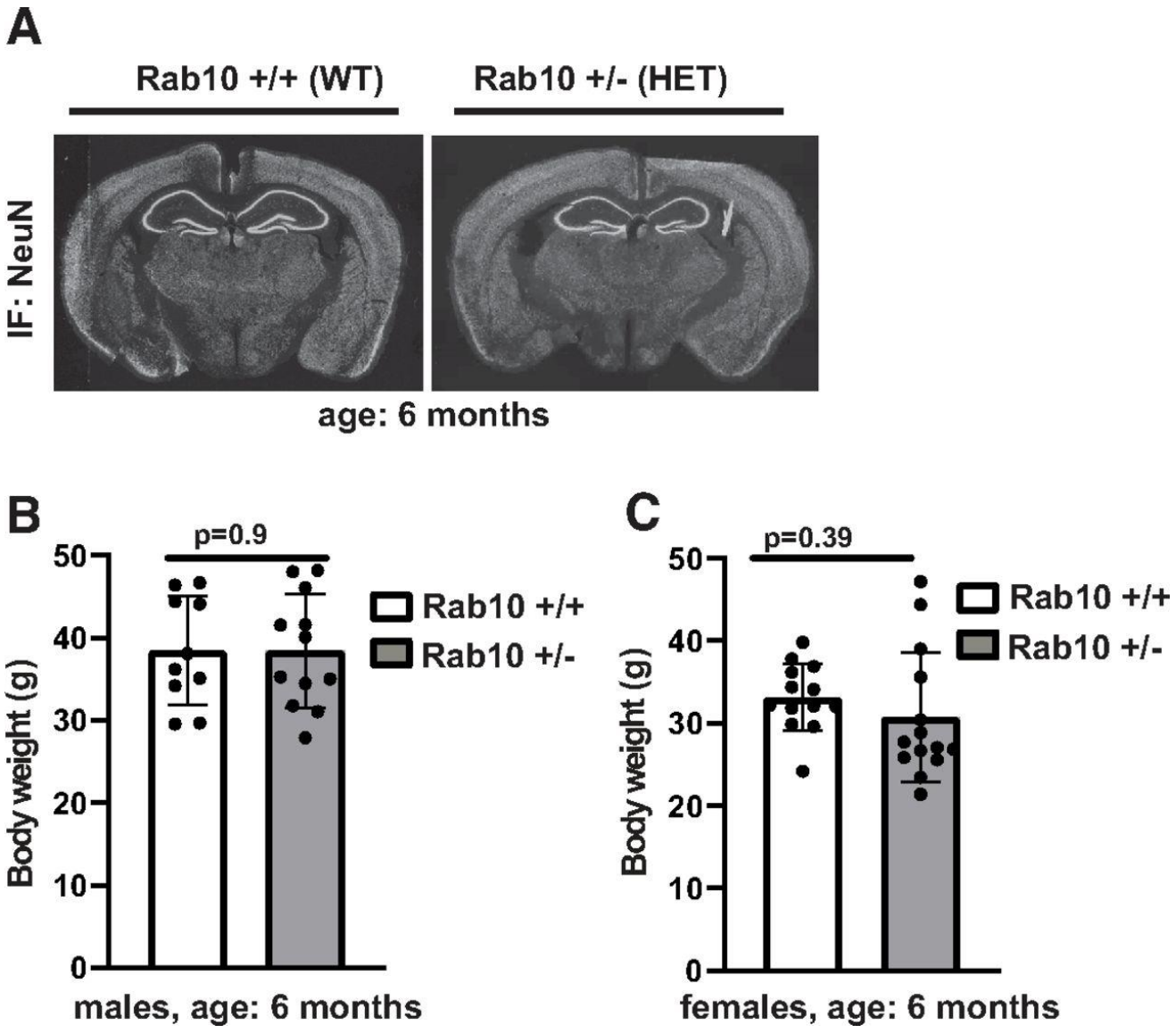
A
Rab10 +/+ (WT)
Rab10 +/- (HET)
IF: NeuN
age: 6 months
B
p=0.9
Body weight (g)
50
40
30
20
10
0
Rab10 +/+
Rab10 +/-
males, age: 6 months
C
p=0.39
Body weight (g)
50
40
30
20
10
0
Rab10 +/+
Rab10 +/-
females, age: 6 months

Figure 2.3.

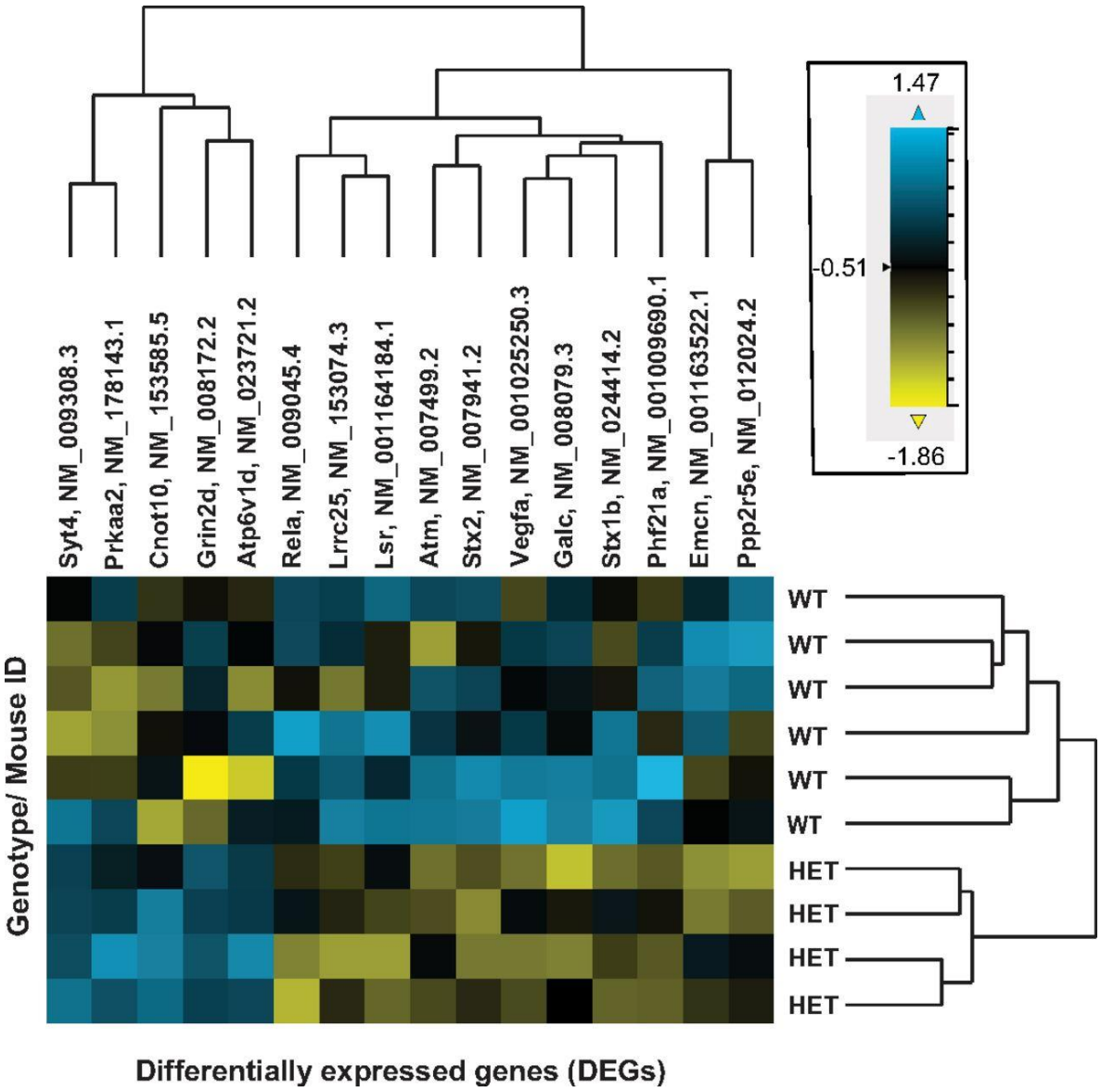
1.47
-0.51
-1.86
Syt4, NM_009308.3
Prkaa2, NM_178143.1
Cnot10, NM_153585.5
Grin2d, NM_008172.2
Atp6v1d, NM_023721.2
Rela, NM_009045.4
Lrrc25, NM_153074.3
Lsr, NM_001164184.1
Atm, NM_007499.2
Stx2, NM_007941.2
Vegfa, NM_001025250.3
Galc, NM_008079.3
Stx1b, NM_024414.2
Phf21a, NM_001009690.1
Emcn, NM_001163522.1
Ppp2r5e, NM_012024.2
WT
WT
WT
WT
WT
WT
HET
HET
HET
HET
Genotype/ Mouse ID
Differentially expressed genes (DEGs)

Figure 2.4.

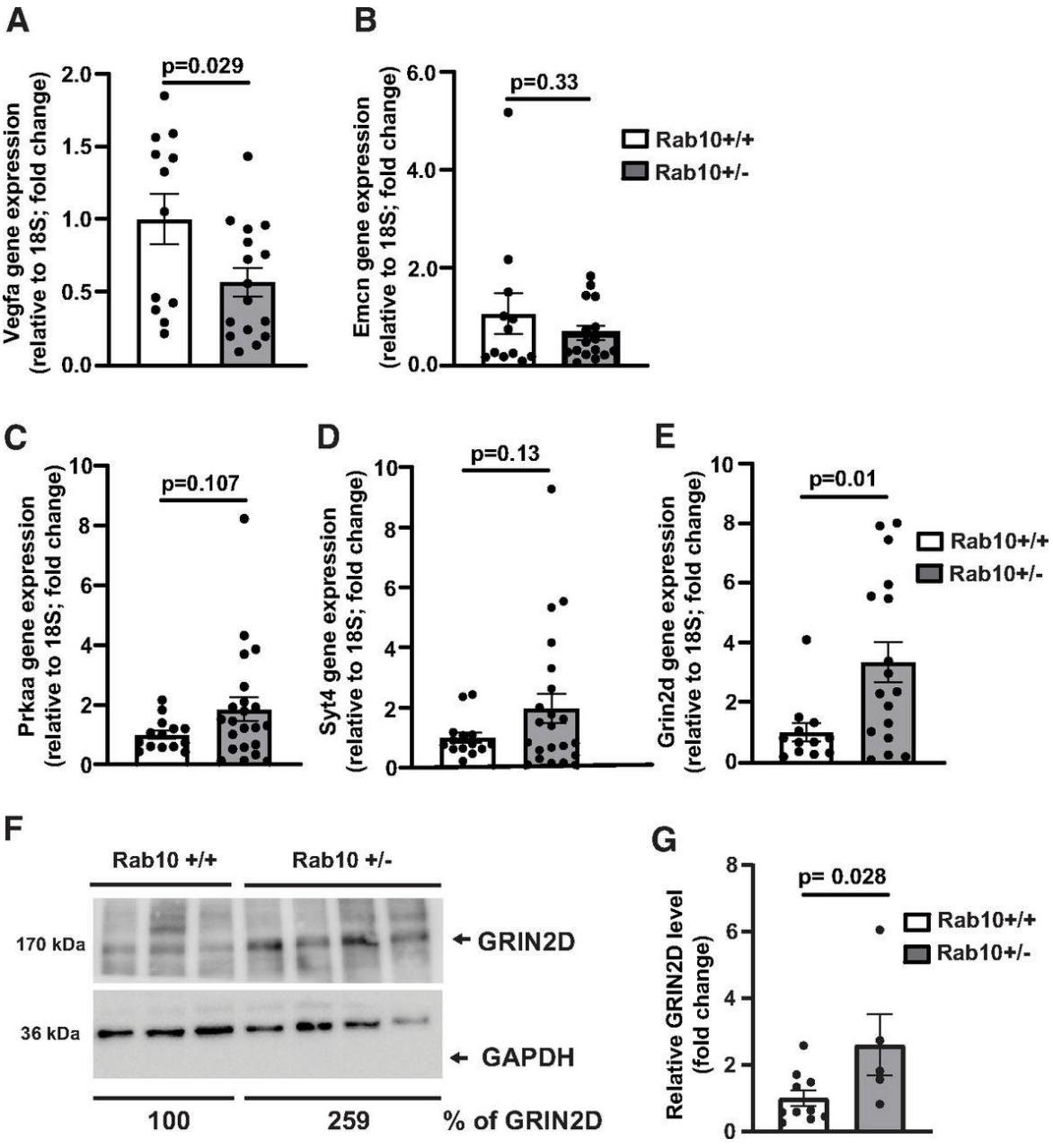
A
p=0.029
Vegfa gene expression (relative to 18S; fold change)
2.0
1.5
1.0
0.5
0.0
B
p=0.33
Emcn gene expression (relative to 18S; fold change)
6.0
4.0
2.0
0.0
Rab10+/+
Rab10+/-
C
p=0.107
Prkaa gene expression (relative to 18S; fold change)
10
8
6
4
2
0
D
p=0.13
Syt4 gene expression (relative to 18S; fold change)
E
p=0.01
Grin2d gene expression (relative to 18S; fold change)
F
Rab10 +/+
Rab10 +/-
170 kDa
← GRIN2D
36 kDa
← GAPDH
100
259
% of GRIN2D
G
p= 0.028
Relative GRIN2D level (fold change)
8
6
4
2
0

Figure 2.5.

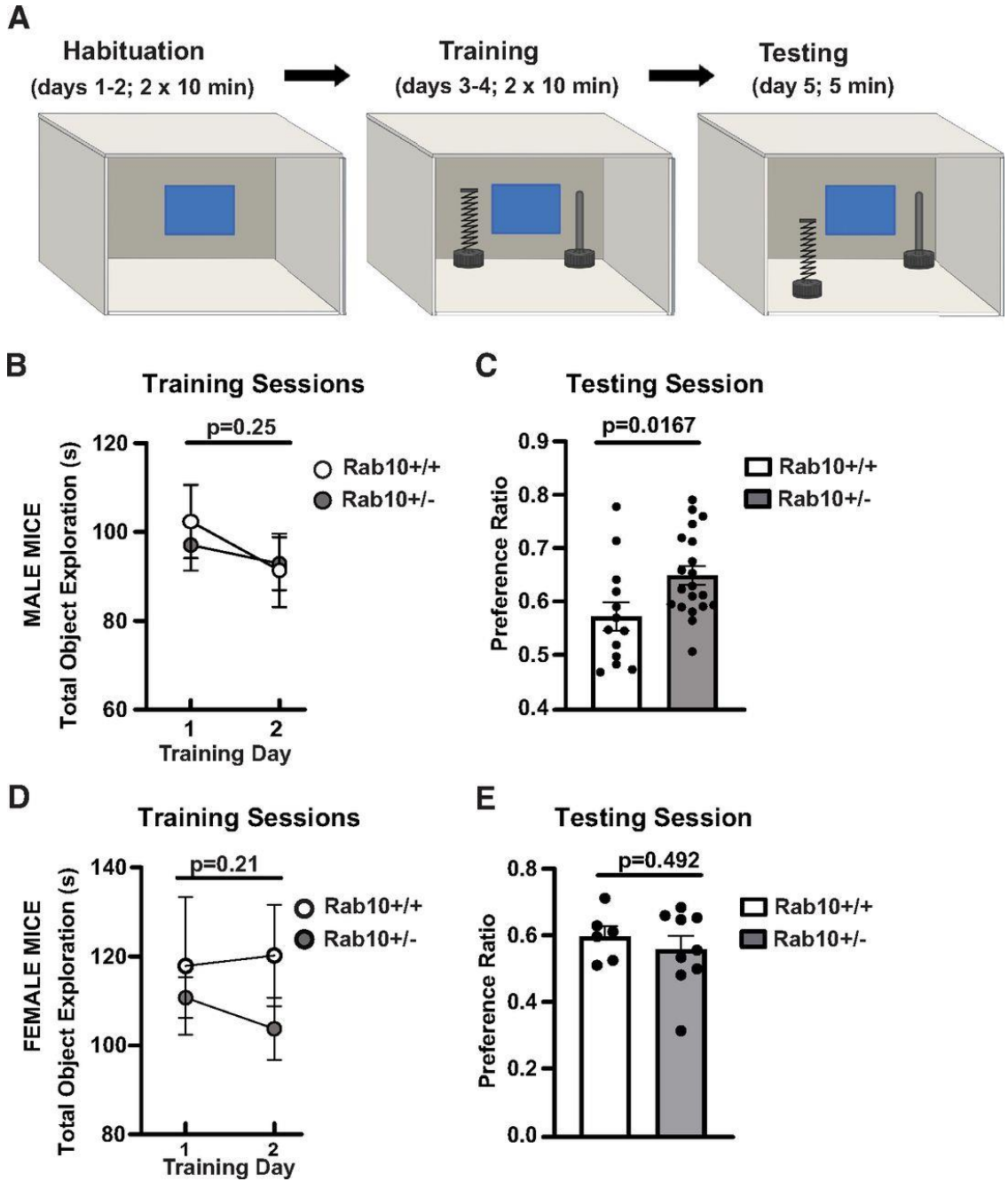
A
Habituation
(days 1-2; 2 x 10 min)
Training
(days 3-4; 2 x 10 min)
Testing
(day 5; 5 min)
B
Training Sessions
p=0.25
MALE MICE
Total Object Exploration (s)
120
100
80
60
1
2
Training Day
Rab10+/+
Rab10+/-
C
Testing Session
p=0.0167
Preference Ratio
0.9
0.8
0.7
0.6
0.5
0.4
Rab10+/+
Rab10+/-
D
Training Sessions
p=0.21
FEMALE MICE
Total Object Exploration (s)
140
120
100
80
1
2
Training Day
Rab10+/+
Rab10+/-
E
Testing Session
p=0.492
Preference Ratio
0.8
0.6
0.4
0.2
0.0
Rab10+/+
Rab10+/-

Figure 2.6.

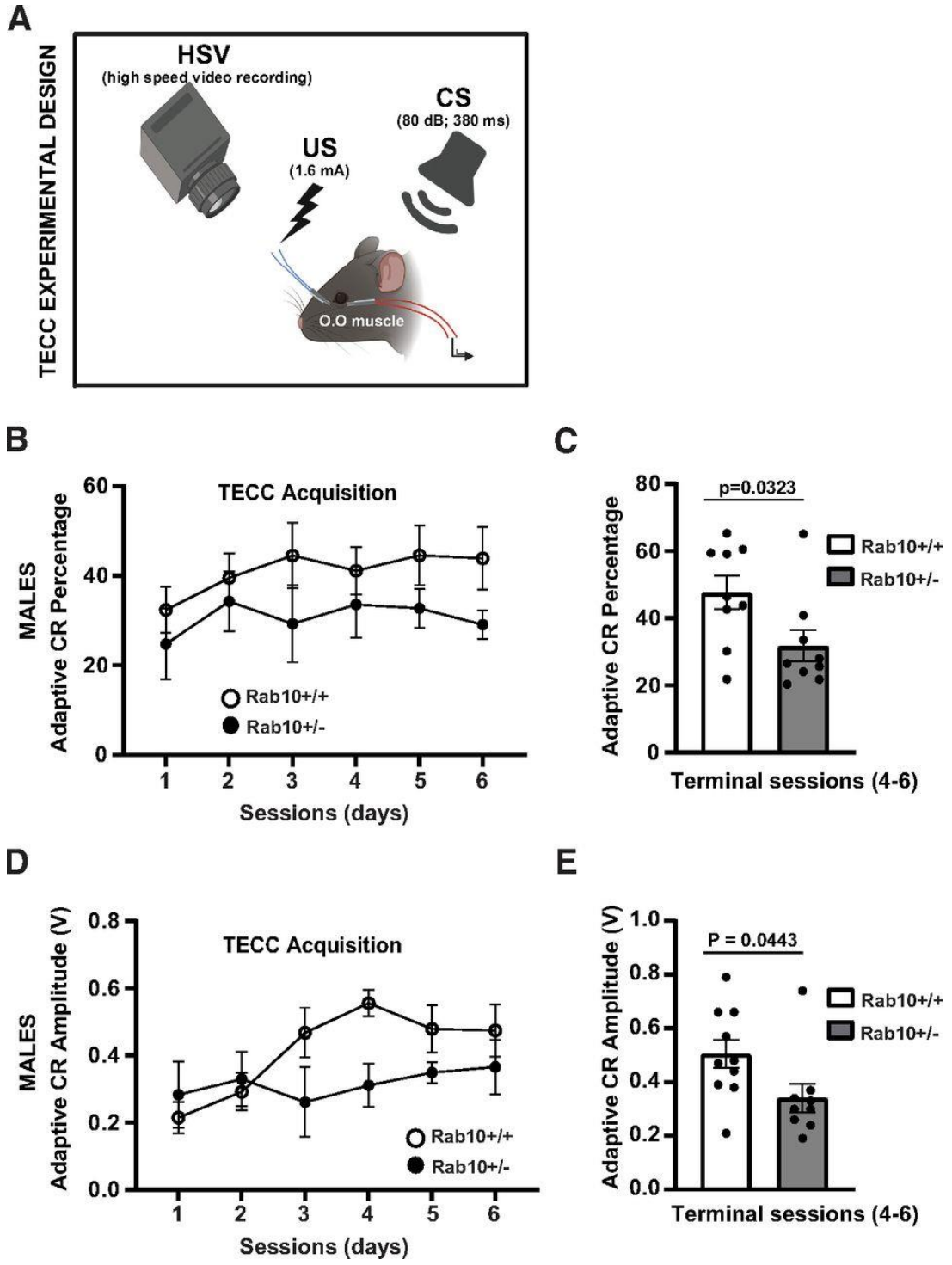
A
TECC EXPERIMENTAL DESIGN
HSV
(high speed video recording)
CS
(80 dB; 380 ms)
US
(1.6 mA)
O.O muscle
B
TECC Acquisition
MALES
Adaptive CR Percentage
Rab10+/+
Rab10+/-
Sessions (days)
C
p=0.0323
Adaptive CR Percentage
Rab10+/+
Rab10+/-
Terminal sessions (4-6)
D
TECC Acquisition
MALES
Adaptive CR Amplitude (V)
Rab10+/+
Rab10+/-
Sessions (days)
E
P = 0.0443
Adaptive CR Amplitude (V)
Rab10+/+
Rab10+/-
Terminal sessions (4-6)

Figure 2.7.

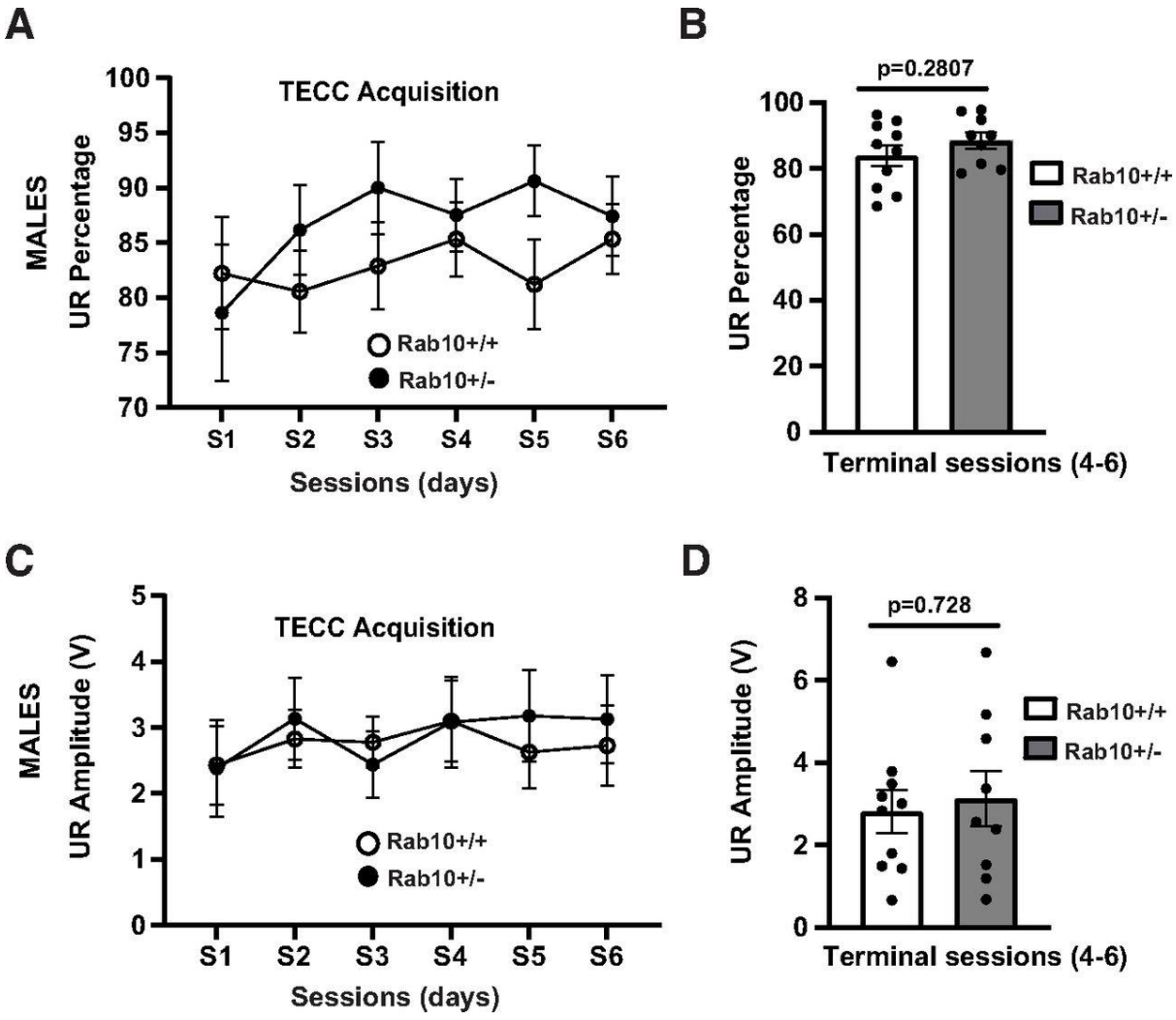
A
TECC Acquisition
MALES
UR Percentage
100
95
90
85
80
75
70
S1
S2
S3
S4
S5
S6
Sessions (days)
Rab10+/+
Rab10+/-
B
p=0.2807
UR Percentage
100
80
60
40
20
0
Terminal sessions (4-6)
Rab10+/+
Rab10+/-
C
TECC Acquisition
MALES
UR Amplitude (V)
5
4
3
2
1
0
S1
S2
S3
S4
S5
S6
Sessions (days)
Rab10+/+
Rab10+/-
D
p=0.728
UR Amplitude (V)
8
6
4
2
0
Terminal sessions (4-6)
Rab10+/+
Rab10+/-

Figure 2.8.

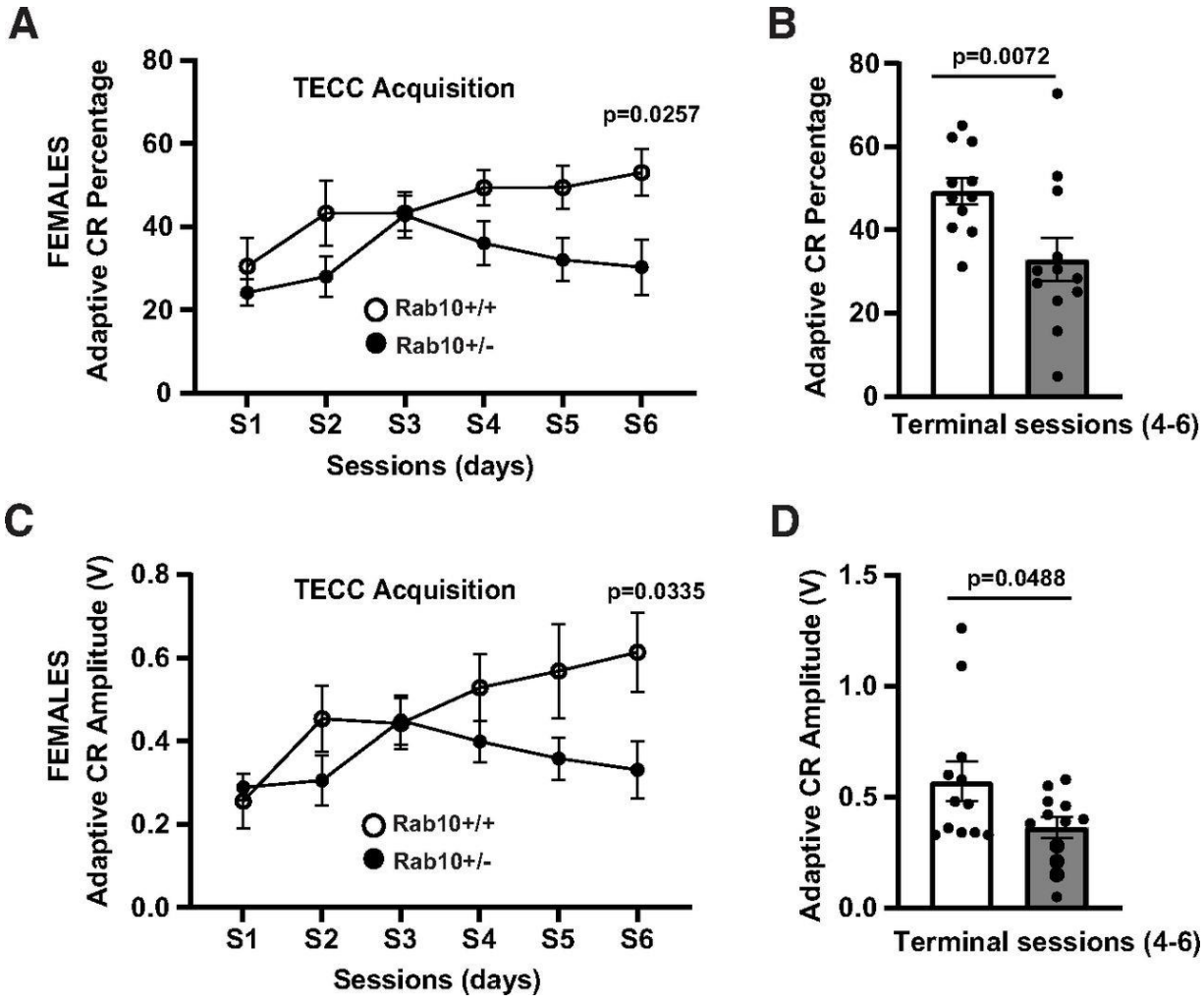
A
FEMALES
Adaptive CR Percentage
TECC Acquisition
p=0.0257
Rab10+/+
Rab10+/-
Sessions (days)
S1
S2
S3
S4
S5
S6
B
p=0.0072
Terminal sessions (4-6)
C
FEMALES
Adaptive CR Amplitude (V)
TECC Acquisition
p=0.0335
D
p=0.0488

Figure 2.9.

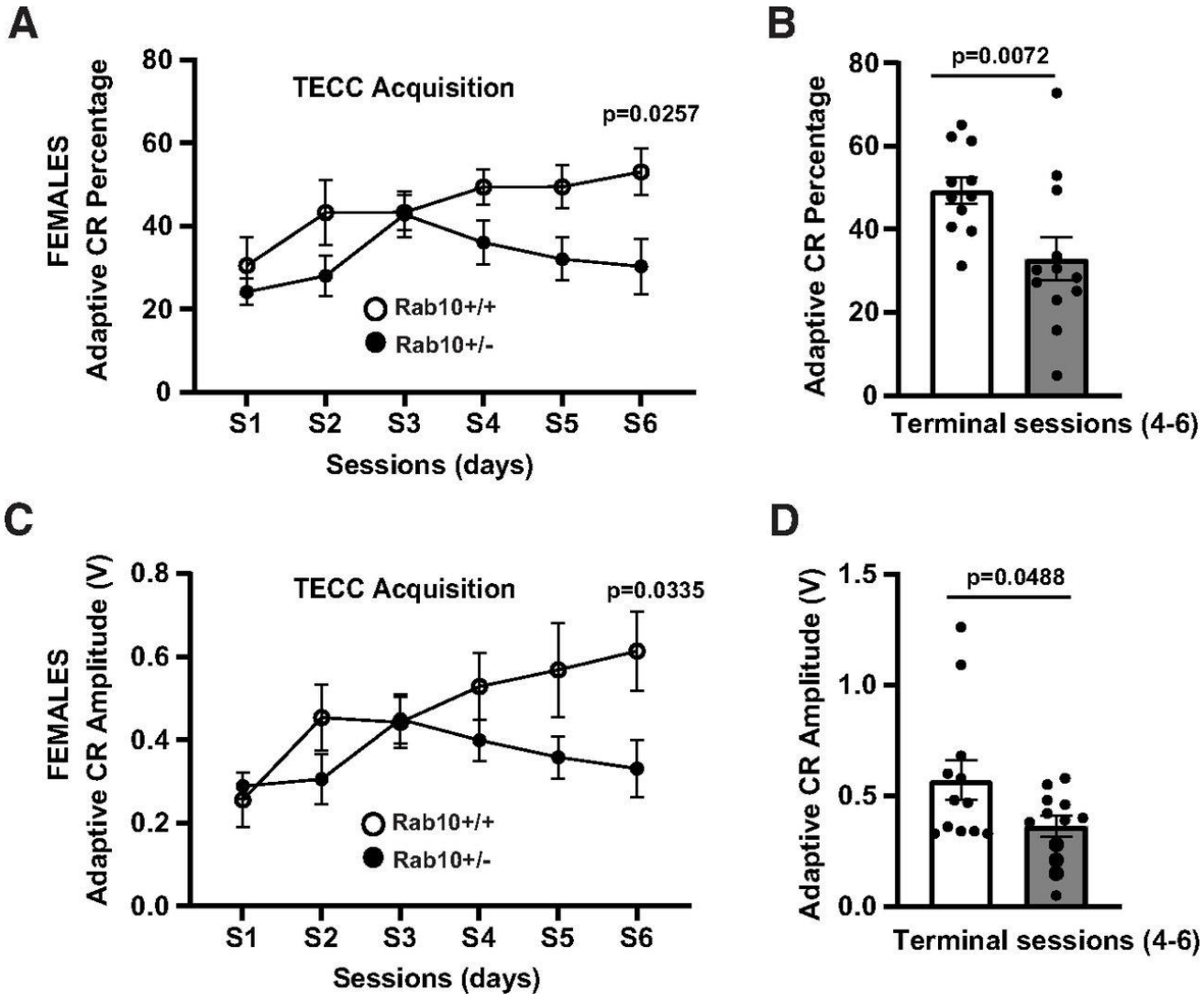
A
FEMALES
Adaptive CR Percentage
TECC Acquisition
p=0.0257
Rab10+/+
Rab10+/-
S1
S2
S3
S4
S5
S6
Sessions (days)
B
p=0.0072
Adaptive CR Percentage
Terminal sessions (4-6)
C
FEMALES
Adaptive CR Amplitude (V)
TECC Acquisition
p=0.0335
Rab10+/+
Rab10+/-
Sessions (days)
D
p=0.0488
Adaptive CR Amplitude (V)
Terminal sessions (4-6)

Table 2.1.

DEG: downregulated in $Rab10^{+/-}$	Accession #	$Rab10^{+/+}$ average normalized count/probe	$Rab10^{+/-}$ average normalized count/probe	*p*-value	*t*-statistics: $Rab10^{+/-}$ vs $Rab10^{+/+}$	95% CI
Stx2	NM_007941.2	79.68 ± 5.14	68.7 ± 2.44	$p = 0.001$	−4.668	4.65, 17.52
Lsr	NM_001164184.1	24.88 ± 3.14	20.12 ± 1.93	$p = 0.016$	−3.033	0.768, 8.947
Lrrc25	NM_153074.3	10.14 ± 3.77	5.45 ± 1.16	$p = 0.018$	−2.959	0.797, 9.738
Vegfa	NM_001025250.3	184.1 ± 23.35	153.22 ± 11.38	$p = 0.019$	−2.917	2.482, 61.126
Galc	NM_008079.3	116.24 ± 13.5	88.47 ± 12.65	$p = 0.021$	−3.179	8.126, 47.326
Phf21a	NM_001109690.1	30.57 ± 7.23	22.73 ± 1.83	$p = 0.022$	−2.955	0.9501, 16.01
Rela	NM_009045.4	55.87 ± 8.51	40.92 ± 6.95	$p = 0.023$	−3.047	3.200, 26.835
Emcn	NM_001163522.1	33.41 ± 5.43	26.31 ± 3.46	$p = 0.033$	−2.582	0.200, 14.410
Atm	NM_007499.2	55.62 ± 6.74	47.89 ± 2.7	$p = 0.041$	−2.483	0.820
Ppp2r5e	NM_012024.2	281.46 ± 17.47	260.16 ± 10.96	$p = 0.044$	−2.385	0.8508. 42.32
Stx1b	NM_024414.2	2874.87 ± 196.82	2661.65 ± 95.64	$p = 0.049$	−2.328	0.035, 435.2

Table 2.2.

DEG: upregulated in $Rab10^{+/-}$	Accession #	$Rab10^{+/+}$ average normalized count/probe	$Rab10^{+/-}$ average normalized count/probe	*p*-value	*t* statistics: $Rab10^{+/-}$ vs $Rab10^{+/+}$	95% CI
Cnot10	NM_153585.5	176.14 ± 8.9	199.06 ± 10.04	$p = 0.008$	3.689	9.032, 36.835
Atp6v1d	NM_023721.2	1610.64 ± 76.48	1721.72 ± 39.5	$p = 0.019$	2.951	−12.974, −206.808
Syt4	NM_009308.3	902.25 ± 44.03	962.42 ± 12.4	$p = 0.019$	3.146	6.351, 112.379
Prkaa2	NM_178143.1	139.58 ± 11.37	155.96 ± 7.9	$p = 0.027$	2.694	9.032, 36.835
Grin2d	NM_008172.2	15.26 ± 4.81	22.48 ± 0.99	$p = 0.039$	2.729	−0.887, −12.210

Table 2.3.

DEG	Neuroinflammation	Neuroplasticity, development, and aging	Metabolism	Compartmentalization and structural integrity	Neuron–glia interaction	Neurotransmission
Stx2 ⬇	–	–	+	+	–	+
Lsr ⬇	–	–	+	–	–	–
Lrrc25 ⬇	+	–	–	–	–	–
Vegfa ⬇	+	+	–	–	–	–
Atp6v0d1 ⬆	–	–	+	+	–	+
Syt4 ⬆	–	–	–	+	–	+
Galc ⬇	+	–	+	–	–	–
Phf21a ⬇	–	+	–	–	–	–
Rela ⬇	–	+	+	–	+	+
Prkaa2 ⬆	–	+	+	–	–	–
Emcn ⬇	–	+	–	–	–	–
Grin2d ⬆	–	–	–	+	–	+
Atm ⬇	–	+	–	–	–	–
Ppp2r5e ⬇	–	–	+	–	–	+
Stx1b ⬇	–	–	–	+	–	+

Chapter 3

Neuro-Immune Crosstalk in Heterozygous Rab10 Knock-Out Mice

Abstract

Alzheimer's disease (AD) is characterized by chronic neuroinflammation, driven in part by aberrant microglial activation and the dysregulation of systemic immune responses. The immune responses, both centrally and peripherally are involved in the progression of AD. This study explores the potential neuroprotective role of Rab10 reduction in AD pathogenesis. The findings demonstrate that Rab10 reduction significantly reduces basal activation status of the microglia in the hippocampus, a critical brain region affected in AD. Additionally, the study reveals a significant decrease in key AD - associated pro-inflammatory cytokine release in organotypic hippocampal slices from $Rab10^{+/-}$ mice. My work also provides evidence that $Rab10^{+/-}$ influences the phenotypes of CD8+ and CD4+ T-cells, with alterations to the effector memory T-cell subsets. Furthermore, this study shows a significant decrease in the number of Natural Killer (NK) cells in $Rab10^{+/-}$ mice, suggesting a role for Rab10 in modulating NK cell-mediated responses. The observed reduction in pro-inflammatory cytokine release by oAβ42, such as IL1-beta, interferon-gamma (IFN-gamma), and tumor necrosis factor-alpha (TNF-α), in $Rab10^{+/-}$ hippocampus underscores the potential for Rab10 modulations as a neuroprotective factor in AD. By attenuating neuroinflammation and modulating immune cell phenotypes, Rab10 reduction offers promising therapeutic avenues for AD treatment or prevention. These findings shed light on the complex interplay between neuroinflammation and peripheral immune responses in AD

pathology. While the study presents Rab10 as a potential target for therapeutic interventions, further research is needed to elucidate the underlying molecular mechanisms and to translate these discoveries into effective treatment strategies for AD.

3.1 Introduction

3.1.1 Background- Alzheimer's disease (AD) has been intensely investigated since it's discovery in 1906. Several factors, including age, sex, genetics, and environment, have been identified as contributors to the development of the disease. Notably, neuroinflammation is considered a significant component in AD (Saw et al., 2023). In affected regions of the brain, amyloid plaques and neurofibrillary tangles are surrounded by higher number of reactive immune cells compared to unaffected areas. Aberrant activation of innate immune signaling pathways is also among the early inflammatory hallmarks of AD (Bivona et al., 2023).

In addition to the well documented involvement of Rab10 in the regulation of intracellular trafficking (Limone et al., 2022), the role of Rab10 in the mechanism of immune responses is an emerging area of research (Russo et al., 2022; Wallings & Tansey, 2019). For example, the Toll-like receptor (TLR)4 receptor complex plays an important role in several inflammatory response pathways (Karimy et al., 2020; Saleh et al., 2021). Recently a group reported that continuous replenishment of TLR4 from the Golgi to the plasma membrane is regulated by the small GTPase Rab10 (Ciesielska et al., 2021). Importantly, another study demonstrated that neutrophils, the most abundant white blood cells and typically the first responders to inflammation, have an increased Rab10 expression in Parkinson's disease patients (Fan et al., 2018). Thus, I hypothesized that reduced Rab10 level might contribute to cognitive resilience through modulation of immune responses.

3.1.2 Main Objective/hypothesis- The research described in this chapter aimed to characterize inflammatory marker phenotypes both peripherally and in the brain of $Rab10^{+/-}$ and $Rab10^{+/+}$ mice.

3.2 Methods

3.2.1 Experimental animals- $Rab10^{+/-}$ and $Rab10^{+/+}$ mice were cared for in accordance with the National Institutes of Health Guide for the Care and Use of Laboratory Animals. The experimental protocols were approved by Institutional Animal Care and Use Committees of East Carolina University. Mice were housed at 20-22°C with a 12-hour light-dark cycle.

3.2.2 Organotypic hippocampal slice culture preparation and treatment- Organotypic mouse hippocampal slices were prepared at postnatal days 6 or 7, as previously described (Stoppini et al., 1991). Briefly, both hippocampi were dissected and sliced at 350 μm thickness using a McIlwain tissue chopper (Ted Pella, Inc). The slices were then placed and cultured on hydrophilic PTFE membranes (Millicell, Millipore) inserted in 6-well plates containing 1 ml of tissue culture medium. One-week later slices were treated with 500 nM of oligomeric Aβ42 or scrambled Aβ42 peptide as a control.

3.2.3 Measurement of cytokine release from hippocampal slice cultures- Samples of collected culture medium were assayed for mouse GM-CSF, IFN-γ, IL-1β, IL-2, IL-4, IL-5, IL-6, IL12p70, IL-13, IL-18, and TNF-α using the ProcartaPlex Mouse Th1/Th2 extended 11-plex kit on a Luminex™ 200™ Instrument System (ThermoFisher) according to the manufacturer's instructions. In brief, samples were thawed on ice; the antibody-coated beads were mixed and washed then incubated overnight at 4 °C with 1:1 diluted standards or samples. After washing,

the beads were incubated with detection antibody mix for 30 min at room temperature. The beads were subsequently washed and incubated for 30 min at room temperature with streptavidin-PE. After washing, the beads were measured with xMAP Technology with a Luminex instrument (Luminex 200, Luminex Corp.) in accordance with the manufacturer's protocols. A five-point standard curve was generated on each plate.

3.2.4. Flow cytometry analyzes of splenic immune cells- Mice were euthanized with 99.9% isoflurane; then death was confirmed decapitation. Immediately after the spleen was removed and placed into ice cold PBS containing 0.2% bovine serum albumin (BSA) and 2 Mm Ethylenediaminetetraacetic acid (EDTA). For mechanical grinding the spleen was placed on a Falcon nylon strainer (Corning Inc., Corning, NY, USA) that was pre-moistened with the PBS + .2% BSA and 2 Mm EDTA. The cell strainer containing the spleen was then placed into a 50 mL conical tube. The rubber end of a plunger for a 10 mL syringe was used to pass the spleen through the cell strainer into tube that contained 10 mL of PBS + .2% BSA and 2 Mm EDTA. Cells were then centrifuged at 400xg for 5 minutes at 4°C then the supernatant was removed. The pellet was resuspended with 10 mL of 1x RBC Lysis Buffer (BioLegend) and incubated for 5 minutes at room temperature. This reaction was halted by adding 30 mL of 1X PBS. Cells were then centrifuged immediately at 400g for 10 minutes at 4°C. Supernatant was decanted and the pellet was resuspended in 3 mL of PBS + 2% BSA. 300 µL from the splenic cell suspension of each mouse were treated with 10 µL of Brilliant Stain Buffer (BD Biosciences, 566349), followed by 5 µL's each of FCR true block and monocyte block reagents and incubated for 20 minutes on ice. Samples for lymphocyte panel were then stained according to manufacturer instructions for CD45.2 (BioLegend, BLG1934), CD8a (BD Biosciences, 563046), CD62L

(BioLegend, BLG10034), CD19 (BioLegend BLG6876), CD80 (BioLegend, BLG6876), CD49b (BD Biosciences, 566392), CD44 (BioLegend, BLG8801), CD11b (BioLegend, BLG10530), CD4 (BD Biosciences, 565974), and TCR β Chain (BioLegend, BLG6996). Live cell populations were gated on the basis of LIVE/DEAD Fixable Blue Dead Cell staining (Invitrogen, L23105). All data were acquired on a Cytek Aurora 5 Laser (Cytek, Fremont, CA). The results were analyzed using FlowJo software (Tree Star, San Carlos, CA). Forward light scatter (area and height) and side light scatter (area and height) gatings were used to gate single live cells.

3.2.5 Immunohistochemistry- For immunofluorescent analysis, six adult mice per group (3-4 months old, 3 females and 3 males) were intracardially perfused with PBS followed by 4% PFA before immunohistochemistry was performed as previously described (Bunner et al., 2020). Briefly, brains were sliced into 20 µm coronal sections using a freezing microtome (Leica VT1000 S) and incubated overnight with anti-GFAP (Cell Signaling 1:500, Danvers, MA, USA) and anti-Iba1 (Santa Cruz 1:500, Santa Cruz, CA) antibodies. This was followed by secondary antibody incubation (Alexa Fluor 488 and Alexa Fluor 594 at 1:1000 dilution for GFAP and Iba1, respectively). Fluorescence images were collected using an optical microscope (Keyence BZ-X800, Osaka, Japan), followed by Image J analysis of mean pixel intensity of the hippocampal area. Two anatomically matched images per mouse were quantified.

3.2.6 Statistical Analysis- Unpaired t-test was used in experiments to compare differences between groups from, mean pixel intensity, and FACS data Kruskal-Wallis one-way ANOVA with Dunn correction was used to compare groups in the Luminex data. All analyses were

performed using GraphPad Prism statistics software, and a *P* value < 0.05 was considered statistically significant.

3.3 Results

3.3.1- Rab10 reduction is associated with decreased baseline expression of inflammatory markers in the hippocampus

Neuroinflammation is due to the reactive activation of microglia and astrocytes, as indicated by increased expression of ionized calcium-binding adaptor protein-1 (Iba1) and glial fibrillary acidic protein (GFAP) respectively (Hauwel et al., 2005). Therefore, we investigated whether reducing the level of Rab10 has any effect on the activation states of microglia and astrocytes using immunohistochemical staining for Iba1 (Figure 3.1) and GFAP (Figure 3.2). Evidence of an inflammatory response includes increased in microglia and astrocyte numbers and the area covered by their processes (Rodríguez-Gómez et al., 2020). We found that $Rab10^{+/-}$ leads to a significant reduction of microglia activation in the hippocampus as shown by a decreased Iba1-labeled area ($p = 0.0114$, $Rab10^{+/+}$ vs $Rab10^{+/-}$ mice, Figure 3.1 [C]). This finding is promising as chronic neuroinflammation facilitated by irregular microglia activation is a hallmark of AD. Reactive microglia contributes to progression of neurodegeneration via the engulfment of synapses (Werneburg et al., 2020). Furthermore, microglia can exacerbate tau pathology and release inflammatory factors that can damage neurons directly or indirectly through the activation of reactive astrocytes (Asai et al., 2015). GFAP immunoreactivity did not show difference between $Rab10^{+/-}$ and $Rab10^{+/+}$ mice (Figure 3.2).

3.3.2.- Rab10$^{+/-}$ alters T-cell effector memory phenotypes in both CD8+ and CD4+ cells

Numerous studies have supported the hypothesis that peripheral inflammatory immune mechanisms contribute to AD pathology (Dá Mesquita et al., 2016). Importantly, it was recently discovered that tau induced neurodegeneration could be attenuated by T-cell activation in the brain of mice (Chen et al., 2023). Here we assessed CD4+ and CD8+ T-cells, that are known to be involved in neurodegenerative disorders such as AD (Town et al., 2005). These cells can be further categorized into memory and naïve phenotypes based on expression of CD62L and CD44 with the CD44^{low}CD62L+ population considered "naïve", CD44^{high}CD62L+ considered "central memory", and the CD44^{high}CD62L^{neg} cells considered "effector memory" (Geginat et al., 2001). To better understand the composition of CD4+ and CD8+ cells in Rab10$^{+/-}$ vs Rab10$^{+/+}$ mice, we evaluated all three of the phenotypes (naïve; central memory; effector memory) in the spleens of both genotypes Our results showed no significant difference between the total percentage of CD8+ and CD4+ cells, along with the naïve and central memory phenotypes between the two T cell types between groups (Figure 3.3 [B,D,E]; Figure 3.4 [B,D,E]). Interestingly the percentage effector memory T-cells were significantly lower in the CD8+ cells of the Rab10$^{+/-}$ mice (Figure 3.3 [D]; p=0.0324). While the average number of central memory T-cells was higher in the CD4+ cells in the Rab10$^{+/-}$ group compared to the Rab10$^{+/+}$ group with an average of close to 3 and .4 respectively, there was no significant difference between genotypes (Figure 3.4 [E], p= .0992). Conversely, the number of effector memory T-cells was significantly higher in the CD4+ cells in Rab10$^{+/-}$ mice (Figure 3.4, [D], p=.0075).

3.3.3- Natural Killer cells are reduced in Rab10$^{+/-}$ mice

Natural killer (NK) cells are cytotoxic lymphocytes that provide rapid response to kill infected and malignant T-cells. NK cells are also known to play a role in inflammatory disorders,

with the ability to both drive inflammation and to restrict the immune response (Sun et al., 2013). Recently NK cells have been implicated in promoting inflammation and exacerbating cognitive decline in AD mouse models (Zhang et al., 2020). Conversely, the depletion of NK cells improved cognitive function and repressed inflammation in AD model mice (Zhang et al., 2020). Here we assessed the percentage of splenic NK cells in $Rab10^{+/-}$ mice compared to their $Rab10^{+/+}$ littermates. NK cells were identified as $CD45.2^{+}CD11b^{+}CD19^{-}$ and TCR-β^{-}CD49b+ lymphocytes. We found that % of NK cells was significantly lower in the spleens of $Rab10^{+/-}$ (p = .0149, Figure 3.4 [C]). Contrarily, the non-NK cell numbers present in the spleens were on average slightly higher in the $Rab10^{+/-}$ mice, without reaching statistical significance (p = .1773, Figure 3.4 [B]).

3.3.4- Rab10 reduction moderates the production of pro-inflammatory cytokines in the hippocampus exposed to oAβ42

A hallmark of Alzheimer's disease is the sustained activation of pro-inflammatory cytokines. Neuroinflammation exacerbates amyloid pathology and that in turn potentiates tau pathology. This cross talk between neuroinflammation, amyloid deposition and tau pathology drives neurodegeneration. We hypothesized that Rab10-dependent resilience against neurodegeneration may be due in part to the modulation of inflammatory cytokine release. We tested this hypothesis using a highly sensitive multiplex immunoassay for key inflammatory cytokines released from hippocampal slices treated with either oligomeric Amyloid-beta (oAβ42) or a scrambled form of Aβ42 peptide as a control. The culture medium from the brain slices was collected and saved immediately before and 24 hours after treatment. As can be seen on Figure 3.5 and 3.6, IL1-Beta, IFN-Gamma, and TNF alpha were significantly elevated in $Rab10^{+/+}$ slices following oAβ42, whereas there was no significant difference in the $Rab10^{+/-}$ slices between the cytokine content

before and after treatment (Figure 3.5 [A], Figure 3.6 [A,D]). The oligomeric peptide treatment groups of both genotypes were significantly higher than both of the groups before peptide treatment and the scramble controls in IFN-Gamma and Il-20p70 (Figure 3.6 [E, F]).

3.4 Discussion-

Our results suggest that Rab10 reduction significantly lowers the baseline activation status of the microglia in the hippocampus. Our findings also shows that this reduction in expression level of Rab10 also reduces key inflammatory cytokine release in organotypic hippocampal slices exposed to o Aβ42. Furthermore, we found evidence that Rab10 reduction also significantly lowers splenic levels of Natural Killer cells and significantly shifts the effector memory phenotype of CD8+ significantly lower and CD4+ significantly higher in the same phenotype. Combined these data indicate that a decrease in the baseline immunity both peripherally and centrally may contribute to the neuroresilience against AD by reduced Rab10 level/activity.

A robust defense mechanism against infections, toxins and injury in the brain is acute inflammation, yet in conditions like AD, the imbalance between anti-inflammatory and pro-inflammatory signaling leads to the development of chronic inflammation (Onyango, 2021). Microglia, the native immune cells of the brain, are critical for tissue maintenance, defense against pathogens and response to injury (Pascoal et al., 2021; Bivona et al., 2023). However aberrant activation of microglia can exacerbate the local neuroinflammation that contributes to the progression of neurodegeneration associated with AD. One prominent inflammatory risk factor for AD is the sustained hippocampal overexpression of interleukin-1beta (IL1-beta) which

mediates chronic neuroinflammation and is produced by microglia (Mrak et al., 2001). In later stages of AD as neurofibrillary tangles increase, Aβ and tau deposits signal microglia triggering the neuroimmune inflammatory response, leading to neurodegeneration (Saw et al., 2023). Furthermore, evidence suggests that tau filaments released from degenerating neurons can re-activate microglial cells, creating a continuous signaling cascade of neurodegeneration (Pascoal et al., 2021). Moreover, in post-mortem brain samples from patients with AD, total microglia have been shown to be elevated as well (Hopperton et al., 2018). A common marker to measure both resting and activated microglia is ionized calcium-binding adaptor molecule-1 (Iba1) (Dursun et al., 2015).

In this study we evaluated whether reduction in Rab10 changes the basal microglial Iba1 level in the hippocampus. To accomplish this, brain sections were immunolabeled with anti-Iba1 antibody. Our findings show a significant reduction in Iba1 immunoreactivity in $Rab10^{+/-}$ mice compared to their $Rab10^{+/+}$ littermates. Increased Rab10 activity induced via leucine-rich repeat kinase 2 induced autophagy-lysosomal dysregulation and NLRP3 inflammasome activation in microglia, was recently shown to cause a neurotoxic environment (Pajarillo et al., 2023). Therefore, Rab10 reduction may have a protective role through decreased basal microglial activation in the brain. Further studies investigating the molecular mediators in neurons and microglia are necessary to better understand the neuroprotective role of reduced Rab10 against neurodegeneration.

Immune dysfunction and the role immunity plays in AD pathogenesis was previously thought to be restricted to the central nervous system, but accumulating evidence have implicated the systemic immune system as well (Bettcher et al., 2021; Streit et al., 2005). Of note, recent studies have shown a homeostatic imbalance of peripheral T-cells in AD (Dansokho et al., 2016).

Altered distribution of phenotypes and activation statuses of different subsets of lymphocytes have been shown to play a role in AD pathogenesis (Dansokho et al., 2016). In line with this research, another recent study showed an increase in the percentage of the central memory and a significant decrease in the effector memory CD4+ T-cell phenotype in AD patients compared to healthy individuals (Garfias et al., 2022). Contrarily, both central memory and effector memory CD8+ T-cells were positively correlated to AD in humans (Gate et al., 2020). T-cell differentiation is critical for combating pathogenic agents. Once a pathogenic cell presents to a naïve or undifferentiated T-cell, the T-cells become active, their number increases at the pathogenic site and differentiate into either effector or central memory cells (Smith-Garvin et al., 2009). The effector T-cells induce the production of pro-inflammatory cytokines that initiate inflammation (Smith-Garvin et al., 2009). With this in mind, we set out to evaluate whether peripherally circulating T-cells are altered in $Rab10^{+/-}$ mice. To accomplish this, we utilized flow cytometry of splenic cells from 3–4-month-old $Rab10^{+/-}$ and $Rab10^{+/+}$ mice.

Busse et al. previously reported an increase in effector and a decrease in central memory in CD8+ T-cells in AD patients (Busse et al., 2021). Our results showed a contrary effect in $Rab10^{+/-}$ mice with effector memory CD8+ cells being significantly lower and the central memory cells being higher, but the difference was not statistically significant. The opposite phenomenon was observed in CD4+ cells in AD patients where the central memory T-cells were increased and the effector memory T-cells were decreased (Garfias et al., 2022). Unlike our results with the CD8+ cells, the CD4+ showed an increase in both effector and central memory cells while the difference between groups was not statistically significant in the central memory cells. Combined these results indicate a role for Rab10 in the control of basal T cell phenotypes in the systemic immune response. Many of these results are the opposite to the AD phenotype.

Thus, our findings are exciting because they point to the possibility of $Rab10^{+/-}$ dependent modulation of systemic immunity as a mechanism of neuroresilience against neurodegeneration. Several different antigens may activate and promote the differentiation of CD8+ and CD4+ T-cells. Therefore, identifying the specific molecular changes involved, particularly in AD, could lead to new therapeutic approaches in the treatment of neurodegenerative disorders.

Another peripheral immune system lymphocyte of interest implicated in AD pathology is the Natural Killer (NK) cell. Several studies have indicated NK cell involvement in AD (Solana et al., 2018; Zhang et al., 2020). Zhang et al. recently identified in AD mouse models a role for NK cells in promoting neuroinflammation and exacerbating cognitive decline (Zhang et al., 2020). The same study showed attenuated neuroinflammation, stimulated neurogenesis, and improved cognitive function in AD mice by depleting NK cells via the introduction of an anti-NK antibody (Zhang et al., 2020). While this study may have shown a wonderful ability to reduce many of the pathological features of AD, the complete depletion of NK cells in humans can be harmful. Our study revealed that reduction of NK cells was significantly lowered in $Rab10^{+/-}$ mice. While this number was lower, it wasn't abolished with the number of NK cells making up 54.84% and 48.99% of the B-cell and T-cell negative lymphocytes for the $Rab10^{+/+}$ and the $Rab10^{+/-}$ groups respectively. Thus, Rab10 reduction may provide a safe therapeutic route to target NK cells as an AD therapeutic strategy. Identifying the molecular mechanisms involved in the Rab10-dependent reduction of NK cell percentage, is another avenue to find therapeutic interventions to treat or prevent AD.

While targeted and timely activation of inflammatory cells and pathways is necessary for combating pathological conditions, chronic inflammation is detrimental. Increased microglial

activation can result in the production of inflammatory cytokines exacerbating Aβ and tau pathologies.

AD remains a devastating disease with unmet therapeutic needs. The development of successful treatments relies on a comprehensive understanding of the cellular and molecular mechanisms involved. To further expand on this, we utilized $Rab10^{+/-}$ and $Rab10^{+/+}$ organotypic hippocampal slice cultures and tested the media for cytokines released in the presence of oAβ42 or scrambled Aβ peptide. Our results showed that IL1-Beta, IFN-Gamma, and TNF alpha were significantly elevated in the culture medium of $Rab10^{+/+}$ after being incubated with oAβ for 24 hours. While the average release was higher in the culture medium from the $Rab10^{+/-}$ slices treated with oAβ, there was no significant difference between the media from oAβ treatment compared to the media from the groups before treatment. IL1-beta was the first cytokine identified to have the ability to affect the brain (Besedovsky et al., 1986) where it was described as an "endogenous pyrogen". Since then, it has been implicated in a number of pathological processes in the brain including AD (Benzing et al., 1999; Lim et al., 2000). Increased IL1-beta expression is significantly higher in activated microglia that surround Aβ plaques (Solana et al., 2018). Besides IL- beta, interferon gamma (IFN-gamma) and tumor necrosis factor alpha (TNF-α) are also significantly elevated in AD (Bermejo et al., 2008). TNF-α, originally recognized for its antitumor ability, is also a major inflammatory cytokine with a prominent role in neuroinflammation. Elevated TNF-α has been found in both AD patients and AD mouse models. In AD transgenic mice, increased TNF-α lead to an increase in both beta and gamma secretase activity, while chronic induction of TNF-α resulted in extensive neurodegeneration (Balkwill et al., 2006). IFN-gamma is also an inflammatory cytokine released from T and NK (Roussos et al., 2015). It can prime microglia resulting in the release of other cytokines thus enhancing the

inflammatory response (Roussos et al., 2015). Our study demonstrated that both IFN-gamma and TNF-α were significantly elevated in $Rab10^{+/+}$ hippocampal slices treated with oAβ compared to the media in the groups before treatment, whereas there was no significant difference between groups when comparing the $Rab10^{+/-}$ hippocampal slice media levels before and after treatment with Aβ. Hence, by lowering TNF-α and INF-gamma levels, it is possible to effectively reduce inflammation in AD patients. As neuroinflammation contributes to neuronal damage and chronic inflammation enhances Aβ accumulation (Leng et al., 2021), Rab10's neuroprotective effect may be due in part by its ability to reduce the level or the production of proinflammatory cytokines. While it is important to note that animal models do not always perfectly mirror the complexity of human diseases, these findings offer promising therapeutic interventions for AD pathology.

Chapter 3 Figures

Figure Legends:

Figure 3.1 Rab10 reduction decreases microglia activation. The number of mice was 6 for $Rab10^{+/+}$ and 6 for $Rab10^{+/-}$ genotype (3 females and 3 males). Two anatomically matched images per mouse were quantified**. A,** Representative Iba1 immunofluorescence in the hippocampus of $Rab10^{+/+}$ mice. **B,** Representative Iba1 immunofluorescence in the hippocampus of $Rab10^{+/-}$ mice. **C,** Quantification of the area covered by microglial cells in the hippocampus of $Rab10^{+/+}$ and $Rab10^{+/-}$ mice. Error bars indicate SEM. Two-tailed unpaired *t* test, $p = .0114$. Scale bars represent 100 µM.

Figure 3.2 Rab10 reduction decreases astrocyte activation. The number of mice was 6 for $Rab10^{+/+}$ and 6 for $Rab10^{+/-}$ genotype (3 females and 3 males). Two anatomically matched images per mouse were quantified**. A,** Representative GFAP immunofluorescence in the hippocampus of $Rab10^{+/+}$ mice. **B,** Representative GFAP immunofluorescence in the hippocampus in $Rab10^{+/-}$ mice. **C,** Quantification of the area covered by astrocytic cells in the hippocampus of $Rab10^{+/+}$ and $Rab10^{+/-}$ mice. Error bars indicate SEM. Two-tailed unpaired *t* test, $p = .1692$. Scale bars represent 100 µM.

Figure 3.3 CD8+ effector memory T-cells are reduced in $Rab10^{+/-}$ mice. The number of mice was 4 for $Rab10^{+/+}$ and 7 for $Rab10^{+/-}$ genotype. **A,** Representative flow cytometry gating strategy showing effector memory, central memory and naïve CD8+ splenic cells. **B,** Quantification of parent percentage of CD8+ cells in the spleen of $Rab10^{+/+}$ and $Rab10^{+/-}$ mice. Error bars indicate SEM. Two-tailed unpaired *t* test, $p = 0.4373$. **C,** Quantification of CD8+ naïve cells in the spleen of $Rab10^{+/+}$ and $Rab10^{+/-}$ mice. Error bars indicate SEM. Two-tailed unpaired *t* test, $p = 0.7212$. **D,** Quantification of CD8+ Effector Memory phenotype cells in the spleen of $Rab10^{+/+}$ and $Rab10^{+/-}$ mice. Error bars indicate SEM. Two-tailed unpaired *t* test, $p = 0.0324$. **E,**

Quantification of CD8+ Central Memory phenotype cells in the spleen of $Rab10^{+/+}$ and $Rab10^{+/-}$ mice. Error bars indicate SEM. Two-tailed unpaired *t* test, $p = 0.2982$.

Figure 3.4 CD4+ effector memory T-cells are increased in $Rab10^{+/-}$ mice. The number of mice was 4 for $Rab10^{+/+}$ and 7 for $Rab10^{+/-}$ genotype. **A,** Representative flow cytometry gating strategy showing effector memory, central memory and naïve CD4+ splenic cells. **B,** Quantification of parent percentage ofCD4+ cells in the spleen of $Rab10^{+/+}$ and $Rab10^{+/-}$ mice. Error bars indicate SEM. Two-tailed unpaired *t* test, $p = 0.4456$. **C,** Quantification of CD4+ naïve cells in the spleen of $Rab10^{+/+}$ and $Rab10^{+/-}$ mice. Error bars indicate SEM. Two-tailed unpaired *t* test, $p = 0.7481$. **D,** Quantification of CD8+ Effector Memory phenotype cells in the spleen of $Rab10^{+/+}$ and $Rab10^{+/-}$ mice. Error bars indicate SEM. Two-tailed unpaired *t* test, $p = 0.0075$. **E,** Quantification of CD8+ Central Memory phenotype cells in the spleen of $Rab10^{+/+}$ and $Rab10^{+/-}$ mice. Error bars indicate SEM. Two-tailed unpaired *t* test, $p = 0.0922$.

Figure 3.5 NK cell numbers are reduced in $Rab10^{+/-}$ mice.

The number of mice was 4 for $Rab10^{+/+}$ and 7 for $Rab10^{+/-}$ genotype. **A,** Representative flow cytometry gating strategy showing NK and Non-NK cells. **B,** Quantification of non-NK cells in the spleen of $Rab10^{+/+}$ and $Rab10^{+/-}$ mice. Error bars indicate SEM. Two-tailed unpaired *t* test, $p = 0.1773$. **C,** Quantification of NK cells in the spleen of $Rab10^{+/+}$ and $Rab10^{+/-}$ mice. Error bars indicate SEM. Two-tailed unpaired *t* test, $p = 0.0149$.

3.6 IL-1 beta, IFN-Gamma, and TNF-Alpha release is lower $Rab10^{+/-}$ hippocampal slices treated with oligomeric Aβ. The number of mice was 4 per genotype from two different litters. Organotypic hippocampal slices were plated in 6-well plates on Millicell inserts (3 slices/insert; slice thickness was 350 μm). Two wells/genotypes were used for each experiment: one was

treated with oligomeric Aβ42, while the other was treated with scrambled Aβ42 as a negative control. A Kruskal-Wallis one way ANOVA with DUNN corrections was performed to compare groups from each cytokine. If significance was observed, multiple comparisons were then performed to find which groups were significantly different. Significantly different groups and their p-values are shown in the graphs. **A,** Quantification of IL-1 Beta. Error bars indicate SEM. Significance was observed between the $Rab10^{+/+}$ pretreatment vs. $Rab10^{+/+}$ post Aβ oligomeric group (p=.0251) **B,** Quantification of IFN-Gamma, Error bars indicate SEM. Significance was observed in the $Rab10^{+/+}$ pretreatment vs. $Rab10^{+/+}$ post Aβ oligomeric group (p=.0251) **C,** Quantification of TNF Alpha. Error bars indicate SEM. Significance was observed in the $Rab10^{+/+}$ pretreatment vs. $Rab10^{+/+}$ post AB oligomeric group (p=.0049) **D,** Quantification of IL-20p70. Error bars indicate SEM. Significance was observed in the $Rab10^{+/+}$ pretreatment vs. $Rab10^{+/+}$ post Aβ oligomeric group (p=.0017). **E,** Quantification of IL-2. Error bars indicate SEM. Significance was observed in the $Rab10^{+/-}$ pretreatment vs. $Rab10^{+/-}$ post Aβ oligomeric group (p=.0474) and the $Rab10^{+/-}$ post Aβ oligomeric vs. $Rab10^{+/+}$ post Aβ oligomeric group (0.100). **F,** Quantification of GM-CSF. Error bars indicate SEM. Significance was observed in the $Rab10^{+/+}$ pretreatment vs. $Rab10^{+/+}$ Post Aβ oligomeric group (p=0.0012).

3.7 IL-4, IL-5, IL-6, IL-13, and IL-18 are not affected by oligomeric Aβ treatment of $Rab10^{+/+}$ and $Rab10^{+/-}$ hippocampal slices

The number of mice was 4 per genotype from two different litters. Organotypic hippocampal slices were plated in 6-well plates on Millicell inserts (3 slices/insert; slice thickness was 350 μm). Two wells/genotype were used for each experiment: one was treated with oligomeric Aβ42, while the other was treated with scrambled Aβ42 as negative control. A Kruskal-Wallis one way

ANOVA with DUNN corrections was performed to compare groups from each cytokine. If significance was observed, multiple comparisons were then performed to find which groups were significantly different. **A,** Quantification of IL-4. Error bars indicate SEM. **B,** Quantification of IL-5. Error bars indicate SEM. **C,** Quantification of IL-6. Error bars indicate SEM. **D,** Quantification of IL-13. Error bars indicate SEM. **E,** Quantification of IL-18. Error bars indicate SEM.

Figure 3.1

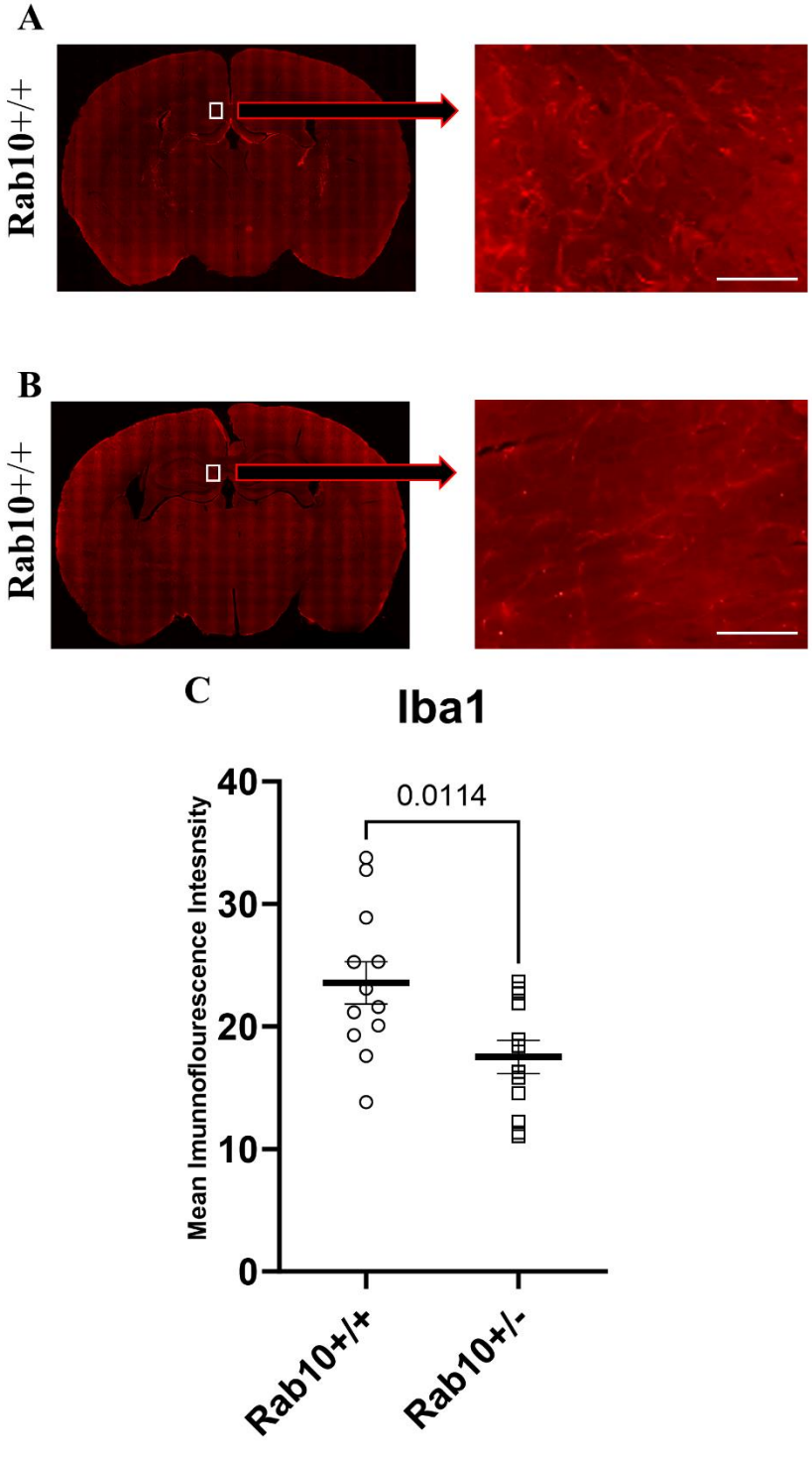
A
Rab10+/+
B
Rab10+/+
C
Iba1
0.0114
Mean Imunnoflourescence Intesnsity
40
30
20
10
0
Rab10+/+
Rab10+/-

Figure 3.2

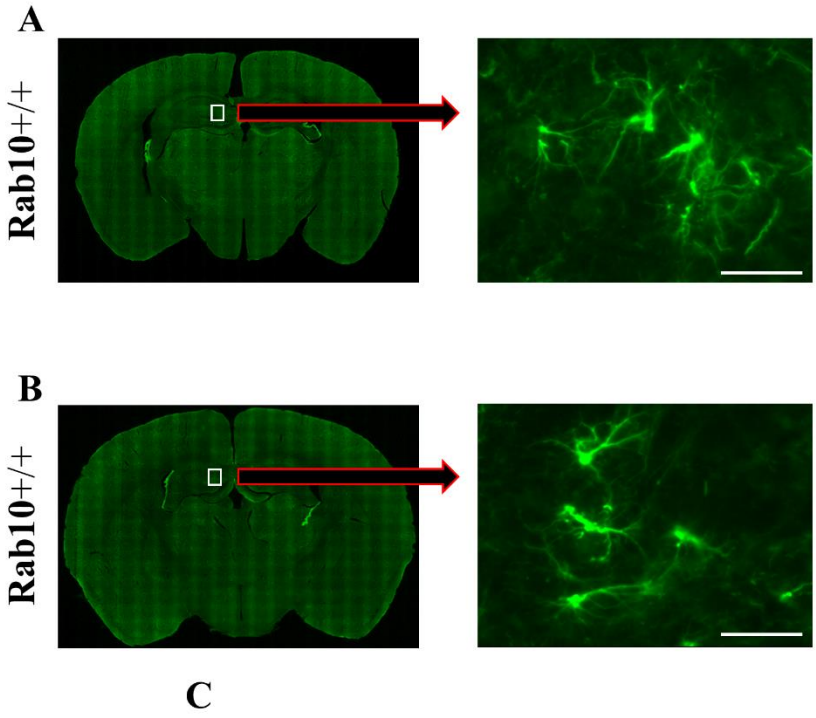
A
Rab10+/+
B
Rab10+/+

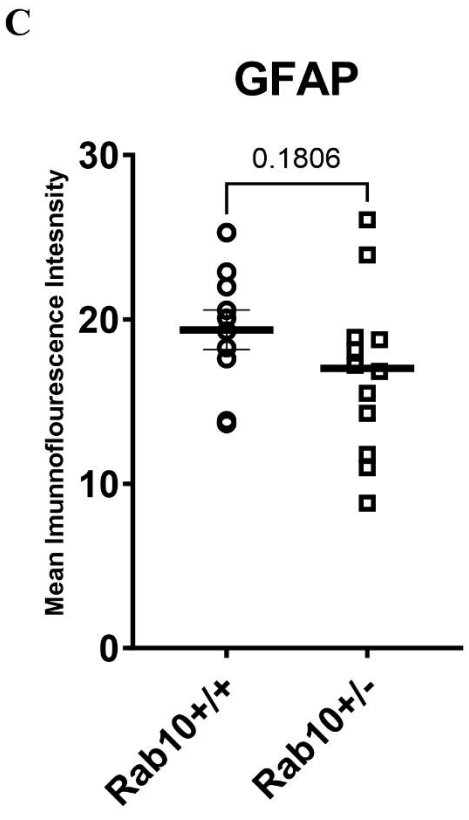
C
GFAP
0.1806
Mean Imunnoflourescence Intesnsity
30
20
10
0
Rab10+/+
Rab10+/-

Figure 3.3

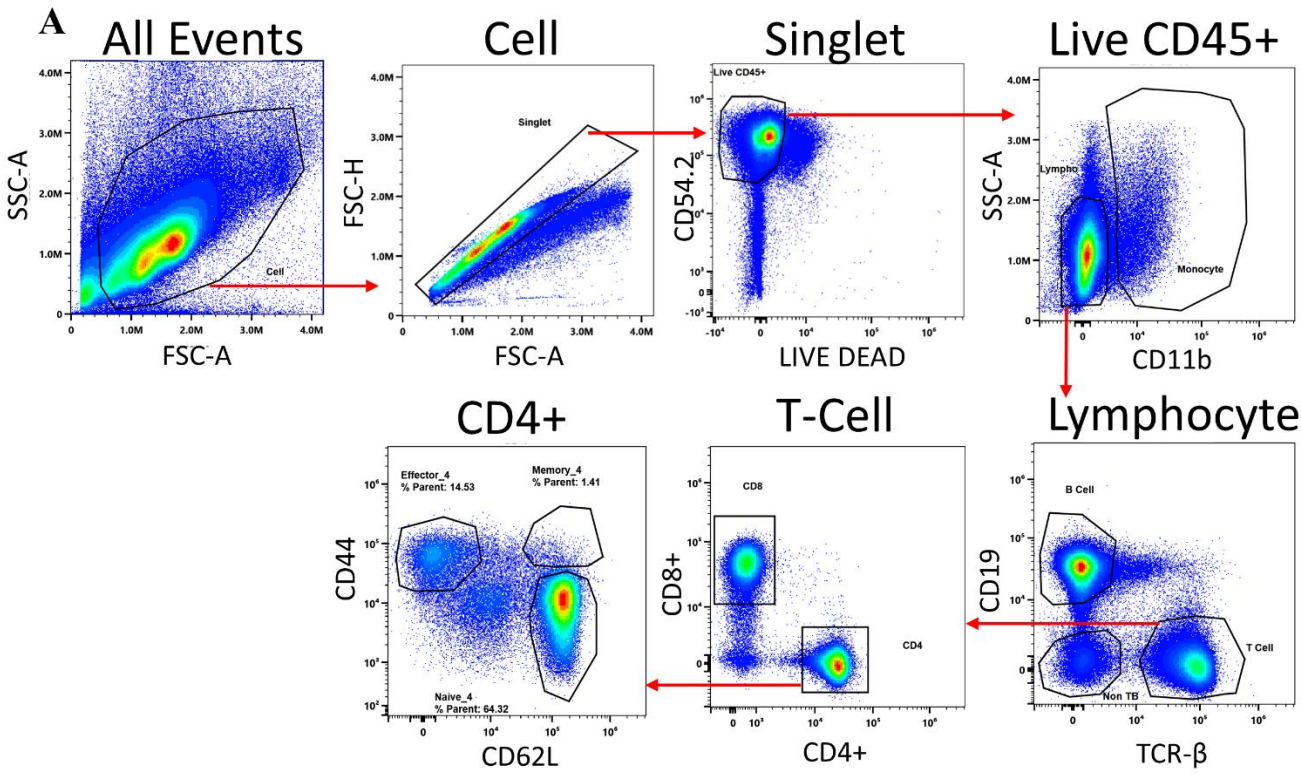
A
All Events
SSC-A
FSC-A
Cell
Cell
FSC-H
FSC-A
Singlet
Singlet
CD54.2
LIVE DEAD
Live CD45+
Live CD45+
SSC-A
CD11b
Lympho
Monocyte
Lymphocyte
CD19
TCR-β
B Cell
T Cell
Non TB
T-Cell
CD8+
CD4+
CD8
CD4
CD4+
CD44
CD62L
Effector_4
% Parent: 14.53
Memory_4
% Parent: 1.41
Naive_4
% Parent: 64.32

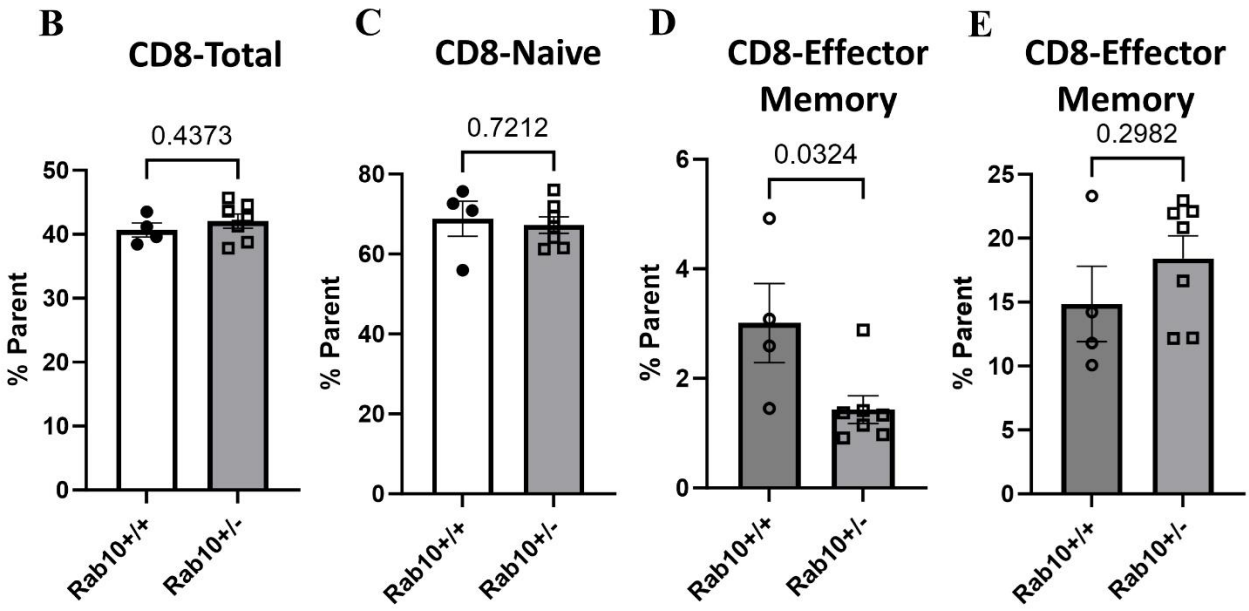
B
CD8-Total
0.4373
% Parent
Rab10+/+
Rab10+/-
C
CD8-Naive
0.7212
% Parent
Rab10+/+
Rab10+/-
D
CD8-Effector Memory
0.0324
% Parent
Rab10+/+
Rab10+/-
E
CD8-Effector Memory
0.2982
% Parent
Rab10+/+
Rab10+/-

Figure 3.4

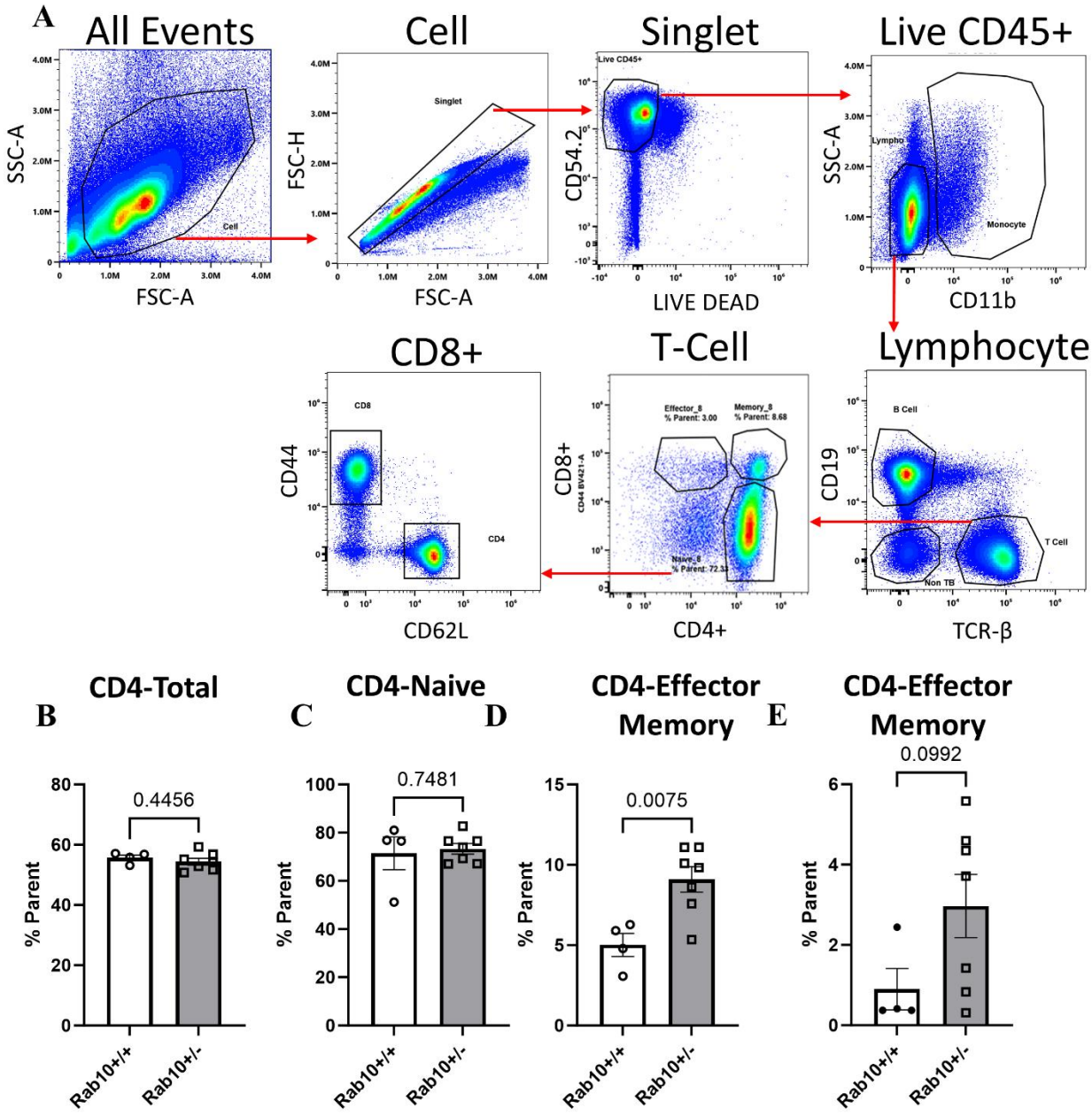
A
All Events
Cell
Singlet
Live CD45+
SSC-A
FSC-A
FSC-H
CD54.2
LIVE DEAD
CD11b
Lymphocyte
CD8+
T-Cell
CD44
CD62L
CD19
TCR-β
CD4+
B
CD4-Total
C
CD4-Naive
D
CD4-Effector Memory
E
CD4-Effector Memory
% Parent
0.4456
0.7481
0.0075
0.0092
Rab10+/+
Rab10+/-

Figure 3.5

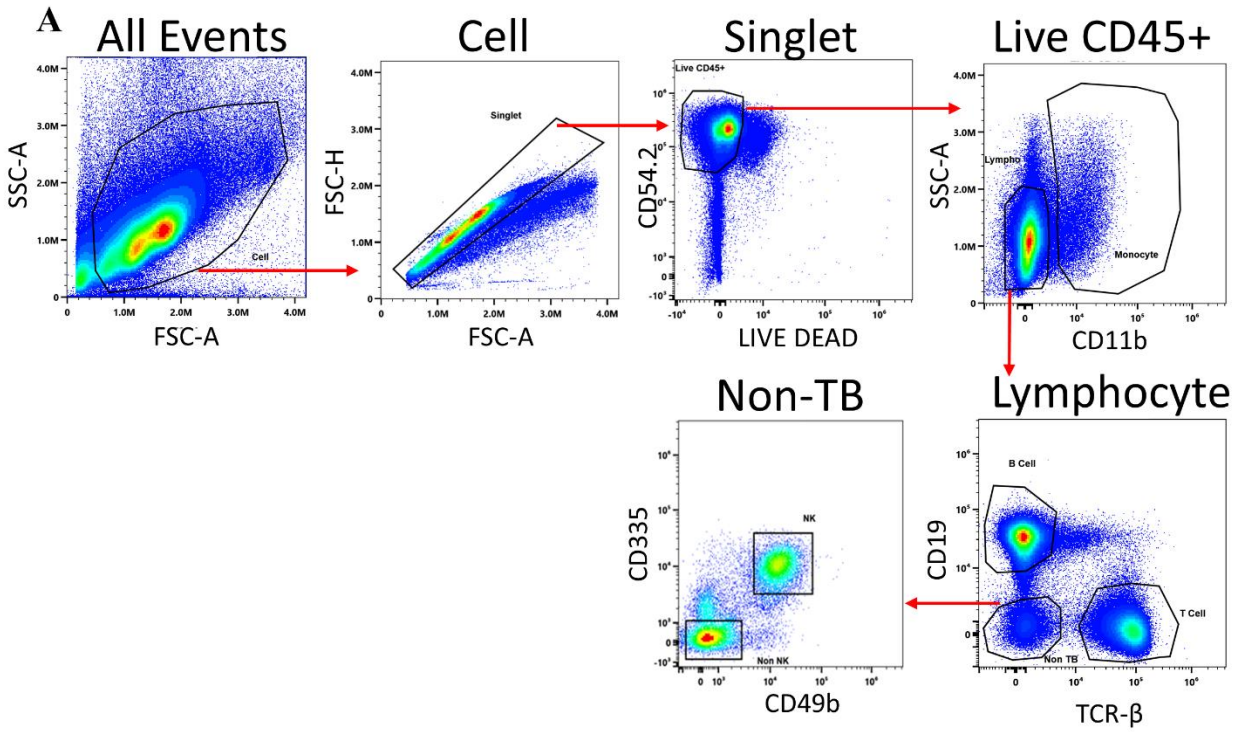
A
All Events
Cell
Singlet
Live CD45+
SSC-A
FSC-A
FSC-H
Singlet
Cell
CD54.2
LIVE DEAD
Live CD45+
SSC-A
CD11b
Lympho
Monocyte
Non-TB
Lymphocyte
CD335
CD49b
NK
Non NK
CD19
TCR-β
B Cell
T Cell
Non TB

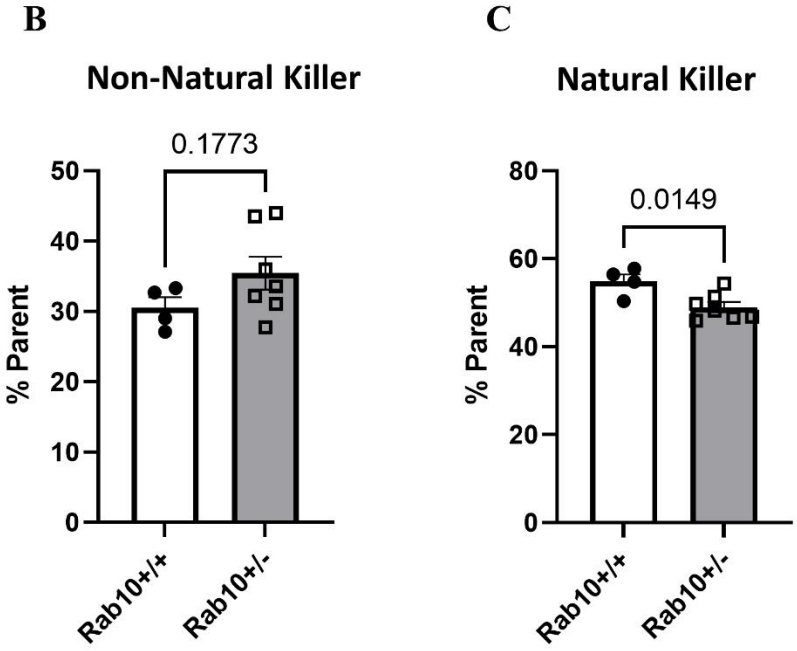
B
Non-Natural Killer
0.1773
% Parent
Rab10+/+
Rab10+/-
C
Natural Killer
0.0149
% Parent
Rab10+/+
Rab10+/-

Figure 3.6

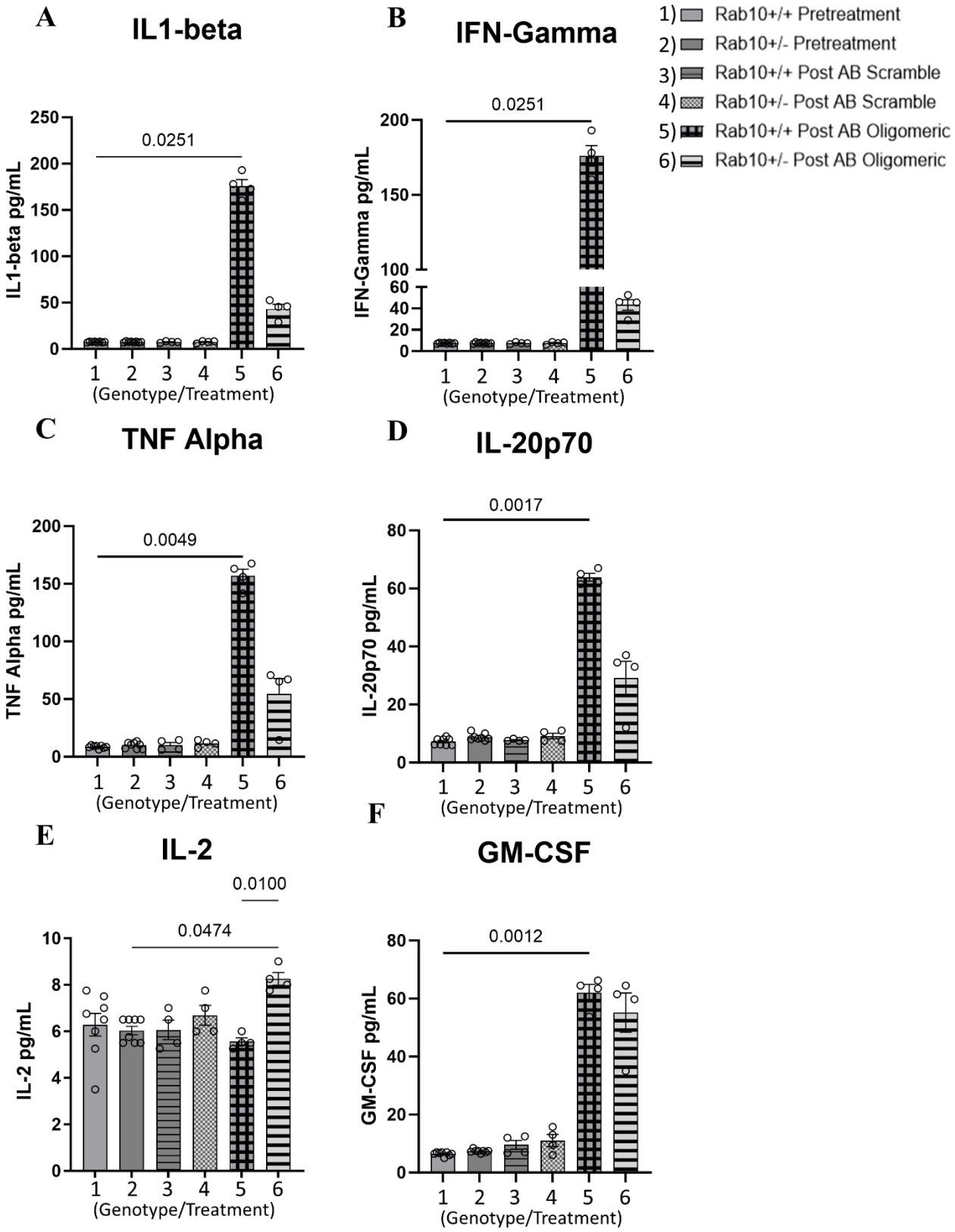
A
IL1-beta
IL1-beta pg/mL
0.0251
(Genotype/Treatment)
B
IFN-Gamma
IFN-Gamma pg/mL
0.0251
(Genotype/Treatment)
1) Rab10+/+ Pretreatment
2) Rab10+/- Pretreatment
3) Rab10+/+ Post AB Scramble
4) Rab10+/- Post AB Scramble
5) Rab10+/+ Post AB Oligomeric
6) Rab10+/- Post AB Oligomeric
C
TNF Alpha
TNF Alpha pg/mL
0.0049
(Genotype/Treatment)
D
IL-20p70
IL-20p70 pg/mL
0.0017
(Genotype/Treatment)
E
IL-2
IL-2 pg/mL
0.0100
0.0474
(Genotype/Treatment)
F
GM-CSF
GM-CSF pg/mL
0.0012
(Genotype/Treatment)

Figure 3.7

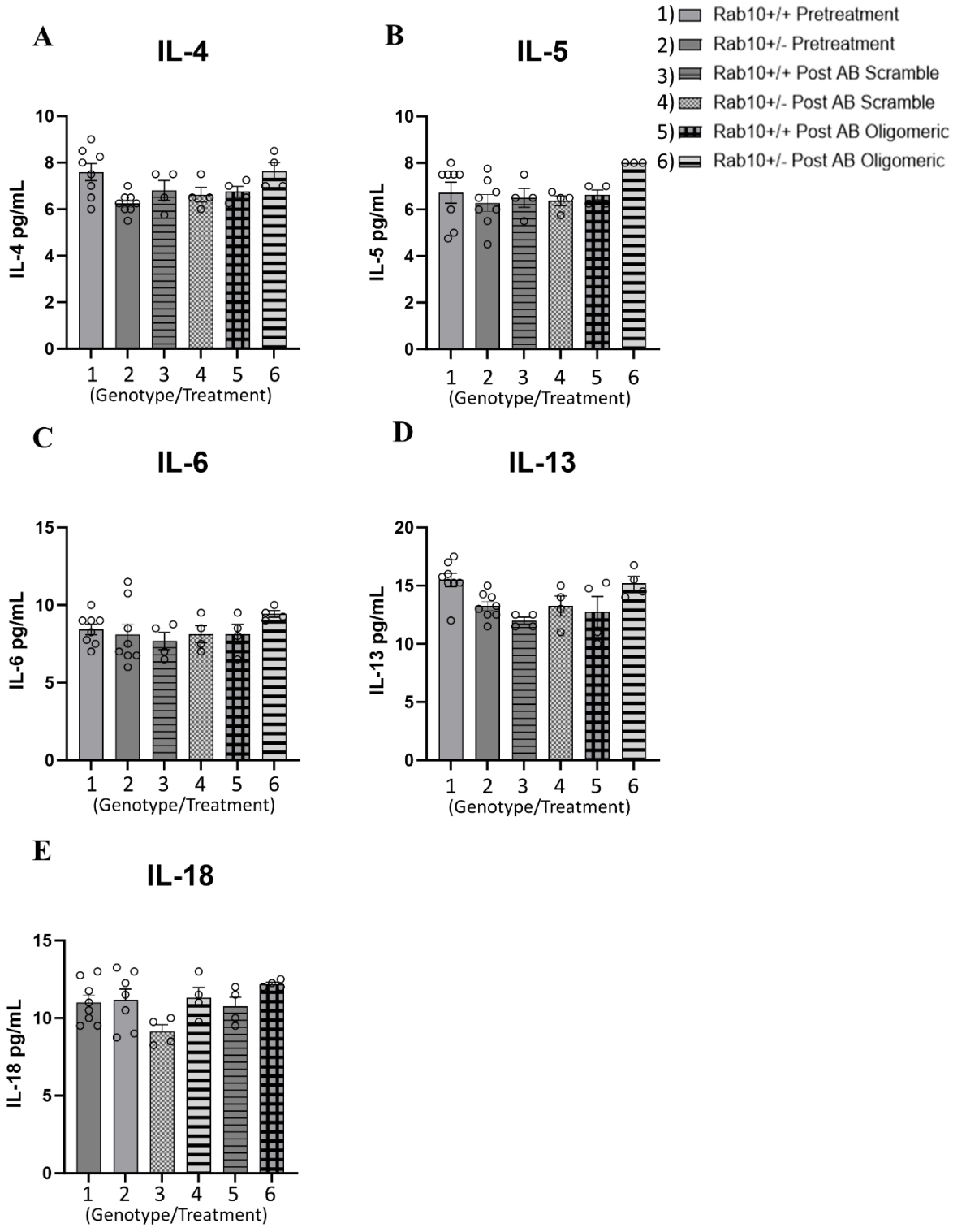
A
IL-4
IL-4 pg/mL
(Genotype/Treatment)
B
IL-5
IL-5 pg/mL
(Genotype/Treatment)
C
IL-6
IL-6 pg/mL
(Genotype/Treatment)
D
IL-13
IL-13 pg/mL
(Genotype/Treatment)
E
IL-18
IL-18 pg/mL
(Genotype/Treatment)
1) Rab10+/+ Pretreatment
2) Rab10+/- Pretreatment
3) Rab10+/+ Post AB Scramble
4) Rab10+/- Post AB Scramble
5) Rab10+/+ Post AB Oligomeric
6) Rab10+/- Post AB Oligomeric

Chapter 4-Conclusions

4.1 Summary of profiling of Rab10 heterozygous mice

After extensive characterization of Rab10 heterozygous mice, it is clear that Rab10 has a prominent role on numerous systems throughout the body. Genetic analysis of $Rab10^{+/-}$ mice show increased activation of pathways involved in neuronal metabolism, structural integrity, neurotransmission, and neuroplasticity. Contrarily they have lower activation of pathways known to be associated with neurodegeneration and aging. Several differentially genes were identified in $Rab10^{+/-}$ mice compared to their $Rab10^{+/+}$ littermates including Stx2, Stx1b, Vegfa, and Lrrc25, Prkaa2, Syt4, and Grin2d. Behavioral testing showed that $Rab10^{+/-}$ mice performed significantly better in the hippocampal-dependent object in place task, whereas their performance was significantly impaired on the trace eyeblink classical conditioning task. Immuno-labeling of Iba1 showed a significant reduction in microglia activation in $Rab10^{+/-}$ mice. Furthermore, Luminex analysis of the culture medium from $Rab10^{+/-}$ and $Rab10^{+/+}$ hippocampal slices incubated with oAβ demonstrated that reducing Rab10 level is sufficient to reduce inflammatory cytokine release such as IL1-beta, IFN-Gamma, and TNF Alpha. Peripherally, Rab10 reduction showed the role of Rab10 in modulation of baseline immune cell distributions: NK cells being lowered and skewing the phenotypes of CD8+ and CD4+ effector memory T-cells significantly lower and higher respectively. Thus, Rab10-dependent neuroresilience is likely a multifactorial phenomenon with potential therapeutic targets within the nervous and immune systems worthy of further research.

4.2 Future Directions:

In this dissertation numerous possible therapeutic targets were identified as possible mediators of Rab10-dependent neuroresilience; however, there are likely other molecular mechanisms involved in the vital functions that it provides. For example, the downstream targets of Rab10 signaling that mediate the differential roles of this signaling protein have yet to be discovered. Spatial gene expression and spatial proteomics could be utilized to help tackle this problem. Also, while a recent study has shown that Rab10 may play a role in microglia activation and our study has shown that Rab10 reduction lowers basal microglia activation, how this happens is unknown as well. Lasty, based on our data Rab10 seems to play a prominent role in inflammation mediation both centrally and peripherally. Further studies elucidating the mechanisms behind this phenomenon could prove not only beneficial for our understanding of Rab10 neuronal resilience, but also reveal future therapeutic targets to combat the dismal prognosis of neurodegenerative disorders such as AD. Development of new tools to specifically manipulate Rab10 levels both peripherally and centrally would also be extremely valuable in elucidating this critical protein's diverse and complex functions.

Bibliography

1. Ali, M., Falkenhain, K., Njiru, B. N., Murtaza-Ali, M., Ruiz-Uribe, N. E., Haft-Javaherian, M., Catchers, S., Nishimura, N., Schaffer, C. B., & Bracko, O. (2022). VEGF signalling causes stalls in brain capillaries and reduces cerebral blood flow in Alzheimer's mice. *Brain*, *145*(4), 1449-1463.
2. Asai, H., Ikezu, S., Tsunoda, S., Medalla, M., Luebke, J., Haydar, T., Wolozin, B., Butovsky, O., Kügler, S., & Ikezu, T. (2015). Depletion of microglia and inhibition of exosome synthesis halt tau propagation. *Nature neuroscience*, *18*(11), 1584-1593.
3. Balkwill, F. (2006). TNF-α in promotion and progression of cancer. *Cancer and Metastasis Reviews*, *25*, 409-416.
4. Barker, G. R. I., & Warburton, E. C. (2015). Object-in-place associative recognition memory depends on glutamate receptor neurotransmission within two defined hippocampal-cortical circuits: a critical role for AMPA and NMDA receptors in the hippocampus, perirhinal, and prefrontal cortices. *Cerebral cortex*, *25*(2), 472-481.
5. Barral, D. C., Ramalho, J. S., Anders, R., Hume, A. N., Knapton, H. J., Tolmachova, T., Collinson, L. M., Goulding, D., Authi, K. S., & Seabra, M. C. (2002). Functional redundancy of Rab27 proteins and the pathogenesis of Griscelli syndrome. *The Journal of clinical investigation*, *110*(2), 247-257.
6. Bellucci, A., Longhena, F., & Spillantini, M. G. (2022). The role of Rab proteins in Parkinson's disease synaptopathy. *Biomedicines*, *10*(8), 1941.
7. Bettcher, B. M., Tansey, M. G., Dorothée, G., & Heneka, M. T. (2021). Peripheral and central immune system crosstalk in Alzheimer disease—a research prospectus. *Nature Reviews Neurology*, *17*(11), 689-701.
8. Bermejo, P., Martín-Aragón, S., Benedí, J., Susín, C., Felici, E., Gil, P., ... & Villar, Á. M. (2008). Differences of peripheral inflammatory markers between mild cognitive impairment and Alzheimer's disease. *Immunology letters*, *117*(2), 198-202.
9. Besedovsky, H., Del Rey, A., Sorkin, E., & Dinarello, C. A. (1986). Immunoregulatory feedback between interleukin-1 and glucocorticoid hormones. *Science*, *233*(4764), 652-654.
10. Bezprozvanny, I., & Hiesinger, P. R. (2013). The synaptic maintenance problem: membrane recycling, Ca 2+ homeostasis and late onset degeneration. *Molecular Neurodegeneration*, *8*, 1-14.
11. Benzing, W. C., Wujek, J. R., Ward, E. K., Shaffer, D., Ashe, K. H., Younkin, S. G., & Brunden, K. R. (1999). Evidence for glial-mediated inflammation in aged APPSW transgenic mice. *Neurobiology of aging*, *20*(6), 581-589.
12. Bivona, G., Iemmolo, M., Agnello, L., Lo Sasso, B., Gambino, C. M., Giglio, R. V., Scazzone, C., Ghersi, G., & Ciaccio, M. (2023). Microglial Activation and Priming in Alzheimer's Disease: State of the Art and Future Perspectives. *International journal of molecular sciences*, *24*(1), 884.
13. Bonifacino, J. S., & Glick, B. S. (2004). The mechanisms of vesicle budding and fusion. *cell*, *116*(2), 153-166.
14. Brighouse, A., Dacks, J. B., & Field, M. C. (2010). Rab protein evolution and the history of the eukaryotic endomembrane system. *Cellular and molecular life sciences*, *67*, 3449-3465.

15. Brown, K. L., Calizo, L. H., Goodlett, C. R., & Stanton, M. E. (2007). Neonatal alcohol exposure impairs acquisition of eyeblink conditioned responses during discrimination learning and reversal in weanling rats. *Developmental psychobiology*, *49*(3), 243-257.
16. Brumfield, A., Chaudhary, N., Molle, D., Wen, J., Graumann, J., & McGraw, T. E. (2021). Insulin-promoted mobilization of GLUT4 from a perinuclear storage site requires RAB10. *Molecular Biology of the Cell*, *32*(1), 57-73.
17. Bunner, W., Landry, T., Laing, B. T., Li, P., Rao, Z., Yuan, Y., & Huang, H. (2020). ARCAgRP/NPY neuron activity is required for acute exercise-induced food intake in un-trained mice. *Frontiers in Physiology*, *11*, 411.
18. Busse, S., Hoffmann, J., Michler, E., Hartig, R., Frodl, T., & Busse, M. (2021). Dementia-associated changes of immune cell composition within the cerebrospinal fluid. *Brain, Behavior, & Immunity-Health*, *14*, 100218.
19. Butterfield, D. A., & Halliwell, B. (2019). Oxidative stress, dysfunctional glucose metabolism and Alzheimer disease. *Nature Reviews Neuroscience*, *20*(3), 148-160.
20. Calin-Jageman, R. J., & Cumming, G. (2019). The new statistics for better science: Ask how much, how uncertain, and what else is known. *The American Statistician*, *73*(sup1), 271-280.
21. Campenot, R. B., & Eng, H. (2000). Protein synthesis in axons and its possible functions. *Journal of neurocytology*, *29*(11-12), 793-798.
22. Carroll, K. S., Hanna, J., Simon, I., Krise, J., Barbero, P., & Pfeffer, S. R. (2001). Role of Rab9 GTPase in facilitating receptor recruitment by TIP47. *Science*, *292*(5520), 1373-1376.
23. Chan, C.-C., Scoggin, S., Wang, D., Cherry, S., Dembo, T., Greenberg, B., Jin, E. J., Kuey, C., Lopez, A., & Mehta, S. Q. (2011). Systematic discovery of Rab GTPases with synaptic functions in Drosophila. *Current Biology*, *21*(20), 1704-1715.
24. Chen, X.-Q., Wang, B., Wu, C., Pan, J., Yuan, B., Su, Y.-Y., Jiang, X.-Y., Zhang, X., & Bao, L. (2012). Endosome-mediated retrograde axonal transport of P2X3 receptor signals in primary sensory neurons. *Cell research*, *22*(4), 677-696.
25. Chen, X., Firulyova, M., Manis, M., Herz, J., Smirnov, I., Aladyeva, E., Wang, C., Bao, X., Finn, M. B., & Hu, H. (2023). Microglia-mediated T cell infiltration drives neurodegeneration in tauopathy. *Nature*, *615*(7953), 668-677.
26. Cheng, D. T., Disterhoft, J. F., Power, J. M., Ellis, D. A., & Desmond, J. E. (2008). Neural substrates underlying human delay and trace eyeblink conditioning. *Proceedings of the National Academy of Sciences*, *105*(23), 8108-8113.
27. Cheng, K. W., Lahad, J. P., Kuo, W.-l., Lapuk, A., Yamada, K., Auersperg, N., Liu, J., Smith-McCune, K., Lu, K. H., & Fishman, D. (2004). The RAB25 small GTPase determines aggressiveness of ovarian and breast cancers. *Nature Medicine*, *10*(11), 1251-1256.
28. Ciesielska, A., Matyjek, M., & Kwiatkowska, K. (2021). TLR4 and CD14 trafficking and its influence on LPS-induced pro-inflammatory signaling. *Cellular and molecular life sciences*, *78*, 1233-1261.
29. Cost, K. T., Williams-Yee, Z. N., Fustok, J. N., & Dohanich, G. P. (2012). Sex differences in object-in-place memory of adult rats. *Behavioral neuroscience*, *126*(3), 457.
30. Cousin, M. A. (2015). Synaptic vesicle endocytosis and endosomal recycling in central nerve terminals: discrete trafficking routes? *The Neuroscientist*, *21*(4), 413-423.
31. Crist, A. M., Hinkle, K. M., Wang, X., Moloney, C. M., Matchett, B. J., Labuzan, S. A., Frankenhauser, I., Azu, N. O., Liesinger, A. M., & Lesser, E. R. (2021). Transcriptomic analysis to identify genes associated with selective hippocampal vulnerability in Alzheimer's disease. *Nature Communications*, *12*(1), 2311.

32. Cruchaga, C., Karch, C. M., Jin, S. C., Benitez, B. A., Cai, Y., Guerreiro, R., Harari, O., Norton, J., Budde, J., & Bertelsen, S. (2014). Rare coding variants in the phospholipase D3 gene confer risk for Alzheimer's disease. *Nature*, *505*(7484), 550-554.
33. D'Adamo, P., Masetti, M., Bianchi, V., Morè, L., Mignogna, M. L., Giannandrea, M., & Gatti, S. (2014). RAB GTPases and RAB-interacting proteins and their role in the control of cognitive functions. *Neuroscience & Biobehavioral Reviews*, *46*, 302-314.
34. Dá Mesquita, S., Ferreira, A. C., Sousa, J. C., Correia-Neves, M., Sousa, N., & Marques, F. (2016). Insights on the pathophysiology of Alzheimer's disease: The crosstalk between amyloid pathology, neuroinflammation and the peripheral immune system. *Neuroscience & Biobehavioral Reviews*, *68*, 547-562.
35. Dansokho, C., Ait Ahmed, D., Aid, S., Toly-Ndour, C., Chaigneau, T., Calle, V., ... & Dorothee, G. (2016). Regulatory T cells delay disease progression in Alzheimer-like pathology. *Brain*, *139*(4), 1237-1251.
36. Davis, K. L., & Powchik, P. (1995). Tacrine. *The Lancet*, *345*(8950), 625-630.
37. de Wit, H., Lichtenstein, Y., Kelly, R. B., Geuze, H. J., Klumperman, J., & van der Sluijs, P. (2001). Rab4 regulates formation of synaptic-like microvesicles from early endosomes in PC12 cells. *Molecular Biology of the Cell*, *12*(11), 3703-3715.
38. Deinhardt, K., Salinas, S., Verastegui, C., Watson, R., Worth, D., Hanrahan, S., Bucci, C., & Schiavo, G. (2006). Rab5 and Rab7 control endocytic sorting along the axonal retrograde transport pathway. *Neuron*, *52*(2), 293-305.
39. Deng, C.-Y., Lei, W.-L., Xu, X.-H., Ju, X.-C., Liu, Y., & Luo, Z.-G. (2014). JIP1 mediates anterograde transport of Rab10 cargos during neuronal polarization. *Journal of Neuroscience*, *34*(5), 1710-1723.
40. Denning, K. M., Smyth, P. C., Cahill, S. F., Finn, S. P., Conlon, E., Li, J., Flavin, R. J., Aherne, S. T., Guenther, S. M., & Ferlinz, A. (2007). A molecular expression signature distinguishing follicular lesions in thyroid carcinoma using preamplification RT-PCR in archival samples. *Modern Pathology*, *20*(10), 1095-1102.
41. Denninger, J. K., Smith, B. M., & Kirby, E. D. (2018). Novel object recognition and object location behavioral testing in mice on a budget. *JoVE (Journal of Visualized Experiments)*(141), e58593.
42. Diekmann, Y., Seixas, E., Gouw, M., Tavares-Cadete, F., Seabra, M. C., & Pereira-Leal, J. B. (2011). Thousands of rab GTPases for the cell biologist. *PLoS computational biology*, *7*(10), e1002217.
43. Dursun, E., Gezen-Ak, D., Hanağası, H., Bilgiç, B., Lohmann, E., Ertan, S., ... & Yılmazer, S. (2015). The interleukin 1 alpha, interleukin 1 beta, interleukin 6 and alpha-2-macroglobulin serum levels in patients with early or late onset Alzheimer's disease, mild cognitive impairment or Parkinson's disease. *Journal of neuroimmunology*, *283*, 50-57.
44. Fan, Y., Howden, A. J., Sarhan, A. R., Lis, P., Ito, G., Martinez, T. N., Brockmann, K., Gasser, T., Alessi, D. R., & Sammler, E. M. (2018). Interrogating Parkinson's disease LRRK2 kinase pathway activity by assessing Rab10 phosphorylation in human neutrophils. *Biochemical Journal*, *475*(1), 23-44.
45. Fontijn, R. D., Goud, B., Echard, A., Jollivet, F., van Marle, J., Pannekoek, H., & Horrevoets, A. J. (2001). The human kinesin-like protein RB6K is under tight cell cycle control and is essential for cytokinesis. *Molecular and cellular biology*, *21*(8), 2944-2955.

46. Fowler, K. S., Saling, M. M., Conway, E. L., Semple, J. M., & Louis, W. J. (2002). Paired associate performance in the early detection of DAT. *Journal of the International Neuropsychological Society*, *8*(1), 58-71.
47. Garfias, S., Domínguez, B. T., Rojas, A. T., Arroyo, M., Rodríguez, U., Boll, C., ... & Fleury, A. (2022). Peripheral blood lymphocyte phenotypes in Alzheimer and Parkinson's diseases. *Neurología (English Edition)*, *37*(2), 110-121.
48. Gate, D., Saligrama, N., Leventhal, O., Yang, A. C., Unger, M. S., Middeldorp, J., ... & Wyss-Coray, T. (2020). Clonally expanded CD8 T cells patrol the cerebrospinal fluid in Alzheimer's disease. *Nature*, *577*(7790), 399-404.
49. Geginat, J., Sallusto, F., & Lanzavecchia, A. (2001). Cytokine-driven proliferation and differentiation of human naive, central memory, and effector memory CD4+ T-cells. *The Journal of experimental medicine*, *194*(12), 1711-1720.
50. Giau, V. V., Bagyinszky, E., Yang, Y. S., Youn, Y. C., An, S. S. A., & Kim, S. Y. (2019). Genetic analyses of early-onset Alzheimer's disease using next generation sequencing. *Scientific reports*, *9*(1), 8368.
51. Ginsberg, S. D., Alldred, M. J., Counts, S. E., Cataldo, A. M., Neve, R. L., Jiang, Y., Wuu, J., Chao, M. V., Mufson, E. J., & Nixon, R. A. (2010). Microarray analysis of hippocampal CA1 neurons implicates early endosomal dysfunction during Alzheimer's disease progression. *Biological psychiatry*, *68*(10), 885-893.
52. Ginsberg, S. D., Mufson, E. J., Alldred, M. J., Counts, S. E., Wuu, J., Nixon, R. A., & Che, S. (2011). Upregulation of select rab GTPases in cholinergic basal forebrain neurons in mild cognitive impairment and Alzheimer's disease. *Journal of chemical neuroanatomy*, *42*(2), 102-110.
53. Griciuc, A., Serrano-Pozo, A., Parrado, A. R., Lesinski, A. N., Asselin, C. N., Mullin, K., Hooli, B., Choi, S. H., Hyman, B. T., & Tanzi, R. E. (2013). Alzheimer's disease risk gene CD33 inhibits microglial uptake of amyloid beta. *Neuron*, *78*(4), 631-643.
54. Guerreiro, R., Wojtas, A., Bras, J., Carrasquillo, M., Rogaeva, E., Majounie, E., Cruchaga, C., Sassi, C., Kauwe, J. S., & Younkin, S. (2013). TREM2 variants in Alzheimer's disease. *New England Journal of Medicine*, *368*(2), 117-127.
55. Hampel, H., Hardy, J., Blennow, K., Chen, C., Perry, G., Kim, S. H., Villemagne, V. L., Aisen, P., Vendruscolo, M., & Iwatsubo, T. (2021). The amyloid-β pathway in Alzheimer's disease. *Molecular psychiatry*, *26*(10), 5481-5503.
56. Hansen, D. V., Hanson, J. E., & Sheng, M. (2018). Microglia in Alzheimer's disease. *Journal of Cell Biology*, *217*(2), 459-472.
57. Hasan, M. T., Hernández-González, S., Dogbevia, G., Trevino, M., Bertocchi, I., Gruart, A., & Delgado-García, J. M. (2013). Role of motor cortex NMDA receptors in learning-dependent synaptic plasticity of behaving mice. *Nature Communications*, *4*(1), 2258.
58. Hauwel, M., Furon, E., Canova, C., Griffiths, M., Neal, J., & Gasque, P. (2005). Innate (inherent) control of brain infection, brain inflammation and brain repair: the role of microglia, astrocytes,"protective" glial stem cells and stromal ependymal cells. *Brain research reviews*, *48*(2), 220-233.
59. Heneka, M. T., Carson, M. J., El Khoury, J., Landreth, G. E., Brosseron, F., Feinstein, D. L., ... & Kummer, M. P. (2015). Neuroinflammation in Alzheimer's disease. *The Lancet Neurology*, *14*(4), 388-405.
60. Homma, Y., Hiragi, S., & Fukuda, M. (2021). Rab family of small GTPases: an updated view on their regulation and functions. *The FEBS journal*, *288*(1), 36-55.

61. Hooper, S., Gaggioli, C., & Sahai, E. (2010). A chemical biology screen reveals a role for Rab21-mediated control of actomyosin contractility in fibroblast-driven cancer invasion. *British journal of cancer*, *102*(2), 392-402.
62. Hopperton, K. E., Mohammad, D., Trépanier, M. O., Giuliano, V., & Bazinet, R. P. (2018). Markers of microglia in post-mortem brain samples from patients with Alzheimer's disease: a systematic review. *Molecular psychiatry*, *23*(2), 177-198.
63. Hunter, M. P., Russo, A., & O'Bryan, J. P. (2013). Emerging roles for intersectin (ITSN) in regulating signaling and disease pathways. *International journal of molecular sciences*, *14*(4), 7829-7852.
64. Hurtado, D. E., Molina-Porcel, L., Iba, M., Aboagye, A. K., Paul, S. M., Trojanowski, J. Q., & Lee, V. M. Y. (2010). Aβ Accelerates the Spatiotemporal Progression of Tau Pathology and Augments Tau Amyloidosis in an Alzheimer Mouse Model. *The American Journal of Pathology*, *177*(4), 1977-1988. https://doi.org/10.2353/ajpath.2010.100346
65. Hutagalung, A. H., & Novick, P. J. (2011). Role of Rab GTPases in membrane traffic and cell physiology. *Physiological reviews*, *91*(1), 119-149.
66. Jackson, A. P., Flett, A., Smythe, C., Hufton, L., Wettey, F. R., & Smythe, E. (2003). Clathrin promotes incorporation of cargo into coated pits by activation of the AP2 adaptor μ2 kinase. *The Journal of Cell Biology*, *163*(2), 231-236.
67. Jennings, D., Huntwork-Rodriguez, S., Henry, A. G., Sasaki, J. C., Meisner, R., Diaz, D., Solanoy, H., Wang, X., Negrou, E., & Bondar, V. V. (2022). Preclinical and clinical evaluation of the LRRK2 inhibitor DNL201 for Parkinson's disease. *Science Translational Medicine*, *14*(648), eabj2658.
68. Jin, E. J., Chan, C.-C., Agi, E., Cherry, S., Hanacik, E., Buszczak, M., & Hiesinger, P. R. (2012). Similarities of Drosophila rab GTPases based on expression profiling: completion and analysis of the rab-Gal4 kit. *PLoS One*, *7*(7), e40912.
69. Jonsson, T., Atwal, J. K., Steinberg, S., Snaedal, J., Jonsson, P. V., Bjornsson, S., Stefansson, H., Sulem, P., Gudbjartsson, D., & Maloney, J. (2012). A mutation in APP protects against Alzheimer's disease and age-related cognitive decline. *Nature*, *488*(7409), 96-99.
70. Jonsson, T., Stefansson, H., Steinberg, S., Jonsdottir, I., Jonsson, P. V., Snaedal, J., Bjornsson, S., Huttenlocher, J., Levey, A. I., & Lah, J. J. (2013). Variant of TREM2 associated with the risk of Alzheimer's disease. *New England Journal of Medicine*, *368*(2), 107-116.
71. Karimy, J. K., Reeves, B. C., & Kahle, K. T. (2020). Targeting TLR4-dependent inflammation in post-hemorrhagic brain injury. *Expert opinion on therapeutic targets*, *24*(6), 525-533.
72. Kim, S., Sato, Y., Mohan, P. S., Peterhoff, C., Pensalfini, A., Rigoglioso, A., Jiang, Y., & Nixon, R. A. (2016). Evidence that the rab5 effector APPL1 mediates APP-βCTF-induced dysfunction of endosomes in Down syndrome and Alzheimer's disease. *Molecular psychiatry*, *21*(5), 707-716.
73. Kiral, F. R., Kohrs, F. E., Jin, E. J., & Hiesinger, P. R. (2018). Rab GTPases and membrane trafficking in neurodegeneration. *Current Biology*, *28*(8), R471-R486.
74. Kishimoto, Y., Nakazawa, K., Tonegawa, S., Kirino, Y., & Kano, M. (2006). Hippocampal CA3 NMDA Receptors Are Crucial for Adaptive Timing of Trace Eyeblink Conditioned Response. *The Journal of Neuroscience*, *26*(5), 1562-1570. https://doi.org/10.1523/jneurosci.4142-05.2006

75. Kotermanski, S. E., & Johnson, J. W. (2009). Mg2+ imparts NMDA receptor subtype selectivity to the Alzheimer's drug memantine. *Journal of Neuroscience*, *29*(9), 2774-2779.
76. Kotermanski, S. E., Wood, J. T., & Johnson, J. W. (2009). Memantine binding to a superficial site on NMDA receptors contributes to partial trapping. *The Journal of physiology*, *587*(19), 4589-4604.
77. Kwak, S. S., Washicosky, K. J., Brand, E., Von Maydell, D., Aronson, J., Kim, S., Capen, D. E., Cetinbas, M., Sadreyev, R., Ning, S., Bylykbashi, E., Xia, W., Wagner, S. L., Choi, S. H., Tanzi, R. E., & Kim, D. Y. (2020). Amyloid-β42/40 ratio drives tau pathology in 3D human neural cell culture models of Alzheimer's disease. *Nature Communications*, *11*(1). https://doi.org/10.1038/s41467-020-15120-3
78. Leng, F., & Edison, P. (2021). Neuroinflammation and microglial activation in Alzheimer disease: where do we go from here?. *Nature Reviews Neurology*, *17*(3), 157-172.
79. Li, S., Hong, S., Shepardson, N. E., Walsh, D. M., Shankar, G. M., & Selkoe, D. (2009). Soluble oligomers of amyloid β protein facilitate hippocampal long-term depression by disrupting neuronal glutamate uptake. *Neuron*, *62*(6), 788-801.
80. Lim, G. P., Yang, F., Chu, T., Chen, P., Beech, W., Teter, B., ... & Cole, G. M. (2000). Ibuprofen suppresses plaque pathology and inflammation in a mouse model for Alzheimer's disease. *Journal of Neuroscience*, *20*(15), 5709-5714.
81. Limone, A., Veneruso, I., D'Argenio, V., & Sarnataro, D. (2022). Endosomal trafficking and related genetic underpinnings as a hub in Alzheimer's disease. *Journal of Cellular Physiology*, *237*(10), 3803-3815.
82. Liu, P., Jenkins, N. A., & Copeland, N. G. (2003). A highly efficient recombineering-based method for generating conditional knockout mutations. *Genome research*, *13*(3), 476-484.
83. Liu, Z., Xu, E., Zhao, H. T., Cole, T., & West, A. B. (2020). LRRK2 and Rab10 coordinate macropinocytosis to mediate immunological responses in phagocytes. *The EMBO journal*, *39*(20), e104862.
84. Lv, P., Sheng, Y., Zhao, Z., Zhao, W., Gu, L., Xu, T., & Song, E. (2015). Targeted disruption of Rab10 causes early embryonic lethality. *Protein & cell*, *6*(6), 463-467.
85. Maccioni, R. B., Farías, G., Morales, I., & Navarrete, L. (2010). The revitalized tau hypothesis on Alzheimer's disease. *Archives of medical research*, *41*(3), 226-231.
86. Mahoney, E. R., Dumitrescu, L., Moore, A. M., Cambronero, F. E., De Jager, P. L., Koran, M. E. I., Petyuk, V. A., Robinson, R. A., Goyal, S., & Schneider, J. A. (2021). Brain expression of the vascular endothelial growth factor gene family in cognitive aging and alzheimer's disease. *Molecular psychiatry*, *26*(3), 888-896.
87. Mahase, E. (2023). Alzheimer's disease: FDA approves lecanemab amid cost and safety concerns.
88. Matanis, T., Akhmanova, A., Wulf, P., Del Nery, E., Weide, T., Stepanova, T., Galjart, N., Grosveld, F., Goud, B., & De Zeeuw, C. I. (2002). Bicaudal-D regulates COPI-independent Golgi–ER transport by recruiting the dynein–dynactin motor complex. *Nature cell biology*, *4*(12), 986-992.
89. Medway, C. W., Abdul-Hay, S., Mims, T., Ma, L., Bisceglio, G., Zou, F., Pankratz, S., Sando, S. B., Aasly, J. O., & Barcikowska, M. (2014). ApoE variant p. V236E is associated with markedly reduced risk of Alzheimer's disease. *Molecular Neurodegeneration*, *9*(1), 1-5.

90. Mendoza, P., Ortiz, R., Diaz, J., Quest, A. F., Leyton, L., Stupack, D., & Torres, V. A. (2013). Rab5 activation promotes focal adhesion disassembly, migration and invasiveness in tumor cells. *Journal of cell science*, *126*(17), 3835-3847.
91. Mignogna, M. L., & D'Adamo, P. (2018). Critical importance of RAB proteins for synaptic function. *Small GTPases*, *9*(1-2), 145-157.
92. Mottola, G. (2014). The complexity of Rab5 to Rab7 transition guarantees specificity of pathogen subversion mechanisms. *Frontiers in cellular and infection microbiology*, *4*, 180.
93. Mrak, R. E., & Griffin, W. S. T. (2001). Interleukin-1, neuroinflammation, and Alzheimer's disease. *Neurobiology of aging*, *22*(6), 903-908.
94. Murphy, K. C. (1998). Use of bacteriophage λ recombination functions to promote gene replacement in Escherichia coli. *Journal of bacteriology*, *180*(8), 2063-2071.
95. Muyrers, J. P., Zhang, Y., Testa, G., & Stewart, A. F. (1999). Rapid modification of bacterial artificial chromosomes by ET-recombination. *Nucleic acids research*, *27*(6), 1555-1557.
96. Nagy, A., Rossant, J., Nagy, R., Abramow-Newerly, W., & Roder, J. C. (1993). Derivation of completely cell culture-derived mice from early-passage embryonic stem cells. *Proceedings of the National Academy of Sciences*, *90*(18), 8424-8428.
97. Onyango, I. G., Jauregui, G. V., Čarná, M., Bennett Jr, J. P., & Stokin, G. B. (2021). Neuroinflammation in Alzheimer's disease. *Biomedicines*, *9*(5), 524.
98. Pajarillo, E., Kim, S., Digman, A., Dutton, M., Son, D. S., Aschner, M., & Lee, E. (2023). The role of microglial LRRK2 kinase in manganese-induced inflammatory neurotoxicity via NLRP3 inflammasome and RAB10-mediated autophagy dysfunction. *Journal of Biological Chemistry*, *299*(7).
99. Park-Windhol, C., Ng, Y. S., Yang, J., Primo, V., Saint-Geniez, M., & D'Amore, P. A. (2017). Endomucin inhibits VEGF-induced endothelial cell migration, growth, and morphogenesis by modulating VEGFR2 signaling. *Scientific reports*, *7*(1), 17138.
100. Parra-Damas, A., Valero, J., Chen, M., Espana, J., Martín, E., Ferrer, I., Rodríguez-Alvarez, J., & Saura, C. A. (2014). Crtc1 activates a transcriptional program deregulated at early Alzheimer's disease-related stages. *Journal of Neuroscience*, *34*(17), 5776-5787.
101. Pascoal, T. A., Benedet, A. L., Ashton, N. J., Kang, M. S., Therriault, J., Chamoun, M., ... & Rosa-Neto, P. (2021). Microglial activation and tau propagate jointly across Braak stages. *Nature medicine*, *27*(9), 1592-1599.
102. Pavlos, N. J., & Jahn, R. (2011). Distinct yet overlapping roles of Rab GTPases on synaptic vesicles. *Small GTPases*, *2*(2), 13441-13453.
103. Portelius, E., Bogdanovic, N., Gustavsson, M. K., Volkmann, I., Brinkmalm, G., Zetterberg, H., Winblad, B., & Blennow, K. (2010). Mass spectrometric characterization of brain amyloid beta isoform signatures in familial and sporadic Alzheimer's disease. *Acta Neuropathologica*, *120*(2), 185-193. https://doi.org/10.1007/s00401-010-0690-1
104. Preman, P., Alfonso-Triguero, M., Alberdi, E., Verkhratsky, A., & Arranz, A. M. (2021). Astrocytes in Alzheimer's disease: pathological significance and molecular pathways. *Cells*, *10*(3), 540.
105. Prokop, S., Miller, K. R., Labra, S. R., Pitkin, R. M., Hoxha, K. h., Narasimhan, S., Changolkar, L., Rosenbloom, A., Lee, V. M.-Y., & Trojanowski, J. Q. (2019). Impact of TREM2 risk variants on brain region-specific immune activation and plaque microenvironment in Alzheimer's disease patient brain samples. *Acta Neuropathologica*, *138*, 613-630.

106. Raiborg, C., Wenzel, E. M., Pedersen, N. M., Olsvik, H., Schink, K. O., Schultz, S. W., Vietri, M., Nisi, V., Bucci, C., Brech, A., Johansen, T., & Stenmark, H. (2015). Repeated ER–endosome contacts promote endosome translocation and neurite outgrowth. *Nature*, *520*(7546), 234-238. https://doi.org/10.1038/nature14359
107. Ridge, P. G., Karch, C. M., Hsu, S., Arano, I., Teerlink, C. C., Ebbert, M. T., Gonzalez Murcia, J. D., Farnham, J. M., Damato, A. R., & Allen, M. (2017). Linkage, whole genome sequence, and biological data implicate variants in RAB10 in Alzheimer's disease resilience. *Genome medicine*, *9*(1), 1-14.
108. Rodriquez, M. T. (2023). Aducanumab, Lecanemab for Early AD: The Clinical Trials That Led to FDA Approval. *Medical Bag*, NA-NA.
109. Rodríguez-Gómez, J. A., Kavanagh, E., Engskog-Vlachos, P., Engskog, M. K., Herrera, A. J., Espinosa-Oliva, A. M., Joseph, B., Hajji, N., Venero, J. L., & Burguillos, M. A. (2020). Microglia: agents of the CNS pro-inflammatory response. *Cells*, *9*(7), 1717.
110. Ross, O. A., Wu, Y. R., Lee, M. C., Funayama, M., Chen, M. L., Soto, A. I., ... & Wu, R. M. (2008). Analysis of Lrrk2 R1628P as a risk factor for Parkinson's disease. *Annals of Neurology: Official Journal of the American Neurological Association and the Child Neurology Society*, *64*(1), 88-92.
111. Roussos, P., Katsel, P., Fam, P., Tan, W., Purohit, D. P., & Haroutunian, V. (2015). The triggering receptor expressed on myeloid cells 2 (TREM2) is associated with enhanced inflammation, neuropathological lesions and increased risk for Alzheimer's dementia. *Alzheimer's & Dementia*, *11*(10), 1163-1170.
112. Rufer, E. S., Tran, T. D., Attridge, M. M., Andrzejewski, M. E., Flentke, G. R., & Smith, S. M. (2012). Adequacy of maternal iron status protects against behavioral, neuroanatomical, and growth deficits in fetal alcohol spectrum disorders.
113. Russo, I., Bubacco, L., & Greggio, E. (2022). LRRK2 as a target for modulating immune system responses. *Neurobiology of Disease*, *169*, 105724.
114. Saleh, H. A., Yousef, M. H., & Abdelnaser, A. (2021). The anti-inflammatory properties of phytochemicals and their effects on epigenetic mechanisms involved in TLR4/NF-κB-mediated inflammation. *Frontiers in immunology*, *12*, 606069.
115. Saraste, J. (2016). Spatial and functional aspects of ER-Golgi Rabs and tethers. *Frontiers in cell and developmental biology*, *4*, 28.
116. Savage, M. J., Kawooya, J. K., Pinsker, L. R., Emmons, T. L., Mistretta, S., Siman, R., & Greenberg, B. D. (1995). Elevated Aβ levels in Alzheimer's disease brain are associated with selective accumulation of Aβ42 in parenchymal amyloid plaques and both Aβ40 and Aβ42 in cerebrovascular deposits. *Amyloid*, *2*(4), 234-240.
117. Saw, A. M., Hrastelj, J., & Robertson, N. P. (2023). Path from discovery to recovery: therapeutic and diagnostic advances in Alzheimer's dementia. *Journal of Neurology*, *270*(8), 4151-4153. https://doi.org/10.1007/s00415-023-11840-w
118. Scarabino, D., Peconi, M., Broggio, E., Gambina, G., Maggi, E., Armeli, F., ... & Businaro, R. (2020). Relationship between proinflammatory cytokines (Il-1beta, Il-18) and leukocyte telomere length in mild cognitive impairment and Alzheimer's disease. *Experimental Gerontology*, *136*, 110945.
119. Scheper, W., Hoozemans, J., Hoogenraad, C., Rozemuller, A., Eikelenboom, P., & Baas, F. (2007). Rab6 is increased in Alzheimer's disease brain and correlates with endoplasmic reticulum stress. *Neuropathology and applied neurobiology*, *33*(5), 523-532.

120. Scheper, W., Zwart, R., & Baas, F. (2004). Rab6 membrane association is dependent of Presenilin 1 and cellular phosphorylation events. *Molecular brain research*, *122*(1), 17-23.
121. Scheper, W., Zwart, R., Van Der Sluijs, P., Annaert, W., Gool, W. v., & Baas, F. (2000). Alzheimer's presenilin 1 is a putative membrane receptor for rab GDP dissociation inhibitor. *Human molecular genetics*, *9*(2), 303-310.
122. Schindelin, J., Arganda-Carreras, I., Frise, E., Kaynig, V., Longair, M., Pietzsch, T., ... & Cardona, A. (2012). Fiji: an open-source platform for biological-image analysis. *Nature methods*, *9*(7), 676-682.
123. Seabra, M. C., Ho, Y. K., & Anant, J. S. (1995). Deficient Geranylgeranylation of Ram/Rab27 in Choroideremia (∗). *Journal of Biological Chemistry*, *270*(41), 24420-24427.
124. Seabra, M. C., Mules, E. H., & Hume, A. N. (2002). Rab GTPases, intracellular traffic and disease. *Trends in molecular medicine*, *8*(1), 23-30.
125. Seabra, M. C., & Wasmeier, C. (2004). Controlling the location and activation of Rab GTPases. *Current opinion in cell biology*, *16*(4), 451-457.
126. Semerdjieva, S., Shortt, B., Maxwell, E., Singh, S., Fonarev, P., Hansen, J., Schiavo, G., Grant, B. D., & Smythe, E. (2008). Coordinated regulation of AP2 uncoating from clathrin-coated vesicles by rab5 and hRME-6. *The Journal of Cell Biology*, *183*(3), 499-511.
127. Shankar, G. M., Li, S., Mehta, T. H., Garcia-Munoz, A., Shepardson, N. E., Smith, I., Brett, F. M., Farrell, M. A., Rowan, M. J., Lemere, C. A., Regan, C. M., Walsh, D. M., Sabatini, B. L., & Selkoe, D. J. (2008). Amyloid-β protein dimers isolated directly from Alzheimer's brains impair synaptic plasticity and memory. *Nature Medicine*, *14*(8), 837-842. https://doi.org/10.1038/nm1782
128. Shin, H.-W., Hayashi, M., Christoforidis, S., Lacas-Gervais, S., Hoepfner, S., Wenk, M. R., Modregger, J., Uttenweiler-Joseph, S., Wilm, M., & Nystuen, A. (2005). An enzymatic cascade of Rab5 effectors regulates phosphoinositide turnover in the endocytic pathway. *The Journal of Cell Biology*, *170*(4), 607-618.
129. Sims, N., Bowen, D., Allen, S., Smith, C., Neary, D., Thomas, D., & Davison, A. (1983). Presynaptic cholinergic dysfunction in patients with dementia. *Journal of neurochemistry*, *40*(2), 503-509.
130. Singh, M., Kaur, M., Kukreja, H., Chugh, R., Silakari, O., & Singh, D. (2013). Acetylcholinesterase inhibitors as Alzheimer an: from nerve toxins to neuroprotection. *European journal of medicinal chemistry*, *70*, 165-188.
131. Skelton, R. W. (1988). Bilateral cerebellar lesions disrupt conditioned eyelid responses in unrestrained rats. *Behavioral neuroscience*, *102*(4), 586.
132. Smith-Garvin, J. E., Koretzky, G. A., & Jordan, M. S. (2009). T cell activation. *Annual review of immunology*, *27*, 591-619.
133. Söderberg, L., Johannesson, M., Nygren, P., Laudon, H., Eriksson, F., Osswald, G., ... & Lannfelt, L. (2023). Lecanemab, aducanumab, and gantenerumab—binding profiles to different forms of amyloid-beta might explain efficacy and side effects in clinical trials for Alzheimer's disease. *Neurotherapeutics*, *20*(1), 195-206.
134. Solana, C., Tarazona, R., & Solana, R. (2018). Immunosenescence of natural killer cells, inflammation, and Alzheimer's disease. *International Journal of Alzheimer's Disease*, *2018*.
135. Stanton, M. E., & Goodlett, C. R. (1998). Neonatal ethanol exposure impairs eyeblink conditioning in weanling rats. *Alcoholism: Clinical and Experimental Research*, *22*(1), 270-275.

136. Stenmark, H. (2009). Rab GTPases as coordinators of vesicle traffic. *Nature reviews Molecular cell biology*, *10*(8), 513-525.
137. Stenmark, H., & Olkkonen, V. M. (2001). The rab gtpase family. *Genome biology*, *2*(5), 1-7.
138. Stoothoff, W. H., & Johnson, G. V. (2005). Tau phosphorylation: physiological and pathological consequences. *Biochimica et Biophysica Acta (BBA)-Molecular Basis of Disease*, *1739*(2-3), 280-297.
139. Stoppini, L., et al. (1991). "A simple method for organotypic cultures of nervous tissue." Journal of neuroscience methods **37**(2): 173-182.
140. Streit, W. J., Conde, J. R., Fendrick, S. E., Flanary, B. E., & Mariani, C. L. (2005). Role of microglia in the central nervous system's immune response. *Neurological research*, *27*(7), 685-691.
141. Sun, H., Sun, C., Tian, Z., & Xiao, W. (2013). NK cells in immunotolerant organs. *Cellular & molecular immunology*, *10*(3), 202-212.
142. Szodorai, A., Kuan, Y.-H., Hunzelmann, S., Engel, U., Sakane, A., Sasaki, T., Takai, Y., Kirsch, J., Müller, U., Beyreuther, K., Brady, S., Morfini, G., & Kins, S. (2009). APP Anterograde Transport Requires Rab3A GTPase Activity for Assembly of the Transport Vesicle. *The Journal of Neuroscience*, *29*(46), 14534-14544. https://doi.org/10.1523/jneurosci.1546-09.2009
143. Tavana, J. P., Rosene, M., Jensen, N. O., Ridge, P. G., Kauwe, J. S., & Karch, C. M. (2019). RAB10: an Alzheimer's disease resilience locus and potential drug target. *Clinical interventions in aging*, 73-79.
144. Taylor, C. A., Yan, J., Howell, A. S., Dong, X., & Shen, K. (2015). RAB-10 regulates dendritic branching by balancing dendritic transport. *PLoS genetics*, *11*(12), e1005695.
145. Teshima, C. W., Dieleman, L. A., & Meddings, J. B. (2012). Abnormal intestinal permeability in Crohn's disease pathogenesis. *Annals of the New York Academy of Sciences*, *1258*(1), 159-165.
146. Thomas, J. D., & Tran, T. D. (2012). Choline supplementation mitigates trace, but not delay, eyeblink conditioning deficits in rats exposed to alcohol during development. *Hippocampus*, *22*(3), 619-630.
147. Thomas, T., Miners, S., & Love, S. (2015). Post-mortem assessment of hypoperfusion of cerebral cortex in Alzheimer's disease and vascular dementia. *Brain*, *138*(4), 1059-1069.
148. Tolosa, E., Vila, M., Klein, C., & Rascol, O. (2020). LRRK2 in Parkinson disease: challenges of clinical trials. *Nature Reviews Neurology*, *16*(2), 97-107.
149. Torres-Acosta, N., O'Keefe, J. H., O'Keefe, E. L., Isaacson, R., & Small, G. (2020). Therapeutic potential of TNF-α inhibition for Alzheimer's disease prevention. *Journal of Alzheimer's Disease*, *78*(2), 619-626.
150. Town, T., Tan, J., Flavell, R. A., & Mullan, M. (2005). T-cells in Alzheimer's disease. *Neuromolecular medicine*, *7*, 255-264.
151. Tran, T. D., Amin, A., Jones, K. G., Sheffer, E. M., Ortega, L., & Dolman, K. (2017). The use of trace eyeblink classical conditioning to assess hippocampal dysfunction in a rat model of fetal alcohol spectrum disorders. *JoVE (Journal of Visualized Experiments)*(126), e55350.
152. Tran, T. D., Jackson, H. D., Horn, K. H., & Goodlett, C. R. (2005). Vitamin E does not protect against neonatal ethanol-induced cerebellar damage or deficits in eyeblink classical conditioning in rats. *Alcoholism: Clinical and Experimental Research*, *29*(1), 117-129.

153. Tran, T. D., Stanton, M. E., & Goodlett, C. R. (2007). Binge-like ethanol exposure during the early postnatal period impairs eyeblink conditioning at short and long CS–US intervals in rats. *Developmental Psychobiology: The Journal of the International Society for Developmental Psychobiology*, *49*(6), 589-605.
154. Tratnjek, L., Živin, M., & Glavan, G. (2013). Up-regulation of Synaptotagmin IV within amyloid plaqueassociated dystrophic neurons in Tg2576 mouse model of Alzheimer's disease. *Croatian medical journal*, *54*(5), 419-428.
155. Tu, S., Okamoto, S.-I., Lipton, S. A., & Xu, H. (2014). Oligomeric Aβ-induced synaptic dysfunction in Alzheimer's disease. *Molecular Neurodegeneration*, *9*(1), 48. https://doi.org/10.1186/1750-1326-9-48
156. Tzeng, H.-T., & Wang, Y.-C. (2016). Rab-mediated vesicle trafficking in cancer. *Journal of biomedical science*, *23*(1), 1-7.
157. Udayar, V., Buggia-Prevot, V., Guerreiro, R. L., Siegel, G., Rambabu, N., Soohoo, A. L., Ponnusamy, M., Siegenthaler, B., Bali, J., & Guerreiro, R. (2013). A paired RNAi and RabGAP overexpression screen identifies Rab11 as a regulator of β-amyloid production. *Cell reports*, *5*(6), 1536-1551.
158. Van Dyck, C. H. (2018). Anti-amyloid-β monoclonal antibodies for Alzheimer's disease: pitfalls and promise. *Biological psychiatry*, *83*(4), 311-319.
159. Vetrivel, K. S., Zhang, Y.-w., Xu, H., & Thinakaran, G. (2006). Pathological and physiological functions of presenilins. *Molecular Neurodegeneration*, *1*, 1-12.
160. Wallings, R. L., & Tansey, M. G. (2019). LRRK2 regulation of immune-pathways and inflammatory disease. *Biochemical Society Transactions*, *47*(6), 1581-1595.
161. Wandinger-Ness, A., & Zerial, M. (2014). Rab proteins and the compartmentalization of the endosomal system. *Cold Spring Harbor perspectives in biology*, *6*(11), a022616.
162. Wang, M., Dong, Q., & Wang, Y. (2016). Rab23 is overexpressed in human astrocytoma and promotes cell migration and invasion through regulation of Rac1. *Tumor Biology*, *37*, 11049-11055.
163. Wang, X., Zimmermann, H. R., & Ma, T. (2019). Therapeutic potential of AMP-activated protein kinase in Alzheimer's disease. *Journal of Alzheimer's Disease*, *68*(1), 33-38.
164. Wang, Z., Edwards, J. G., Riley, N., Provance, D. W., Karcher, R., Li, X.-d., Davison, I. G., Ikebe, M., Mercer, J. A., & Kauer, J. A. (2008). Myosin Vb mobilizes recycling endosomes and AMPA receptors for postsynaptic plasticity. *cell*, *135*(3), 535-548.
165. Wareham, L. K., Liddelow, S. A., Temple, S., Benowitz, L. I., Di Polo, A., Wellington, C., Goldberg, J. L., He, Z., Duan, X., & Bu, G. (2022). Solving neurodegeneration: Common mechanisms and strategies for new treatments. *Molecular Neurodegeneration*, *17*(1), 23.
166. Werneburg, S., Jung, J., Kunjamma, R. B., Ha, S.-K., Luciano, N. J., Willis, C. M., Gao, G., Biscola, N. P., Havton, L. A., & Crocker, S. J. (2020). Targeted complement inhibition at synapses prevents microglial synaptic engulfment and synapse loss in demyelinating disease. *Immunity*, *52*(1), 167-182. e167.
167. Wheeler, D. B., Zoncu, R., Root, D. E., Sabatini, D. M., & Sawyers, C. L. (2015). Identification of an oncogenic RAB protein. *Science*, *350*(6257), 211-217.
168. Wimo, A., Seeher, K., Cataldi, R., Cyhlarova, E., Dielemann, J. L., Frisell, O., Guerchet, M., Jönsson, L., Malaha, A. K., Nichols, E., Pedroza, P., Prince, M., Knapp, M., & Dua, T. (2023). The worldwide costs of dementia in 2019. *Alzheimer's & Dementia*. https://doi.org/10.1002/alz.12901

169. Winkler, J., Suhr, S., Gage, F., Thal, L., & Fisher, L. (1995). Essential role of neocortical acetylcholine in spatial memory. *Nature*, *375*(6531), 484-487.
170. Withington, C. G., & Turner, R. S. (2022). Amyloid-related imaging abnormalities with anti-amyloid antibodies for the treatment of dementia due to Alzheimer's disease. *Frontiers in Neurology*, *13*, 862369.
171. Wu, J. (2002). Theoretical study on shear stress generated by microstreaming surrounding contrast agents attached to living cells. *Ultrasound in medicine & biology*, *28*(1), 125-129.
172. XiangWei, W., Kannan, V., Xu, Y., Kosobucki, G. J., Schulien, A. J., Kusumoto, H., Moufawad El Achkar, C., Bhattacharya, S., Lesca, G., & Nguyen, S. (2019). Heterogeneous clinical and functional features of GRIN2D-related developmental and epileptic encephalopathy. *Brain*, *142*(10), 3009-3027.
173. Xu, B.-H., Li, X.-X., Yang, Y., Zhang, M.-Y., Rao, H.-L., Wang, H.-Y., & Zheng, X. S. (2015). Aberrant amino acid signaling promotes growth and metastasis of hepatocellular carcinomas through Rab1A-dependent activation of mTORC1 by Rab1A. *Oncotarget*, *6*(25), 20813.
174. Yan, T., Wang, L., Gao, J., Siedlak, S. L., Huntley, M. L., Termsarasab, P., Perry, G., Chen, S. G., & Wang, X. (2018). Rab10 phosphorylation is a prominent pathological feature in Alzheimer's disease. *Journal of Alzheimer's Disease*, *63*(1), 157-165.
175. Yu, D., Ellis, H. M., Lee, E.-C., Jenkins, N. A., Copeland, N. G., & Court, D. L. (2000). An efficient recombination system for chromosome engineering in Escherichia coli. *Proceedings of the National Academy of Sciences*, *97*(11), 5978-5983.
176. Zhang, G., & Stackman Jr, R. W. (2015). The role of serotonin 5-HT2A receptors in memory and cognition. *Frontiers in pharmacology*, *6*, 225.
177. Zhang, M., Chen, L., Wang, S., & Wang, T. (2009). Rab7: roles in membrane trafficking and disease. *Bioscience reports*, *29*(3), 193-209.
178. Zhang, Y., Buchholz, F., Muyrers, J. P., & Stewart, A. F. (1998). A new logic for DNA engineering using recombination in Escherichia coli. *Nature genetics*, *20*(2), 123-128.
179. Zhang, Y., Fung, I. T. H., Sankar, P., Chen, X., Robison, L. S., Ye, L., D'Souza, S. S., Salinero, A. E., Kuentzel, M. L., & Chittur, S. V. (2020). Depletion of NK cells improves cognitive function in the Alzheimer disease mouse model. *The Journal of Immunology*, *205*(2), 502-510.
180. Zhou, Y., Fu, Y., Yin, W., Li, J., Wang, W., Bai, F., Xu, S., Gong, Q., Peng, T., & Hong, Y. (2021). Kinetics-driven drug design strategy for next-generation acetylcholinesterase inhibitors to clinical candidate. *Journal of medicinal chemistry*, *64*(4), 1844-1855.
181. Zimmermann, H. R., Yang, W., Kasica, N. P., Zhou, X., Wang, X., Beckelman, B. C., Lee, J., Furdui, C. M., Keene, C. D., & Ma, T. (2020). Brain-specific repression of AMPKα1 alleviates pathophysiology in Alzheimer's model mice. *The Journal of clinical investigation*, *130*(7), 3511-3527.
182. Zoncu, R., Perera, R. M., Sebastian, R., Nakatsu, F., Chen, H., Balla, T., Ayala, G., Toomre, D., & De Camilli, P. V. (2007). Loss of endocytic clathrin-coated pits upon acute depletion of phosphatidylinositol 4, 5-bisphosphate. *Proceedings of the National Academy of Sciences*, *104*(10), 3793-3798.
183. Zou, W., Yadav, S., DeVault, L., Jan, Y. N., & Sherwood, D. R. (2015). RAB-10-dependent membrane transport is required for dendrite arborization. *PLoS genetics*, *11*(9), e1005484

Appendix A: IACUC Approval – AUP 105a

EAST CAROLINA UNIVERSITY
ANIMAL USE PROTOCOL (AUP) FORM
LATEST REVISION APRIL 2017

Project Title:
Identifying new signaling pathways involved in Alzheimer's disease

	Principal Investigator	Secondary Contact
Name	Erzsebet Szatmari	Karen Eastwood
Dept.	Physical Therapy	Physical Therapy
Office Ph #	252-737-7154	252-744-6238
Cell Ph #	919-597-1055	252-531-9603
Pager #	N/A	N/A
Home Ph #	N/A	N/A
Email	szatmarie18@ecu.edu	eastwoodk@ecu.edu

For IACUC Use Only

AUP #	P105a		
New/Renewal	Renewal		
Full Review/Date 06/20/2022	DR/Date		
Approval Date	7/8/2022		
Study Type	Alzheimer's Disease		
Pain/Distress Category	C		
Surgery	Survival	Multiple	
Prolonged Restraint			
Food/Fluid Regulation			
Other			
Hazard Approval/Dates	Rad	IBC 05/20/2022	EHS 10/7/2021
OHP Enrollment			
Mandatory Training			
Amendments Approved			

I. Personnel

A. Principal Investigator(s):
Erzsebet Szatmari, PhD

B. Department(s):
Physical Therapy

C. List all personnel (PI's, co-investigators, technicians, students) that will be working with live animals and describe their qualifications and

Appendix A: IACUC Approval – AUP 105a

EAST CAROLINA UNIVERSITY
ANIMAL USE PROTOCOL (AUP) FORM
LATEST REVISION APRIL 2017

Project Title:
Breeding protocol for ADAP1/Centaurin α1 knockout and Rab10 +/- mice

	Principal Investigator	Secondary Contact
Name	Erzsebet Szatmari	Karen Eastwood
Dept.	Physical Therapy	Physical Therapy
Office Ph #	252-737-7154	252-744-6238
Cell Ph #	919-587-1055	252-531-9603
Pager #	Click here to enter text.	Click here to enter text.
Home Ph #	919-587-1055	Click here to enter text.
Email	szatmarie18@ecu.edu	eastwoodk@ecu.edu

For IACUC Use Only

AUP #	P104a		
New/Renewal	Renewal		
Full Review/Date 4/18/2022	DR/Date		
Approval Date	5/20/2022		
Study Type	Breeding – Alzheimer disease		
Pain/Distress Category			
Surgery	Survival	Multiple	
Prolonged Restraint			
Food/Fluid Regulation			
Other			
Hazard Approval/Dates	Rad	IBC 4/13/2022	EHS 10/7/2021
OHP Enrollment			
Mandatory Training			
Amendments Approved			

I. Personnel

A. Principal Investigator(s):
Erzsebet M. Szatmari, PhD

B. Department(s):
Physical Therapy

C. List all personnel (PI's, co-investigators, technicians, students) that will be working with live animals and describe their qualifications and experience with these specific procedures. If people are to be trained, indicate by whom: